



12-2017

Evaluation of Inveon Pre-Clinical Positron Emission Tomography (PET) Scanner Geant4 Application for Tomographic Imaging (GATE) Model for Multi-Positron Emission Particle Tracking (M-PEPT)

Roque Antonio Santos Torres
University of Tennessee

Recommended Citation

Santos Torres, Roque Antonio, "Evaluation of Inveon Pre-Clinical Positron Emission Tomography (PET) Scanner Geant4 Application for Tomographic Imaging (GATE) Model for Multi-Positron Emission Particle Tracking (M-PEPT)." PhD diss., University of Tennessee, 2017.

https://trace.tennessee.edu/utk_graddiss/4825

This Dissertation is brought to you for free and open access by the Graduate School at Trace: Tennessee Research and Creative Exchange. It has been accepted for inclusion in Doctoral Dissertations by an authorized administrator of Trace: Tennessee Research and Creative Exchange. For more information, please contact trace@utk.edu.

To the Graduate Council:

I am submitting herewith a dissertation written by Roque Antonio Santos Torres entitled "Evaluation of Inveon Pre-Clinical Positron Emission Tomography (PET) Scanner Geant4 Application for Tomographic Imaging (GATE) Model for Multi-Positron Emission Particle Tracking (M-PEPT)." I have examined the final electronic copy of this dissertation for form and content and recommend that it be accepted in partial fulfillment of the requirements for the degree of Doctor of Philosophy, with a major in Nuclear Engineering.

Arthur Ruggles, Major Professor

We have read this dissertation and recommend its acceptance:

John D. Auxier II, Lawrence Heilbronn, Dustin Osborne

Accepted for the Council:

Carolyn R. Hodges

Vice Provost and Dean of the Graduate School

(Original signatures are on file with official student records.)

**Evaluation of Inveon Pre-Clinical Positron
Emission Tomography (PET) Scanner Geant4
Application for Tomographic Imaging (GATE)
Model for Multi-Positron Emission Particle
Tracking (M-PEPT)**

A Dissertation Presented for the
Doctor of Philosophy
Degree
The University of Tennessee, Knoxville

Roque Antonio Santos Torres
December 2017

ACKNOWLEDGEMENTS

Thanks to God for all the miracles that has done in my life.

Thanks to my parents for the support and the love they have given me.

Thanks to Dr. Arthur Ruggles for his guidance and patience. He is the best mentor anyone could want.

Thanks to my girlfriend Fernanda for her support and infinite love.

Thanks to my friends in the United States, especially Cody Wiggins, who has been almost a second advisor in my work.

Thanks to all my friends in Ecuador. I have missed you so much.

Thanks to the Fulbright Program, the Department of Nuclear Engineering at UTK, and the Escuela Politecnica Nacional for their economic support.

ABSTRACT

A Sodium-22 point source of activity 10 μCi [microcurie] is moved through an Inveon Pre-Clinical Positron Emission Tomography (PET) scanner, and the scan data are sent to Multi-Positron Emission Particle Tracking (M-PEPT) software to recreate the particle track. A Geant4 Application for Tomographic Imaging (GATE) model of the Inveon is used to simulate the scanner response to point source movements identical to those prescribed in experiments. Simulated and physical experiment outcomes are compared to qualify the GATE model for the M-PEPT application. GATE over predicts the number of detected coincident lines (CL). The standard deviation of particle positions predicted by M-PEPT using GATE data is similar to the standard deviation produced by M-PEPT using scanner data.

TABLE OF CONTENTS

Chapter One Introduction	1
Chapter Two Literature Review	3
1. Positron Emission Tomography General Review	3
2. Inveon PET Scanner	9
3. Positron Emission Particle Tracking	11
4. Geant4 Application for Tomographic Emission (GATE)	15
5. GATE digitizer.....	17
6. Summary and Objectives	19
Chapter Three Materials and Methods	21
1. Evaluation of the Inveon PET scanner	21
General setup parameters used in Inveon	21
Point sources and phantom support	21
Multiple Positron Emission Particle Tracking (M-PEPT) code	24
Efficiency curve and evaluation of the Inveon	25
2. Moving Particle Experimental Setup.....	25
3. GATE Model and Simulation Setup.....	27
Inveon GATE model.....	27
Source definition for static particle simulation	32
Inveon GATE model efficiency curve and evaluation.....	35
Comparison of experimental and simulated moving particles.....	35
Chapter Four Results and Discussion	37
1. Evaluation of the Inveon	37
CL count in M-PEPT and in Inveon.....	37
Efficiency curve of the Inveon	37
2. Evaluation of GATE simulated Inveon.....	40
Sources definition in GATE	40
Inveon efficiency curve.....	54
3. Evaluation of the standard deviation in reconstructed positions.....	54
4. GATE simulation of moving point source.	59
Trajectory alignment and movement.....	59
Evaluation of the standard deviation in the reconstructed position	67
Evaluation of the standard deviation in the reconstructed position in x and y direction.....	70
Chapter Five Conclusions, and Future work	84
1. Conclusions	84
2. Future Work.....	85
Chapter Six Additional Contribution To M-PEPT development	86
1. Feature Point Identification Method Evaluation	86
2. Movement of several particles in GATE (General Movement)	86
3. Activated Yeast Simulation	87
4. Funding.....	89
List of References	94

Appendix	97
Appendix 1: Design drawings of the phantom support	98
Appendix 2: Mac file for the definition of the source	99
Appendix 3: Inveon header file	100
Appendix 4: Standard deviation distribution for the three velocities tested and at the different repetitions.	101
Appendix 5: GateFileCreator	104
Appendix 6: Examples of Mac files	109
Appendix 7: Example of placement file (for Yeast simulation).....	110
Appendix 8: Comparison between definition of movements	111
Vita	112

LIST OF TABLES

Table 3.1. Dimensions of additional elements in Inveon Model (Lee et al, 2013)	29
Table 3.2. Parameters used in the GATE digitizer of the Inveon	33
Table 3.3. Prescribed initial position and velocity used in GATE simulations	36
Table 4.1. Efficiency of the Inveon as function of the energy window	41
Table 4.2. CL count for the six models of source definition	46
Table 4.3. Results obtained at different time slice prescribed in GATE simulation. 5 ms time slice is used for GATE Simulations of moving sources.	55
Table 4.4. Comparison of simulated and experimental CL available for detection.	66
Table 4.5. Average slope and average Intercept and their standard deviations for experimental and simulated data sets (velocity = 0.18 cm/s, x = 0, y = 0, Energy Window 425 – 625 keV)	68
Table 4.6. Experimental and simulated intercepts for a particle moving at 0.18 cm/s along the z axis of the detection bore.	69
Table 4.7. Average position for the x and y at different velocities and different location inside the Inveon's FOV	73

LIST OF FIGURES

Figure 2.1. Typical positron energy distribution.....	4
Figure 2.2. Graphic scheme of the positron annihilation process	5
Figure 2.3. Scheme of the definition of Coincident Line and Acceptance Angle in a PET scanner (Saha, 2016).....	7
Figure 2.4. Graphical representation of the possible accidental CL that can be detected in a PET scanner.....	8
Figure 2.5. Inveon picture with dimensions	10
Figure 2.6. Scheme of a multi-wire chamber.....	12
Figure 2.7. Evolution of the algorithm proposed by Wiggins et al (Wiggins et al., 2016).	14
Figure 2.8. Average measured uncertainty for FPI M-PEPT method as function of the axial direction in each spatial directions for a elastic circular pipe (Patel et al., 2017).	16
Figure 2.9. GATE architecture scheme (S. Jan, 2014)	18
Figure 2.10. GATE information flow	20
Figure 3.1. Transmission scan of the cubic source and the support phantom	22
Figure 3.2. Picture of the cubic support monted on the support phantom.....	23
Figure 3.3. Image of the cubic source placed at the center of the FOV	26
Figure 3.4. Visualization of Inveon model in GATE (Lee et al., 2013).....	30
Figure 3.5. Scehematic representation of the input file organization for GATE simulation	31
Figure 4.1. Comparison between CL count in inveon log file and M-PEPT's CL count	38
Figure 4.2. CL count at different time windows and at different locations inside the FOV.....	39
Figure 4.3. CL count comparison between simulated and experimental setups. The source defintion used is back to back gamma emission plus positron emission.....	42
Figure 4.4. Comparison in CL representation for a simulated and experimental point source at center FOV. Back to back gamma emission plus positron emission source defintion.	43
Figure 4.5. CL detection sites distribution along the z direction for experimental and simulated particle located at the center of the FOV and at 25 mm away from the center in the z direction.....	45
Figure 4.6. Comparison of the CL distance distribution, relative to the center of the particle, for the three model of source defintinon in GATE.....	47
Figure 4.7. Comparison of experimental and simulated CL in the region 30 to 35 mm in the z direction	48
Figure 4.8. Detectio sites distribution along z for a particle located at the center of the FOV and 25 mm away in the z direction.	50

Figure 4.9. Comparison of the Experimental and simulated CL representation inside a box of 5X5X5 mm around the center of the FOV.....	51
Figure 4.10. CL plot and CL distance distribution for a point source modeled with the positron emission model but without the presence of the phantom support	53
Figure 4.11. Experimental and simulated CL count rate as function of the energy window used in the Inveon setup	56
Figure 4.12. Experimental CL count comparison to Simulated CL count as function of the axial position along the center line of the FOV. 425 – 625 keV positron emission source.	57
Figure 4.13. Comparison of the prescribed position in GATE and measured position for the simulated static data	58
Figure 4.14. Comparison of the variation of the standard deviation in the detection of a static particle at different locations along the z direction	60
Figure 4.15. Overlapping of experimental and simulated trajectories reconstructed by M-PEPT.	61
Figure 4.16. Overlapping of experimental and simulated trajectory in a 3D plot. The velocity of the particle is 0.18 cm/s (Energy window 425 – 625)	62
Figure 4.17. CL 3D representation at z = -50 mm and at the center (z = 0 mm) of the FOV for a moving particle. The velocity is 0.18 cm/s (Energy window 425 – 625 keV).....	64
Figure 4.18. Comparison of the CL count available for detection for a particle moving at 0.18 cm/s (Energy window 425 – 625 keV).....	65
Figure 4.19. Variation in the standard deviation along the z directions for different velocities.	71
Figure 4.20. Frontal and lateral view of the FOV of the Inveon when a particle is moving at 0.18 cm/s	72
Figure 4.21. Variation in experimental and simulated standard deviation along the z direction for x and y positions	74
Figure 4.22. Variation CL count as function of position super imposed on position reconstruction as function of position for a particle moving at 0.18cm/s.....	75
Figure 4.23. Close up of the CL count vs time superimposed to position reconstruction vs time	76
Figure 4.24. Detection site distribution for experimental and simulated results ..	78
Figure 4.25. Standard deviation comparison for different grid size. Particle moving at 0.18 cm/s.	79
Figure 4.26. Standard deviation comparison for different grid size. Particle moving at 0.22 cm/s.	80
Figure 4.27. Standard deviation comparison for different grid size. Particle moving at 0.45 cm/s.	81
Figure 4.28. Comparison frame by frame of the CL representation of a particle moving inside the FOV	82

Figure 6.1. Comparison of the CL count available for detection for a particle moving at 0.18 cm/s without the phantom support. (Energy window 425 – 625 keV).....	88
Figure 6.2. Superimposition of the particles detected in M-PEPT and their trajectories prescribed in GATE for a simulation of 20 F-18 particles of 50 Bq each. Only 17 particles are detected.....	90
Figure 6.3. Comparison of the prescribed position in GATE and the detected particles in M-PEPT.....	91
Figure 6.4. Absolute difference of the values prescribed for position in GATE and those detected with M-PEPT. The difference in the time mark of detection is also included.	92
Figure A.1. Standard deviation comparison for 0.18 cm/s.....	101
Figure A.2. Standard deviation comparison for 0.22 cm/s.....	102
Figure A.3. Standard deviation comparison for 0.45 cm/s.....	103

CHAPTER ONE

INTRODUCTION

Positron Emission Particle Tracking (PEPT) is a concept presented by Shaw in 1978 in a US patent (Shaw, 1978). Shaw proposed using positron emitting particles in flowing blood inside a coincidence camera to reconstruct the trajectory followed by those particles. The location of the particle is identified as where several Coincidence Lines (CL) nearly intersect. A CL is the line formed by two coincident gammas emitted from the positron-electron annihilation.

Shaw's idea was later used to implement an algorithm to detect a single positron emitting particle using a gamma camera set up for coincidence detection (Parker et al., 1993). The algorithm determines the location of the particle as the point in space where the sum of the distances to CL nearby is minimum. With this algorithm, Parker was able to reconstruct the trajectory of a particle moving within a granular media inside a rotating drum (Parker et al., 1993).

Bickell et al uses a Positron Emission Tomography scanner to track a radiotracer using a different method (Bickell et al., 2012). His method divides the FOV into a 3D grid, and counts how many CL intersect each grid volume, referred to here as a voxel. The location of the particle is taken as the centroid of a Gaussian curve fitted in the grid with highest CL count (Bickell et al., 2012). This method is able to find more than one radiotracer at a time provided that the number of particles is previously known.

The use of a grid with scalar counts of CL intersections as introduced by Bickell is later treated using a clustering technique to locate regions in the grid corresponding to particles (Wiggins et al, 2016). The location of the particle is identified as the centroid of the cluster generated by applying the G-Means technique to the 3D grid data (Wiggins et al., 2016). This technique is able to identify several particles at the time without knowing the number of tracers in advance. For this reason, this technique is known as Multiple-Positron Emission Particle Tracking (M-PEPT).

M-PEPT was further improved using the Feature Point Identification (FPI) method to locate the particle (Wiggins et al., 2017). In FPI, the field of view of the PET scanner is divided into a 3D grid and a CL count is performed in each grid volume. Then the data are conditioned using the FPI method adapted from imaging processing to locate point sources.

Both version of M-PEPT have been tested for several point sources in motion as well as for point sources in stationary position (Wiggins et al., 2017). Additionally, M-PEPT has been used to measure the features of flow in a rectangular cross-section channel with obstructions (Langford et al., 2016), and in pulsatile flow (Patel et al., 2017). In the work developed by Langford et al, a comparison of the

information retrieved by M-PEPT with the information provided by High Speed Video (HSV) is performed. This comparison shows good agreement between the two measurements. However, since the two measurements were not simultaneous, and the flow patterns are complicated, the actual precision of individual trajectory measurement is not fully known. Prescribed position or trajectory typical of a particle in flow is required in order to further understand M-PEPT performance.

In this research point source motion is physically achieved by using the bed motion control of the Inveon. The Inveon is a PET scanner designed for rats and mice, and contains 25,600 Lutetium Orthosilicate (LSO) crystal detectors. A Na22 point source of 10 μ Ci activity is moved to specific locations inside the FOV, and also traverses the scanner bore at three specific velocities. Tracer locations and trajectories are then reconstructed by providing the scanner data to M-PEPT.

Additionally, Geant4 Application for Tomographic Emission (GATE) is introduced as a tool to simulate the PET scanner response to radiotracers moving inside the scanner field of view (FOV). GATE is a Monte Carlo software that is able to simulate the response of different scanners (Sarrut and et al., 2014). In this research, a published GATE model of the Inveon validated for tomography is used for simulations of point source detection (Lee et al., 2013).

This research tests GATE as a simulation tool for the Inveon in the M-PEPT application. The aim is to validate GATE for M-PEPT measurement so that GATE simulation can be used as a surrogate to the scanner. Combination of GATE simulation with Computer Fluid Dynamics (CFD) simulation is envisioned where particle trajectories predicted by the CFD simulation are provided to the GATE simulation to produce synthetic scanner data. Those data may then be provided to M-PEPT to reproduce the prescribed trajectories. This allows an examination of the goodness of the M-PEPT measurement for the specific application, and may offer an efficient approach to testing M-PEPT improvements.

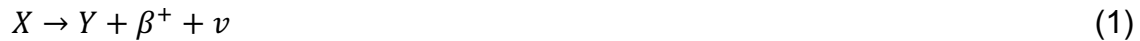
The combination of CFD and GATE and M-PEPT is also useful to define activity of the tracers and to identify scanner settings and M-PEPT settings best suited to a measurement challenge.

CHAPTER TWO

LITERATURE REVIEW

1. Positron Emission Tomography General Review

Positron Emission Tomography (PET) generates a 3D image (i.e., tomograph) of positron emitter activity inside a scanner Field of View (FOV). Positron emitters are isotopes that have a proton excess in their nucleus. This excess makes these atoms unstable. In order to achieve stability, these isotopes release positrons in a process described by (Turner, 2007).



The total energy released in the decay from X to Y is shared by the positron, β^+ , and the emitted neutrino, ν . The positrons emitted have a distribution of energy similar to that presented in Figure 2.1.

The total energy that the positron can have is given by the equation (2)

$$Q_\beta = \Delta_P - \Delta_D - 2m_e c^2 \quad (2)$$

Where Δ_P is the mass excess of the parent, Δ_D is the mass excess of the daughter, m_e is the mass of electron at rest and c is the speed of light.

The energy that a positron carries out determines how far it can travel inside a medium before it annihilates. The annihilation of a positron occurs when it interacts with an electron present in the medium. First a positron – electron complex is formed, similar to a hydrogen atom, then they annihilate and release two gamma rays (Phelps, 2006). These gamma rays each have energy of 511 keV, and are emitted in opposite directions. This process is explained graphically in Figure 2.2. If the two gammas are detected by two different sensors, the line that joins these two sensors, a Coincidence Line, passes near the location of the source. This feature is used in PET scanners to define an image of the activity distribution (Phelps, 2006).

The detection of the annihilation photon in a PET scanner occurs in a scintillator material. The annihilation photon deposits its energy inside the scintillator in the form of a photoelectric effect or a Compton scattering. Both process leave an excited atom inside the scintillator that emits a new photon when it decays to its base state. Scintillator material in the form of crystals are common in PET scanners such as Bismuth Germinate Oxide (BGO), Lutetium Orthosilicate (LSO), and Thallium doped-Sodium Iodide NaI(Tl) (Saha, 2016).

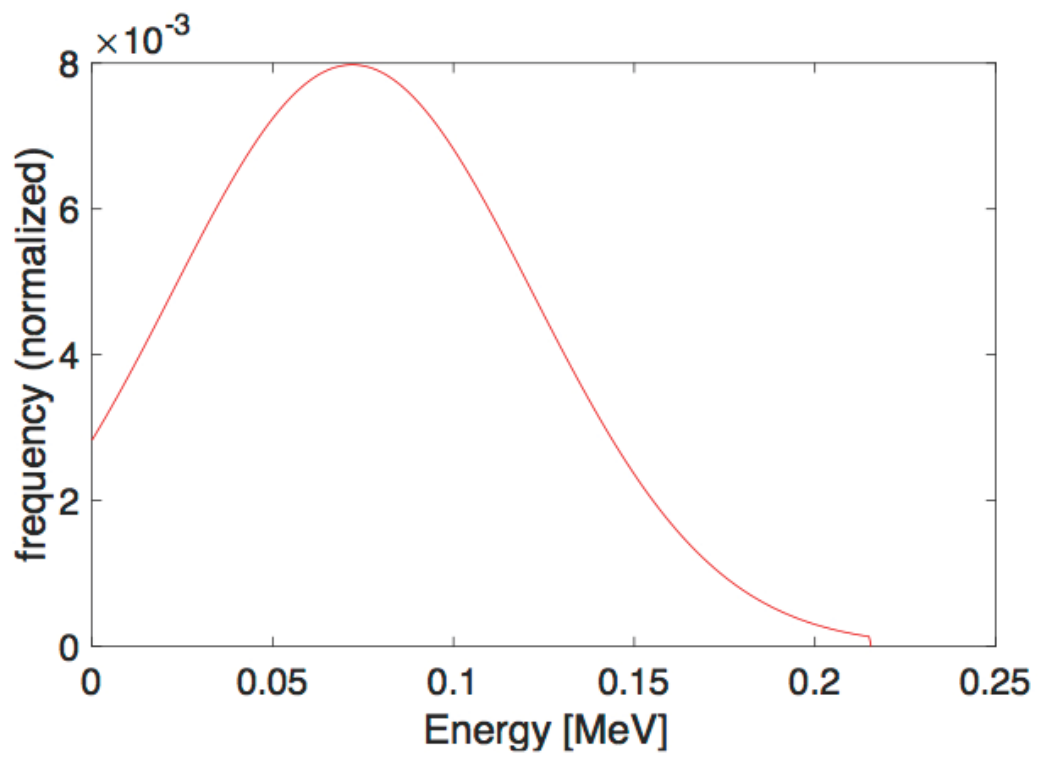


Figure 2.1. Typical positron energy distribution

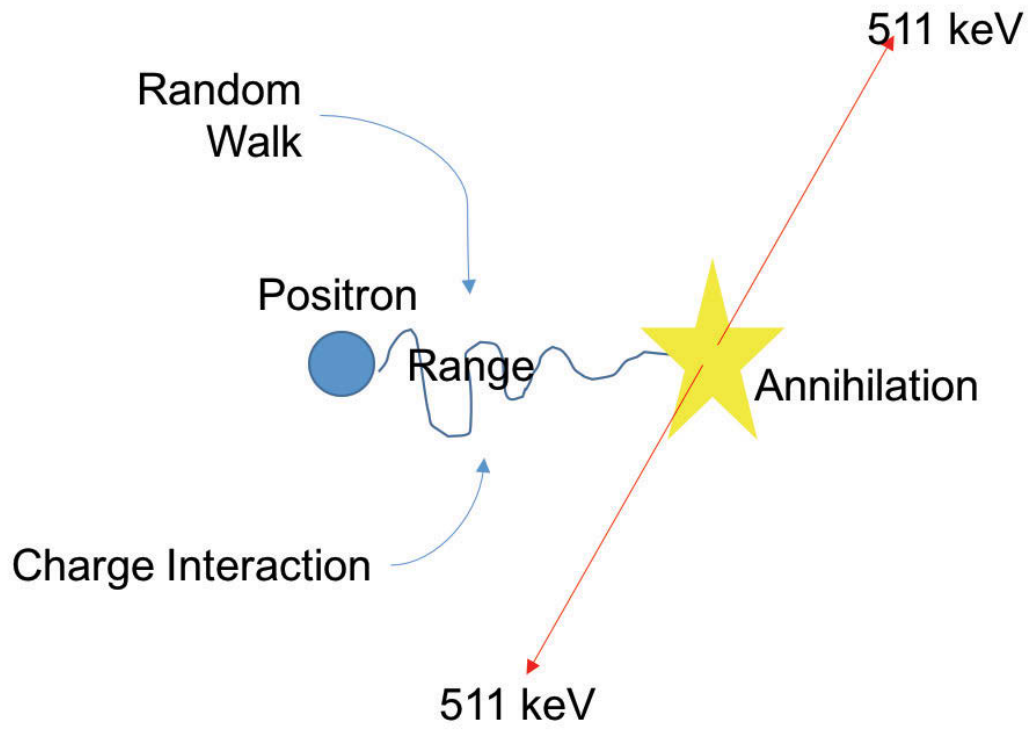


Figure 2.2. Graphic scheme of the positron annihilation process

The crystal detectors are often arranged in blocks that form a ring as shown in Figure 2.3A. Each block of detectors points to the center of the scanner, and they are connected to Photo Multiplier Tubes (PMT) that translate the de-excitation photon into an electric pulse. When photons are detected at two locations during a short time interval (coincidence window), a coincidence line is defined. An example of coincidence lines (CL) is presented in Figure 2.3A (Saha, 2016).

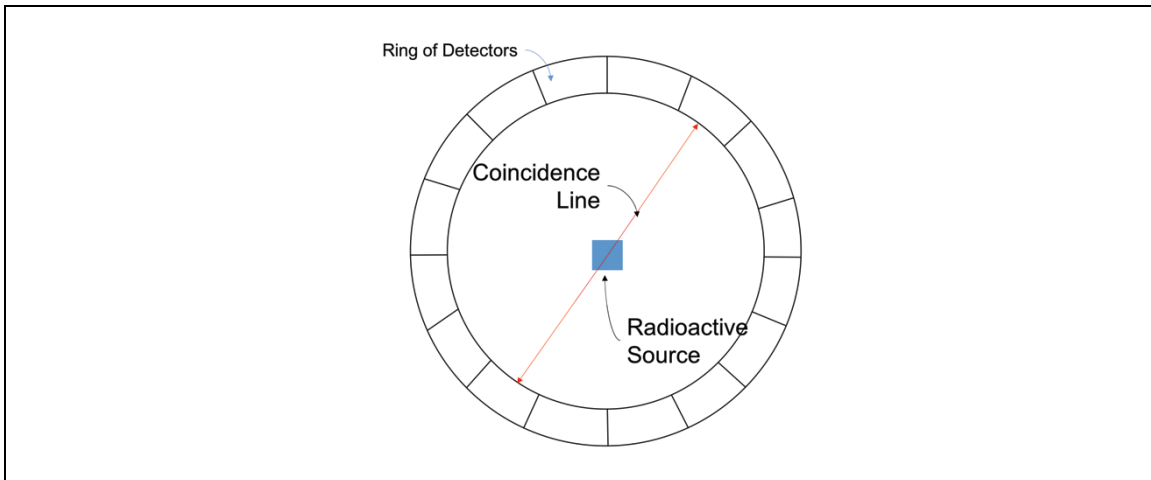
The number of lines that are able to be produced is limited by the acceptance angle of the detector. Figure 2.3B presents a graphic example of such angle. This angle can be customized by the user within pre-defined limits. A large acceptance angle increases the field of view of each crystal, but may also reduce tomographic resolution (Saha, 2016).

The line that lies between two crystals is called Line of Response (LOR). The number of LOR is determined by the number of crystals and the acceptance angle (Phelps, 2006). When the detection of two annihilation photons occurs along a LOR, a Coincidence Line (CL) is recorded that corresponds to one of the available LOR. The acquisition software uses the CLs to recreate an image.

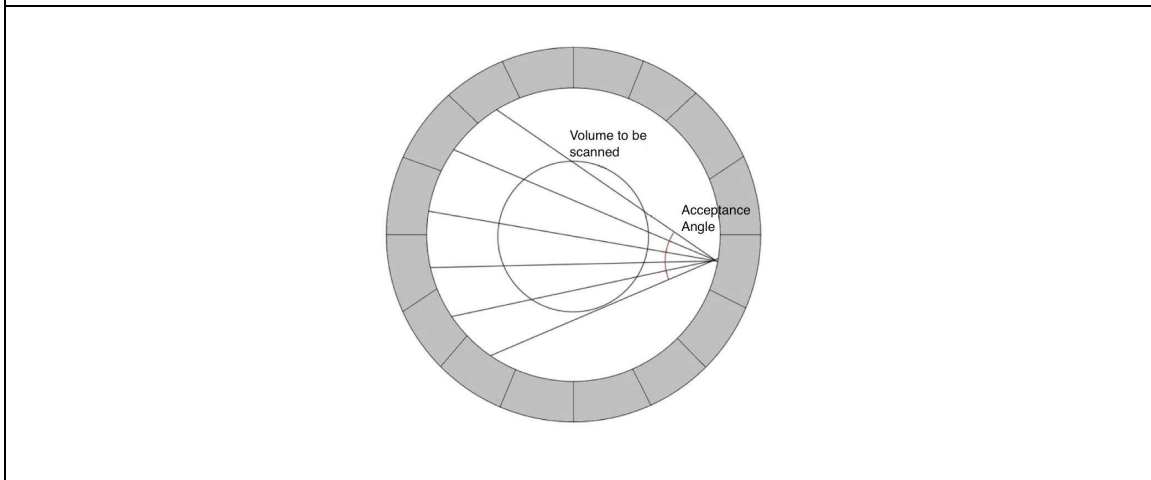
A CL detection begins with photon production at two crystal detectors, followed by PMT response, energy discrimination and a circuit that counts two single detections as a coincidence event (or CL) when they are registered inside a coincidence time window (Phelps, 2006), (Saha, 2016). There is a processing time to this process, and within this time, any detections in that detector block will not be registered by the machine. This time is known as dead time, and it affects the number of CLs that can be counted per unit time. An additional factor that contributes to the dead time is the time elapsed in the decay of the excited atom in the detector material. This time is called the scintillation decay time (Phelps, 2006).

There are some physical processes, like time of flight, scintillation decay time, and scatter inside the medium that make coincident detections less than perfectly coincident. The coincidence window is around 3 to 4 ns for the Inveon PET scanner with LSO crystals.

Accidental CLs are also created during a scan. These are events that do not necessarily correspond to the detection of two annihilation photons from the same positron emission. Among the origins of these CLs are: a) Scattered coincidence photons, b) random coincidences and c) multiple coincidences (Phelps, 2006). Figure 2.4 shows examples of these accidental CL. The random and multiple coincidences produce untrue CL, and occur more often when the count rate is high.



A) Ring of detectors of a PET scanner and a CL line



B) Acceptance angle in a PET scanner

Figure 2.3. Scheme of the definition of Coincident Line and Acceptance Angle in a PET scanner (Saha, 2016)

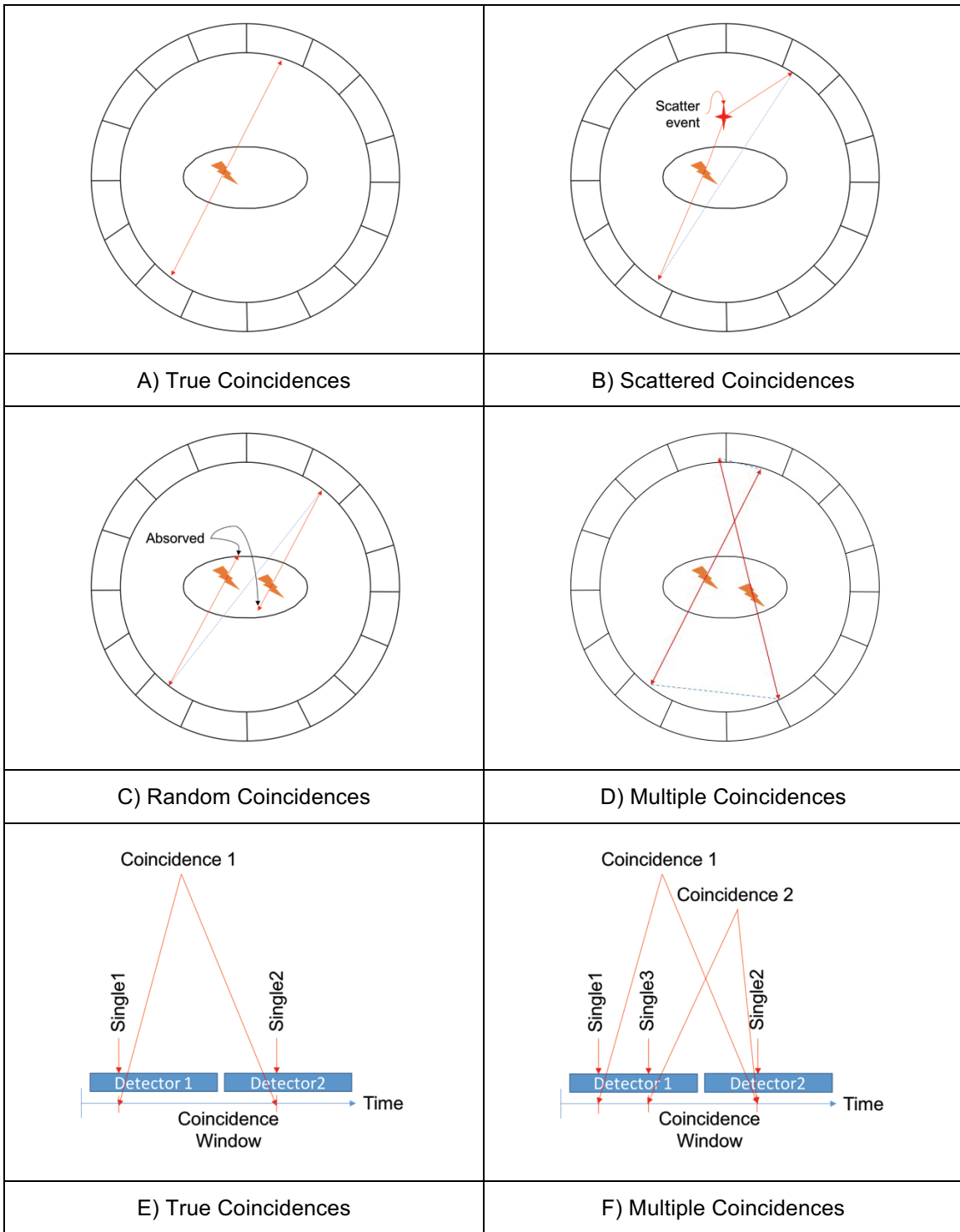


Figure 2.4. Graphical representation of the possible accidental CL that can be detected in a PET scanner.

2. Inveon PET Scanner

The Inveon is a PET scanner produced by Siemens to image small animals. For this reason, its dimensions allow it to be much more portable than scanners designed for humans. This feature makes it very valuable for research groups with small space available. Figure 2.5 shows a picture of the Inveon with dimensions.

The detector blocks are made of an array of 20×20 LSO crystals. Each crystal has dimensions 1.5×1.5×20 mm, with the 20 mm dimension oriented along the radius of the scanner bore. The arrays are placed in four rings, so they form eighty rows in the direction of the bed movement. Sixteen blocks comprise each Inveon detection ring, such that 25,600 crystals (4rings×16blocks×400crystals) surround the field of view. This scanner is capable of collecting near 3 million true CL per second (Siemens, 2011). Activity in the scanner bore is near 3 mCi to achieve 3 million true CL per second.

LSO crystals have a density of 7.4 gm/cm³, and a linear attenuation coefficient of 0.87 1/μm. The majority of annihilation photons interact inside the 20 mm maximum interaction range (Saha, 2016). This feature is complemented with a low scintillation decay time (40 ns) and medium relative light output (75% of NaI(Tl), or 29 photons per keV of photon energy). The last parameter measures the ability of the crystal to produce de-excitation photons per keV of annihilation photon absorbed.

The LSO crystals present the problem of the ¹⁷⁶Lu decay. This natural isotope of the lutetium decays via the emission of an electron of 88 keV, and by the emission of x rays at 400 keV (McIntosh et al., 2011). The presence of the x rays can create photon production inside the detector and random CL that can blur the image. This disadvantage can be controlled by defining a restricted energy window. The annihilation photons have an energy of 511 keV, but scatter and oblique detection may reduce this value. Therefore, the restricted energy window reduces the scanner efficiency slightly. For this dissertation, the energy window used is 425 to 625 keV, while the default setting is 350 to 625 keV.

The detector blocks with 400 crystals each are coupled to 64 channel Position Sensitive Photo Multiplier Tubes (PSPMT). The circuitry of this PSPMT identifies the position of interaction to the nearest crystal centroid. This feature provides to the Inveon a spatial resolution of 1.4 mm Full Width Half Maximum (FWHM) at the center of the field view (Siemens, 2011). The Full Width Half Maximum (FWHM) is defined using a known activity and a specially designed phantom (NEMA NU4, 2008).

The detection efficiency is measured as 6.14% at the center of the FOV using the



Figure 2.5. Inveon picture with dimensions

default energy window of 350-625 keV. This value is close to the 6.72% reported in (Bao et al., 2009). The detection efficiency is the CL count rate registered over the activity of the source. Some authors also call this parameter sensitivity, but this term is more related to the CL count to the concentration of the positron emitter inside the volume. The detection efficiency has a peak at the center of the Field of View (FOV), and decays near linearly as one moves to the edges of the field of view.

3. Positron Emission Particle Tracking

Positron Emission Particle Tracking (PEPT) is a technique that uses the back to back annihilation photons detected by a PET scanner to determine the location of the source particle. If a scan of a moving source particle is performed continuously, the trajectory of this particle can be reconstructed by dividing the scan data into time intervals, and using data from each interval to locate the particle in that time. This technique was proposed by Shaw in 1978 (Shaw, 1978). He proposed the detection of gallium hydroxide particles distributed inside the blood flow. This detection would be done in the region of the heart by high resolution high speed gamma detectors. He also suggested that these detectors might have been multi-wire proportional chambers coupled to a 1mm lead converter (Shaw, 1978). Proportional chambers are gas filled detectors that collect the energy deposited in their volume. An anode placed at the center of the chamber collects the electrons liberated inside the gas after an interaction. The energy deposited is proportional to the energy of the incident radiation (particle or photon). Multi-wire proportional chambers use the same principle, but have several anodes, so the detection is position sensitive (Prosper et al, 2003). An example of a multi-wire gas detector is presented in Figure 2.6.

Parker et al (Parker et al., 1993) took this idea and proposed an algorithm to detect one particle inside a gamma camera set up for coincidence detection (Parker et al., 1993). The algorithm estimates the location of a particle by finding a point in space that minimizes the sum of the perpendicular distance to the CL nearby. Particle tracking begins by dividing the scanner output into an array of time intervals. Particle locations are evaluated using CL in each time interval. The particle trajectory is constructed from the array of particle locations. This technique was able to find and track one particle, and it was applied to the study of flow features of particulate media inside a rotating drum (Parker et al., 1993). Since only one particle was located inside the FOV, it was assumed that each CL comes from the decay of this particle. Based on this premise, the uncertainty of particle location is inversely proportional to the square root of the CL count.

Bickell et al (Bickell et al., 2012) proposed a new algorithm based on the back to back projection method used to reconstruct images in PET. The method divides

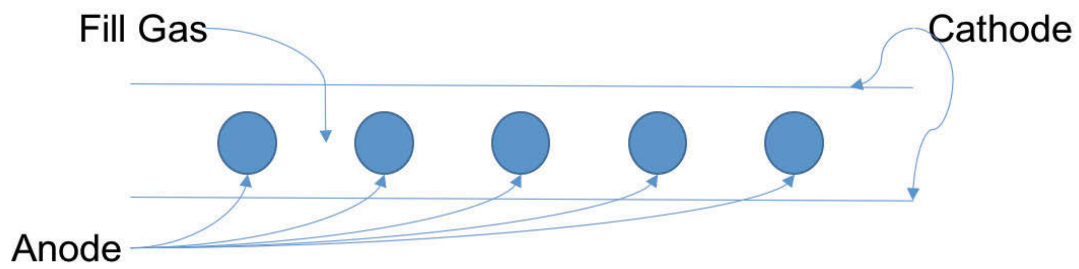


Figure 2.6. Scheme of a multi-wire chamber

the FOV into a 3D grid and then counts the number of CL that pass inside each box of the grid. The result of this step is a matrix that represents the CL distribution inside the FOV of the scanner. The box inside the grid with highest CL count is then used to fit a 3D Gaussian distribution of the count. The centroid of this Gaussian distribution is considered to be the location of the particle. Bickell consider the uncertainty of this method to be proportional to the Full Width Half Maximum of the distribution divided by the square root of the CL count. The algorithm was able to find more than one particle, but it was necessary to approximately know their locations in advance. This method was tested with several particles moving in circular paths (Bickell et al., 2012).

Wiggins et al use the same grid density concept, and combine it with the G-means clustering technique. The algorithm proposed by Wiggins divides the FOV into a 3D grid and counts the CL that pass through each volume. Then the grid element with maximum CL count is found. A fraction of this maximum count is subtracted from all the other members of the grid, and the boxes with a negative difference are set to zero. The fraction used is based on the particle activity and on the background count. The remaining data are grouped into clusters using a series of statistical tests (Wiggins et al., 2016). The centroid of these clusters are considered the location of the particle. The evolution of this algorithm is depicted in Figure 2.7.

The trajectories in Wiggin's work are found by matching two particles at different time frames that have a displacement less than a value d_{max} , which is equal to the time step times the maximum expected velocity of the particle. This process is done through the Munkres algorithm (Munkres, 1957), (Kuhn, 2005).

G-means technique has been tested with particles moving in known paths as well as particles moving inside flowing fluids. Wiggins et al first tested G-means with a set of particles moving inside a P4 PET scanner (Wiggins et al., 2016). Langford et al uses G-means to compare the fluid characteristics derived by M-PEPT and High Speed Video (HSV) techniques for flow in a rectangular channel. The measurements were not simultaneous, so time averaged flow parameters were used for data comparisons. The results of the measurements are very similar (Langford et al., 2016). However, specific parametric uncertainties in individual trajectories could not be established.

More recently, Wiggins et al (Wiggins et al., 2017) propose the feature point identification (FPI) approach to M-PEPT which is an adaptation of a widely used image processing method (I.F. Sbalzarini, 2005). The algorithm starts by dividing the FOV into a 3D grid and counting the CL that pass through each element. This grid is smoothed using a box-car average over a cubic region to precondition the data. The particle positions in FPI are estimated by finding the local maxima of the CL count in the smoothed grid. Two requirements are tested for a voxel to be

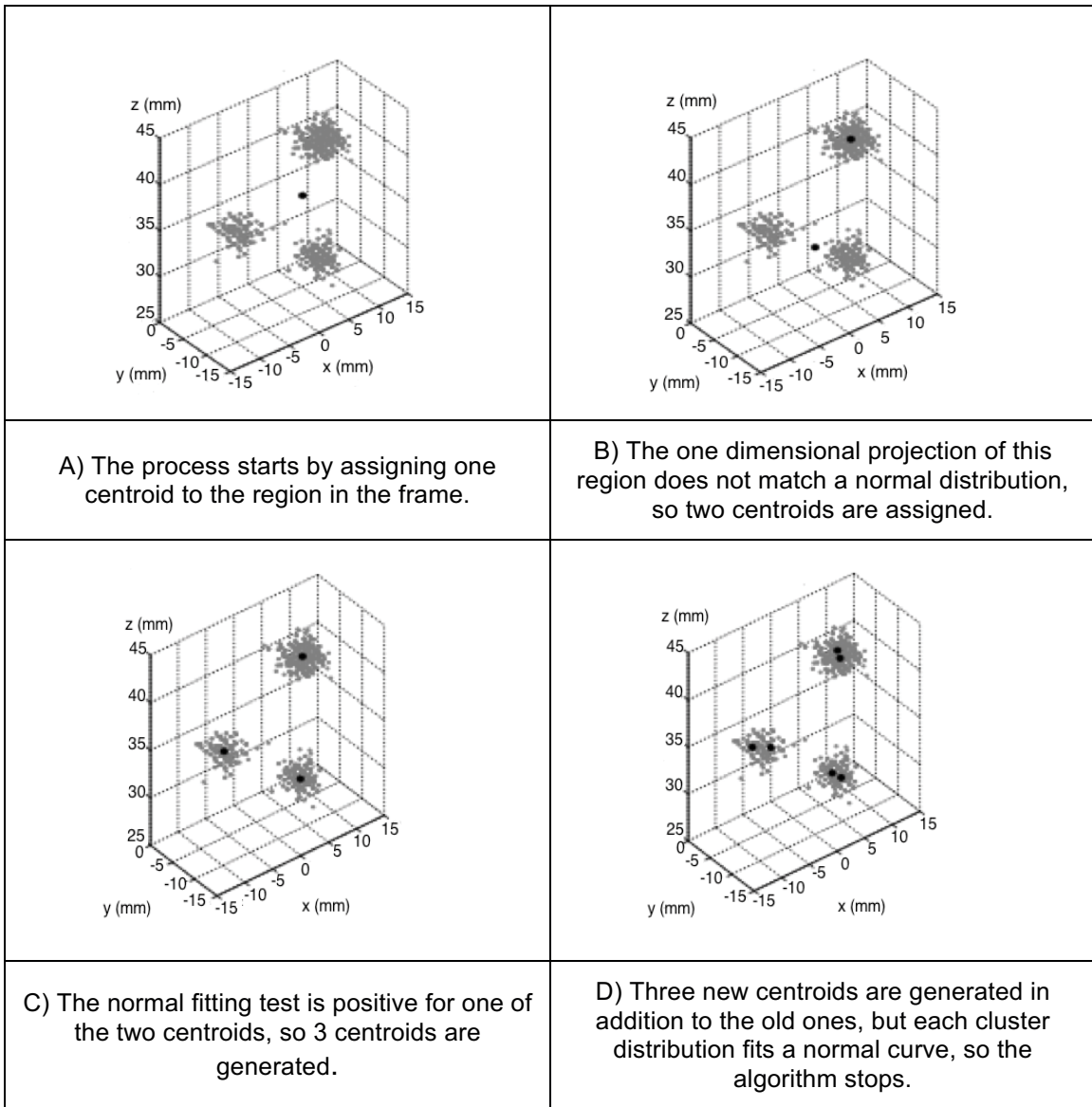


Figure 2.7. Evolution of the algorithm proposed by Wiggins et al (Wiggins et al., 2016).

used as a local maximum. First, the CL count is in the upper r^{th} percentile. The r^{th} value is based on the noise present in the data. Second, the CL count in the voxel must be greater than neighbors within a cube of $2w+1$ side. W , which is the length of the boxcar, can be set by the user. In case of a tie between two voxels within this cube, the principle first come/first served is used. So only the first voxel detected by the algorithm is considered.

The FPI method has been used to identify up to 100 stationary particles in the field of view, and up to 17 moving particles simultaneously inside the field of view. Wiggins et al (Wiggins et al., 2017) uses the GATE model of the Inveon to test the ability of the FPI and G-means methods to identify 100 particles placed on a sphere around the center of the FOV. While G-means was able to find only 13 of the particles, FPI identified all of them with position uncertainty less than 0.35 mm in the three directions. However, the GATE simulation was not validated for M-PEPT application and was known to overestimate the number of CL produced by the source. Wiggins normalizes results according to the number of CL (Wiggins et al., 2017) to accommodate this deficiency. The over estimation in CL is examined in this dissertation in the Results section.

Patel et al use the FPI method to study the properties of pulsatile flow in an elastic circular section pipe. M-PEPT using FPI was used to locate and link particles inside this fluid, and to derive the velocity field. They determine that the uncertainty in the location of the particles for the FPI method is inversely proportional to the number of CL available to locate the particle. The number of CL used for location correspond to those inside the neighborhood of length $2w+1$. The location precision therefore is best at the center of the field of view where scanner efficiency is highest, and the number of detected true CL are maximum, and degrades as the particle approaches the edges of the FOV where efficiency diminishes. Wiggins et al defines the uncertainty as the standard deviation of the mean of the particle data for the flow measurement, with several thousand particle trajectories present, with each trajectory including near 100 positions (Patel et al., 2017). Figure 2.8. shows the predicted uncertainty as a function of axial location in FOV.

4. Geant4 Application for Tomographic Emission (GATE)

Prior validation of the results provided by M-PEPT has been done mainly for experimental data. Further refinement of M-PEPT precision knowledge requires very precise source location control or measurement. A definite source location and trajectory can be generated in simulation and used in GATE to generate synthetic scanner data. The synthetic data can be used to generate M-PEPT results, and the predicted trajectories can be compared to the exact prescribed trajectories.

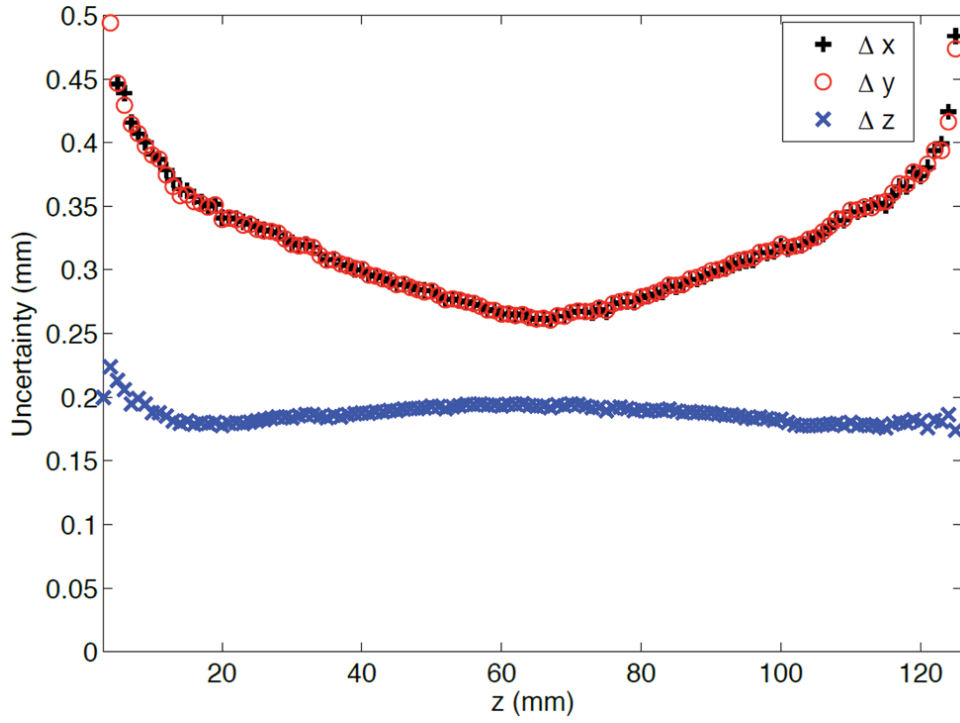


Figure 2.8. Average measured uncertainty for FPI M-PEPT method as function of the axial direction in each spatial directions for a elastic circular pipe (Patel et al., 2017).

The Geant4 part of GATE simulates the interaction of radioactive particles with matter through Monte-Carlo (Agostinelli et al., 2003). Each simulation must be coded in C++ and be compiled before it can be performed. This makes the use of Geant4 complicated for users without experience programming.

GATE is an application developed in Geant4 that is already compiled and ready to be used. It already includes all the modules required to simulate the interaction of electrons, positrons, alpha, gamma and x rays with matter. Moreover, it includes features that simulate some of the components of the electronic chain of PET scanners. GATE can be used without knowledge of C++.

GATE architecture comprises four layers of code. The first layer has the tools provided by Geant4 that will be useful in PET simulation. This tool includes the mechanisms that manage geometry, cross sections and other physical data. The second layer includes mechanisms proper to GATE like time management, radioactive decay and electronic chain simulation (Jan, 2004). The next layer comprises elements derived from the first two levels. The mechanisms of this layer are related to specific shapes and volumes as well as the movement of geometric forms and sources. The user layer is the last level. This includes the dedicated scripting that allows the user to control and perform the simulations through the macro language. This language is a series of commands that can be executed line by line in a dynamic window, or through an input file called macro file. Figure 2.9 summarize GATE architecture (S. Jan, 2014).

One of the most important features of GATE is its ability to simulate a time dependent process. This feature permits the simulation of decaying isotopes and moving sources. Since GEANT4 does not allow the movement of volumes, GATE splits the simulation into time slices. At each slice, all the volumes are considered at rest, so GEANT4 is able to compute the radiation interactions within all bodies in the system. Finally, GATE synchronizes all the volume positions with the activities of the sources, so the simulation can continue. When the time slices are small enough, based on the rate of change of the simulation, the results are very smooth and recreate the movement of volumes and sources (S. Jan, 2014).

5. GATE digitizer

GATE simulation of PET scanner electronic chain is done through the digitizer module. This module has some sub modules that mimic features of the real PET scanners like energy blurring, energy window, electronic noise, dead time and logic for the coincidence sorting. The digitizer takes GEANT4 output called hits and transforms them into singles. Then the digitizer produces coincidences out of the singles using a coincidence sorter module that mimics PET circuitry. The

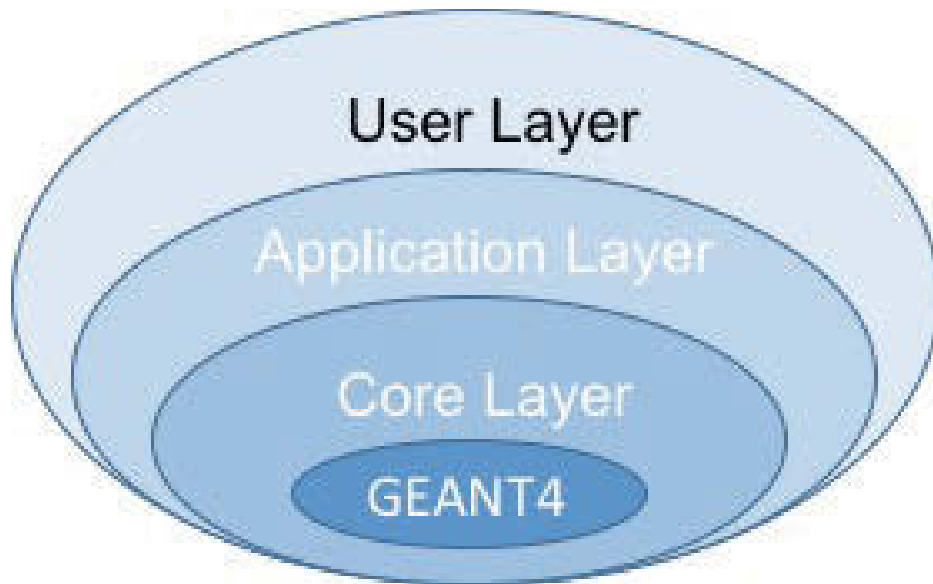


Figure 2.9. GATE architecture scheme (S. Jan, 2014)

complete process followed by GATE to produce coincidences is in Figure 2.10 (S. Jan, 2014). More details about GATE operation are provided in the Method and Material chapter of this dissertation.

6. Summary and Objectives

M-PEPT is a technique that uses the back to back photons produced after the annihilation of a positron emitted by a source in order to locate the position of the source. This positron emitting source may be incorporated in a fluid in order to derive information such as velocity and acceleration in the flow. M-PEPT has been used in different equipment and flow channels and is a technique that can be used in different fields from engineering to medicine.

In order to test M-PEPT abilities in a precise and flexible manner, a simulation tool is required. The source location and trajectory values are prescribed in a simulation and provided to GATE to generate synthetic scanner data. Synthetic scanner data are then provided to M-PEPT and the trajectories are reconstructed and compared to the prescribed trajectories. This improves the understanding of M-PEPT and streamlines further testing of the technique. This work evaluates the performance of GATE scanner simulation in comparison to real scanner data, and then applies simulated data and scanner data for stationary and moving point sources to the M-PEPT measurement. This dissertation offers an evaluation of GATE for M-PEPT applications.

In this dissertation a GATE model of an Inveon pre-clinical PET scanner is assessed with specific attention to attributes important to M-PEPT. A published GATE model of the Inveon that was validated for PET application is used for the simulations (Lee et al., 2013). The results of point source position and trajectory measurements generated in GATE simulation are processed with FPI M-PEPT and are compared to M-PEPT prediction using data from an actual Inveon with identical source position and movements. A ^{22}Na point source of 10 μCi , encapsulated, and held in a phantom to introduce some scattering, is used in the physical tests and in simulation. Direct comparisons of the GATE simulation and physical scanner data are performed initially, followed by comparison of the M-PEPT reproduction of particle positions and movements created using simulated and real scanner data.

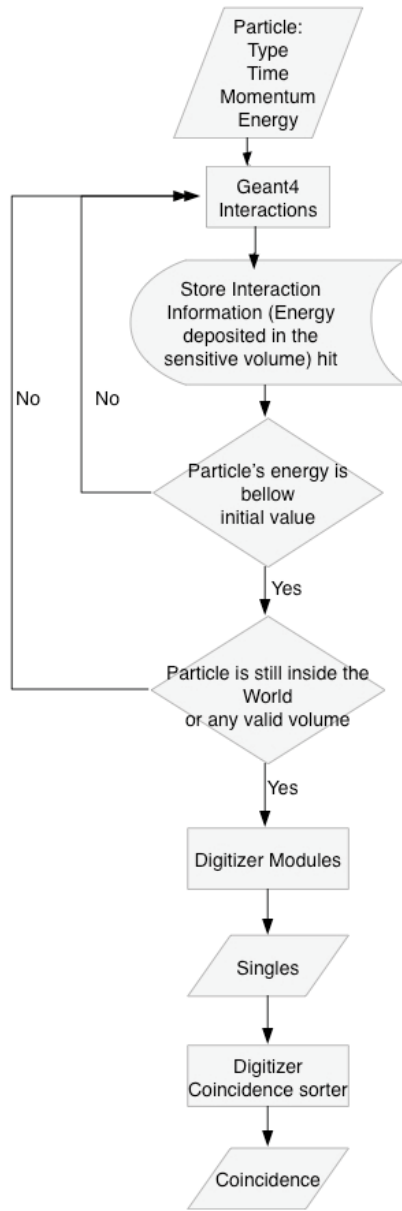


Figure 2.10. GATE information flow

CHAPTER THREE

MATERIALS AND METHODS

1. Evaluation of the Inveon PET scanner

General setup parameters used in Inveon

The experiments are performed in a Inveon dedicated PET (DPET) 120 scanner serial number 1036, property of the University of Tennessee, Knoxville. The control of the machine is done through a HP computer model Z829 serial number 10528959 with Windows XP. The software used for this purpose is the Inveon Acquisition Workstation 2 (IAW2) provided by Siemens. The energy window used for the experiments is 425 to 625 keV, unless otherwise indicated. The coincidence window set for the experiments is 3.438 ns.

The CL count (number of events) is registered through the default histogramming algorithm provided by IAW2. The histogram settings used correspond to the default values. The mode is set to emission, the delays are subtracted, the sinogram width is equal to 128, the span is 3 and the ring difference is 79. For the reconstruction algorithm all the default settings in the software are kept.

Point sources and phantom support

The point source used is provided by Spectrum Techniques, Inc. Oak Ridge, TN. The source is enclosed in a 12.5 mm HDPE cube that has a 2.38 mm hole drilled to a depth of 6.35 mm in the center of one side. Inside this hole, ^{22}Na radioactive material is placed forming a near 2 mm diameter sphere near the center of the cube. The hole is sealed using a method developed by the source provider, SpectrumTechniques, Inc., Oak Ridge TN.

In order to handle this source, a HDPE support half cylinder is fabricated. The drawing designs are in the Appendix 1. The radius of the half cylinder is 31.75 mm and the length is 139.7 mm. Over the flat face of this support, five square holes are machined to depth of 6.35 mm. The purpose of these holes is to handle the cubic source in a stable manner. Figure 3.1 provides a CT scan of the source placed in the center position on the support. A picture of the support is presented in Figure 3.2. The shape of this support is based on the phantom provided by the Siemens Molecular Imaging to perform the daily calibration of the scanner.

The location and the movement of the particles is managed by the Inveon bed motion control. This control moves the bed in the horizontal (z) and vertical (y) direction. Specific x and y coordinates can be input through the IAW with a precision of 0.1 mm. The movement of the bed can be coordinated with PET data acquisition to extend the effective field of view of the scanner by moving the subject (e.g., snake or lizard) through the scanner FOV. The user defines the

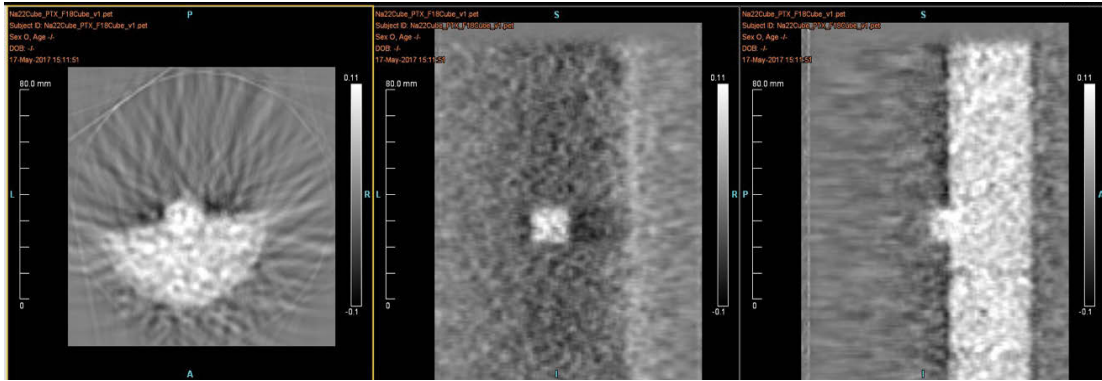


Figure 3.1. Transmission scan of the cubic source and the support phantom

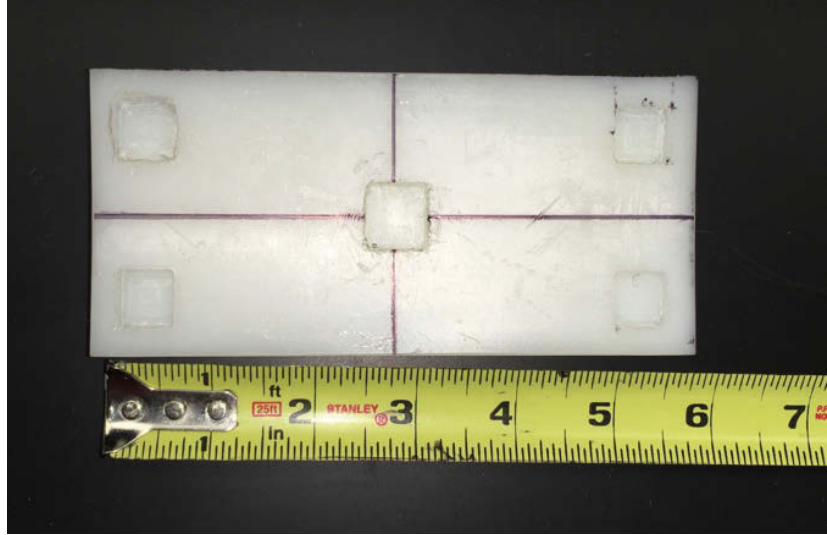


Figure 3.2. Picture of the cubic support mounted on the support phantom

time of the scan, the length of the volume to be scanned, and the number of times the volume will pass through the FOV. The combination of these parameters will determine a velocity for the bed motion. These parameters are specified by the user in the Acquisition protocol window. Once these parameters are set, the user defines the initial position of the volume. This is done for our experiments through the alignment of the front end of the support with the positioning laser on the Inveon. Once the support phantom is aligned, this point is considered the initial position for the experiment.

Multiple Positron Emission Particle Tracking (M-PEPT) code

The results provided by the Inveon and by GATE are processed by the multiple Positron Emission Particle Tracking (M-PEPT) software developed in the University of Tennessee, Knoxville. This software requires an input file that can be a list mode file for the scanner results or a text file for GATE results. The user is able to define which identification algorithm is to be used to detect the particle. Two options are available: G-means and FPI. The user also can define which linking algorithm to employ. The options are Munkres based nearest neighbor identification and Munkres with multi frame projection.

Other advanced options are available in M-PEPT:

- The maximum expected velocity at which the particle(s) is moving
- The maximum number of time steps allowed for linking
- The lower level discriminator for counts per time step
- The fraction of peak value used as particle intensity threshold
- The number of neighboring grid elements (voxels) for local maxima calculation, w

The identification algorithm used in M-PEPT is FPI. Munkres based nearest neighbor identification linking is used to reconstruct the trajectories. The grid size used is 1 mm. Different time steps are used in order to study the standard deviation of the results. The boxcar size used is set to the default value ($w=3$). The rest of the advanced features in M-PEPT are set to their default values.

The CL count provided by M-PEPT are compared with the results registered by the Inveon. For this purpose, a particle source is placed inside the scanner FOV, and a 10 second scan is performed. This process is performed in a series of positions along the scanner primary axis. The results written in the Inveon log file are registered. The list mode file obtained is processed with M-PEPT and the CL count provided by this software is also registered. Finally, M-PEPT and Inveon CL count results are compared.

Efficiency curve and evaluation of the Inveon

The efficiency is defined as the CL detected by the scanner divided by the product of the activity of the source times the branching ratio for positron particles. This concept of efficiency is similar to some definitions of sensitivity (Lu et al., 2013). However, the sensitivity can be 2 dimensional or 3 dimensional. In order to measure the efficiency variation along the z direction, the following protocol, based on (Lu et al., 2013), is used.

1. A point source is placed in the center of FOV. This point is the origin of the z axis.
2. A 10 second scan is taken at this position
3. The source is moved 1 mm away from the origin and a new 10 second scan is taken.
4. The step 3 is repeated in the range -5 to 5 mm around the center of the FOV.
5. The source is moved in steps of 5 mm in the range 5 to 55 mm, and a 10 second scan is taken at each position.
6. The step 5 is repeated in the range -5 to -55 mm.

The location of the source at the center of the FOV is done through the bed motion control. The following procedure is followed:

1. Draw marks indicating the center of the source and of the support.
2. Align these marks with Inveon positioning laser.
3. Choose the option "Move to the center of FOV" on the touch screen.

The location of the source at the center of FOV is corroborated visually with the reconstructed image provided by the IAW. If the radioactive spot of the source coincides with the cross hair pointer in screen, the source is aligned at the center. Figure 3.3 shows an aligned source image reconstruction.

The same procedure is repeated for scanning times of 10, 30, and 60 seconds. These scans are performed the same day, so the activity of the source remains constant (^{22}Na decays 1% of its initial activity in 14.6 days). With this procedure the CL count per second is measured as function of position. With the source located at the center of the FOV three different energy windows are tested in order to check the change in the CL count. The energy windows used are: 400 – 650 keV, 375 – 675 keV, and 350 – 700 keV. Additionally, the standard 350 – 650 keV is also checked.

2. Moving Particle Experimental Setup

The cubic Na-22 source, 10 μCi strength is moved inside the Inveon bore at three different velocities. As mentioned before, these velocities are achieved by the combination of three parameters: scanning time, volume length and number of passes through the FOV. Each velocity is repeated six times. The velocities are nominally: 0.18 cm/s, 0.22 cm/s and 0.45 cm/s. The source is placed at the

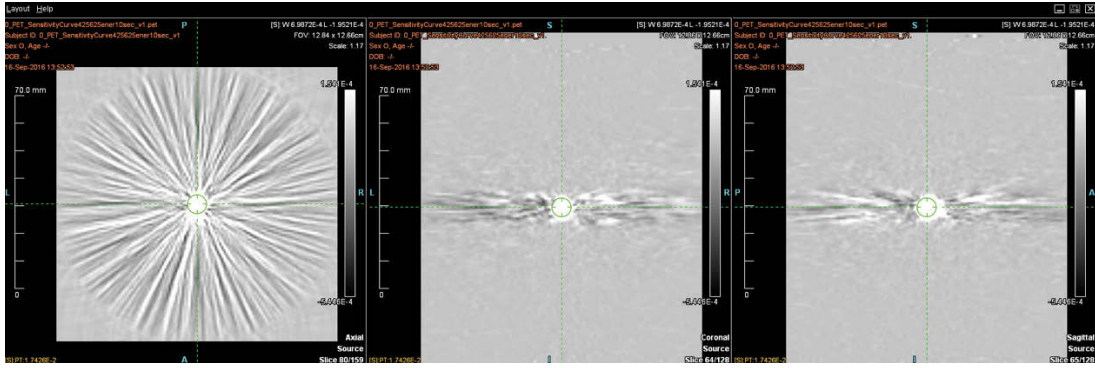


Figure 3.3. Image of the cubic source placed at the center of the FOV

center of the phantom showed in Figure 3.2 for each experiment. This plastic phantom is used to avoid any movement of the source while it is traversing inside the Inveon. The front end of the phantom is aligned with the laser and it is marked as the starting point for a continuous scan. The phantom and the source are not moved after each traverse.

3. GATE Model and Simulation Setup

Inveon GATE model

The model developed by Lee et al (Lee et al., 2013) is used to simulate the real Inveon in this work. The model is based in a Cylindrical PET system. In GATE a system is a template of predefined geometry that emulates a scanner, and it is required to produce and store the hit information that will generate the singles and the coincidences of the simulation. GATE Cylindrical PET system is meant to simulate most animal PET scanners. The system is contained in the world, which is the GATE term for the entire simulated domain. Transport simulation terminates at the end of the world. The world in Lee's model is a cube of 50 cm length. The Cylindrical PET system is comprised of 5 hierarchic levels:

- A) **World cylindrical PET:** is defined as a cylinder inside the world with non-zero inner radius. In the model of the Inveon, this level represents the inner space at which the detectors will be placed. The cylinder inner radius is 80.5 mm and the outer radius is 90.5 mm.
- B) **r sector:** Represents the block of detectors in the radial direction, which in the Inveon sum up to 16. In Lee's model the r sector corresponds to the structure called Head, which is a box of 20×31.8×127.8 mm.
- C) **Module:** Represents the block of detectors in the axial direction. There are 4 blocks in this direction in the Inveon. The dimensions in the model are: 20×32×32 mm.
- D) **Sub-module:** Not present in Lee's model.
- E) **Crystal:** Which represents the space at which the LSO detector will be placed. It must be inside the module. In Lee's model, crystal is a box of 1.59×1.59 mm called Crystal. This structure is repeated 400 times per module.
- F) **Layer:** This level is the LSO detector. In Lee's model this is a square of 1.59×1.59 mm called LSO. This structure is repeated 400 times per module.

In GATE only the elements attached to the sensitive detector are able to store hits. Hits represent the energy deposited in this element. GATE has two sensitive detectors: attachCrystalSD and attachPhantomSD. The first stores the information of the interactions occurring in the crystal detectors, and the second stores the information for interactions somewhere else inside the cylindrical PET

system. In Lee's model the LSO elements are attached to the detector attachCrystalSD.

Other elements that affect the scatter fraction of photons are present in Lee's model. The back end and front end Tungsten shielding is present in the model. The light guides that couple the crystals to the PSPMTs are modeled. The back compartments that contain the detectors and electronics are also modeled. In Table 3.1 the general dimensions of these elements are listed. Figure 3.4 shows an image of the GATE Inveon model developed by Lee, with the support and source used in these experiments added.

Lee's model is distributed through the internet freely. It consists of 3 basic macro files: `inveonDigitizersimple.mac`, which has the settings for the electronic chain simulation; `inveonPET.mac` that describes the Inveon geometry and defines the acquisition settings, and `physics.mac`, which activates the physical process used to simulate the interaction of the radioactive particles. There are other macro files describing several other phantoms and sources used in the medical imaging field, but that are not used in this work.

No major change is done to the model, however, the configuration of the macro files is changed in order to facilitate the debugging and the creation of several sources. Figure 3.5 shows the configuration of the macro files used in this work. Each block represents a macro file.

Brief descriptions of the files in the GATE model follow.

- a) Master1: Is the file that executes all the other macros. It defines the type of output to be used, and the starting and finishing acquisition times.
- b) Geometry: It defines the Inveon geometry.
- c) Volume inside the detector: It refers to the physical element that is inside the Inveon's FOV. In the case of the Inveon evaluation, this volume corresponds to a representation of the support phantom depicted in Figure 3.2. In other experiments it can be a cylinder of water or air that will contain the moving particles.
- d) Creation of particles: It defines the geometry of the volumes that will contain the sources in the experiments.
- e) Particle Velocities: It defines the velocities, or the type of movement that the particles will have. If the type of movement used is general, then this file will call the placement files, which have the position of the particles as a function of time.
- f) Particle initial position: It states the initial position of the particle that will be moved during the simulation.
- g) Physics: It defines the physical process that will simulate the radioactive particle interaction with matter. Detail of this file is in the next section.

Table 3.1. Dimensions of additional elements in Inveon Model (Lee et al, 2013)

Element	Shape	Dimensions
Tungsten shield	Cylinder	Rmax = 120 mm Rmin = 50 mm Height = 10 mm
Light guide	Box	XLenght = 10 mm YLength = 32 mm ZLength = 1 mm
Back compartment	Box	XLenght = 10 mm YLength = 1.59 mm ZLength = 1.59 mm

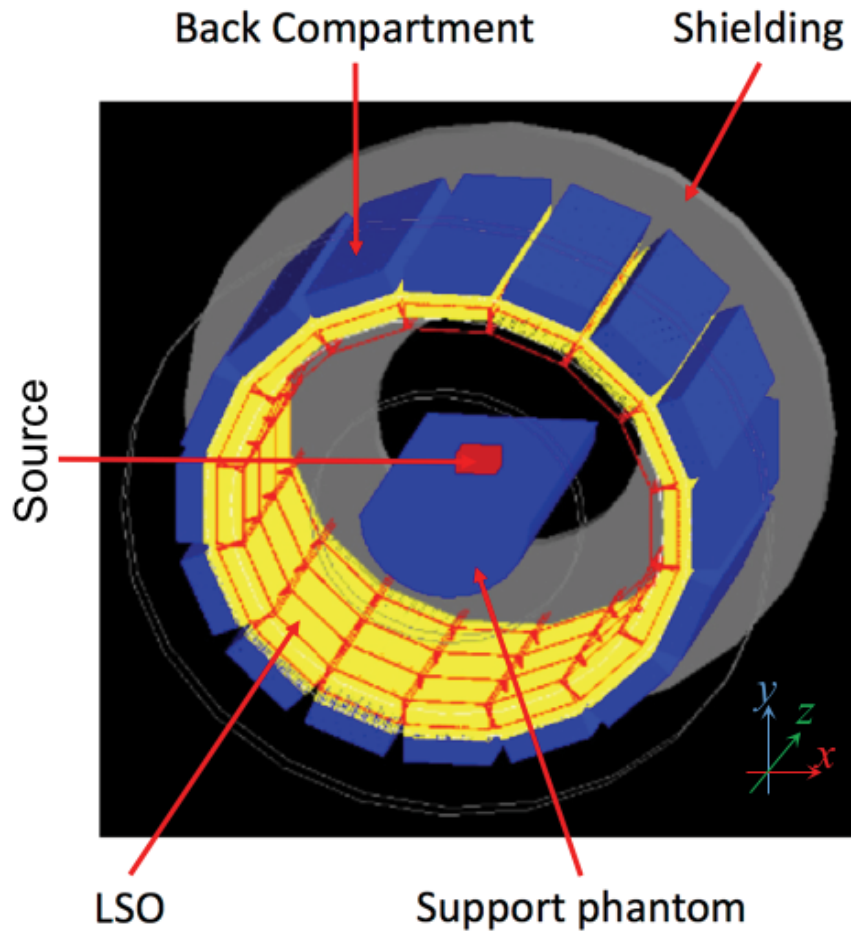


Figure 3.4. Visualization of Inveon model in GATE (Lee et al., 2013)

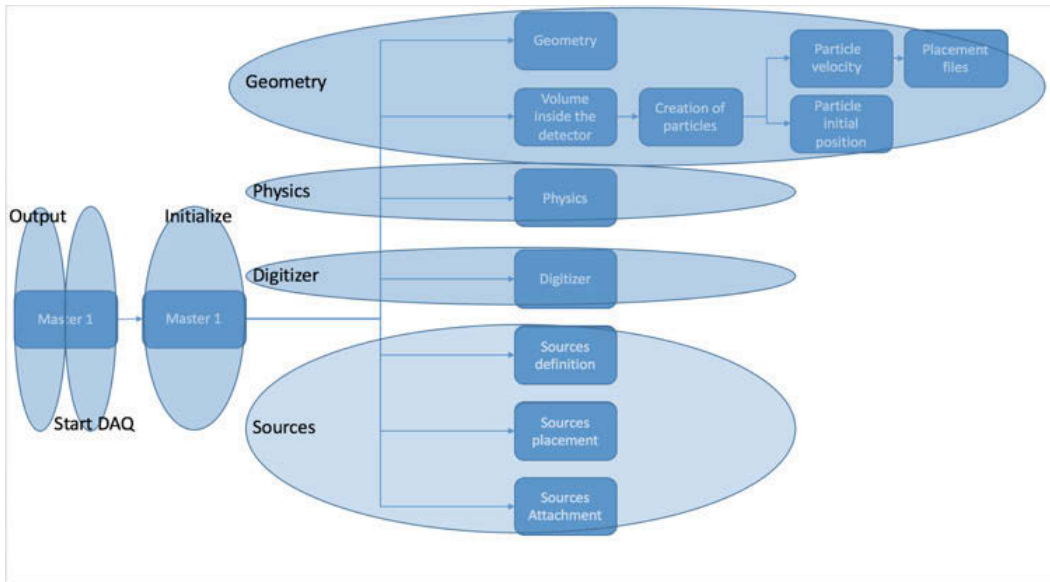


Figure 3.5. Schematic representation of the input file organization for GATE simulation

- h) Digitizer: It has the settings to simulate the electronic chain of the Inveon. The main features are listed in Table 3.2
- i) Sources definition: It defines the main characteristics of the source, like isotope, activity, half-life, positron energy, etc. More details on this file are in the next section.
- j) Source placement: It indicates the location of the source relative to the volume to be moved.
- k) Source attachment: It attaches the sources to the volume.

Source definition for static particle simulation

The definition of the source has the following elements: type of source, energy at which the emissions are released, the activity of the source and the half-life of the isotope, the angle of emission, and geometric shape.

The type of the source defines the way in which the isotope is modeled. When the source is defined as an ion source, GATE uses the GEANT4 data base to drive the decay and particle emission. The source can also be defined as gamma source emitting two back to back photons in all directions. In this case it is not important which isotope is being used and the user specifies that the gammas emitted are mono energetic with an energy equal to 511 keV. Another source definition option allows defining of the particle that is being emitted (positron or electron) and associated energy. Finally, GATE offers the definition of the source by using helper key words that includes several features of the emitter.

The energy at which the emissions are released indicates the kinetic energy of the subatomic particles released from the isotope nucleus. When the source definition is done through the helper key words, this feature is enabled. In all the other cases, the distribution of the emissions has to be specified. This specification can be done by using one of the built-in energy distributions available in GATE. In this research the mono-energetic (Mono) and the user defined histogram (UserSpectrum) are used.

The activity of the source is the number of decays per unit of time of the radioactive source. It can be expressed in Becquerel or Curie, and it has to be specified for all the source definition types. The half-life indicates the time at which the activity of the sample decays to half its initial value. It has to be specified only for the ion source definition.

The angle of emission indicates the direction at which the subatomic particles or photons are emitted. Two angles define this direction. Theta, which indicates the angles along the z axis, and phi which indicates the angles along the traverse direction (XY plane). For an isotropic source, theta has to be defined between 0° to 180° and phi has to be defined between 0° to 360°.

Table 3.2. Parameters used in the GATE digitizer of the Inveon

Parameter	Value
Blurring	0.146
Energy of reference	511 keV
Energy thresholder	425 keV
Energy upholder	625 keV
Dead time	7000000 ps
Type of dead time	paralyzable
Coincidence window	3.438 ns

The source can be shaped as point, surface, volume or beam. When the source is defined as point, it is dimensionless and it has to be placed in a single point inside the GATE coordinate system. If the source is a surface or a volume, it can be defined as sphere, ellipsoid, cylinder or parallelepiped. In this case the geometric center of the shape has to be placed in a single point inside GATE coordinate system. A beam source has a Gaussian shape. The centroid of the Gaussian has to be placed in single point inside the GATE coordinate system.

Four source definitions are investigated in this research to simulate a ^{22}Na source:

- 1) Particle emission + back to back emission
- 2) Back to back emission
- 3) Particle emission
- 4) Isotope Decay

A point source is considered in all four definitions. It is assumed that the source emits isotropically. The activity of the source used is $6.26 \mu\text{Ci}$ for the static particles and $7.66 \mu\text{Ci}$ for moving particles. These values have to be corrected with the branching ratio of Na-22, which is set equal to 0.898. Additionally, these activities correspond to the actual source activity corrected with time.

The performance of the source in the simulation is affected by the physics setup. The most important factor to be considered is the physics list to be used during the simulation. The physics list is a collection of models that reproduce the interaction of radioactive particles with matter. Geant4 offers a recommendation of physics list to be used. Two physics lists are considered for the source definition:

- 1) QGSP_BERT_EMV: This lists calls hadronic models and hadronic cross sections to simulate the particle interaction. This list is recommended for medical applications.
- 2) Emstandard_opt3: This list is required to simulate decaying isotopes.

Additional physical processes in the simulation are activated in Lee's model:

- A) Photoelectric
- B) Compton
- C) Raleigh Scattering
- D) Electron Ionisation
- E) Bremsstrahlung
- F) Positron annihilation
- G) Single scattering for electrons and positrons
- H) Radioactive decay, only for the sources

An example of the mac file used in the definition of the source is in the Appendix 2.

Inveon GATE model efficiency curve and evaluation

The experimental setup used to evaluate the efficiency of the actual Inveon is modeled in GATE. A semi cylinder of 31.75 mm radius represents the support phantom used to handle the sources. Plastic is the material selected from the data base used in this semi cylinder. Then, a plastic cube of 12.5 mm side is generated. A point source inside the cube is defined. This source is Na -22 of 10 μ Ci that emits positrons. This geometric system is the representation of cubic source package and the support phantom used in the actual experiments.

The same locations used in the experimental setup are prescribed in GATE. The source is placed at the center of the FOV and then moves 1mm in the range -5 to 5 mm around the center of the FOV. Movement increments are 5 mm outside the center region. At each location a 10 second scan is specified. The time slice used in GATE simulation is 5 ms. Independent simulations are performed for each location of the source.

Experimental and simulated data are processed with M-PEPT. The grid size used is 1 mm. Four time steps are used: 0.1, 0.5, 1.0 and 2.5 seconds in order to evaluate the standard deviation of the reconstructed location. The boxcar size used is the default value of 3 grid elements. The FPI method of identification is used.

For GATE simulation, a Dell workstation with 32 cores is used. This computer runs on UBUNTU 14.04, and GEANT 10.1.3 is preinstalled as requisite for running GATE 7.1. GATE's installation has OpenGL for visualization. The installation settings also have enabled the split features in order to use the full 32 cores of the WorkStation. The job splitting is done through the code gjs (included in GATE download). The multi-process is managed through HTC Condor.

Comparison of experimental and simulated moving particles

The geometric system previously defined is used in the moving particle simulated experiments. The system consists of a cube of 12.5 mm side centered in a semi cylinder of 31.75 mm radius. The velocity of the sources is defined by the results obtained from M-PEPT using experimental data. The initial positions are determined by overlapping the simulated results and experimental results. This procedure is done for three nominal velocities and repeated six times. Table 3.3 specifies the values prescribed in the simulation.

Table 3.3. Prescribed initial position and velocity used in GATE simulations

Nominal velocity	Prescribed initial position in GATE	Prescribed velocity in GATE
0.18 cm/s	-135.5 mm	0.179 cm/s
0.22 cm/s	-135.9 mm	0.225 cm/s
0.45 cm/s	-136.5 mm	0.461 cm/s

CHAPTER FOUR

RESULTS AND DISCUSSION

1. Evaluation of the Inveon

CL count in M-PEPT and in Inveon

Figure 4.1 shows the relationship between Inveon recorded and M-PEPT recorded CL count and the location of the particle along the z direction. Data are obtained by placing the source and taking a 10 second scan at each location. The grid used in M-PEPT is 1 mm and time step is 100 ms. The error is defined as:

$$\%Error = \frac{CLCount_{inveon} - CLCount_{M-PEPT}}{CLCount_{inveon}} \times 100 \quad (3)$$

$CLCount_{inveon}$ is the sum of histogrammed and unhistogrammed CL count registered by the software in the Inveon image header file, and $CLCount_{M-PEPT}$ is the total CL count recorded by the M-PEPT code. An example of the file produced in the Inveon is presented in Appendix 3.

The maximum error registered is 0.016% at the edges of the FOV. The very first and the very last 5 or so CL addresses recorded in a list mode file are not considered by M-PEPT, causing this small discrepancy in the recorded counts. The CL count not considered by M-PEPT is less than 10 for any position, but the total CL recorded are less near the edges of the FOV causing the percent error to be larger near the ends of the FOV.

Efficiency curve of the Inveon

Figure 4.2A shows the results for the CL count rate for different prescribed scan times. Figure 4.2B shows the efficiency as a function of position along the z direction. The energy window used is 425-625. As expected, the CL count rate does not change with the scan time defined in the Inveon. However, the Inveon does not necessarily perform the scan in the prescribed time. The Inveon scans for more time than is set up in the GUI. The actual time used in the scan is registered in the log file generated after histogramming. This effect is more common on small scan times.

The maximum efficiency of the Inveon for a 425-625 keV energy window is 5.22% at the center of the FOV. The efficiency decreases at the edges. This value is of the same order as other values reported (Bao et al., 2009). The Inveon efficiency at the center of the FOV for a 350 to 625 keV energy window is 6.14%. Efficiencies at other energy windows for the Inveon studied in this

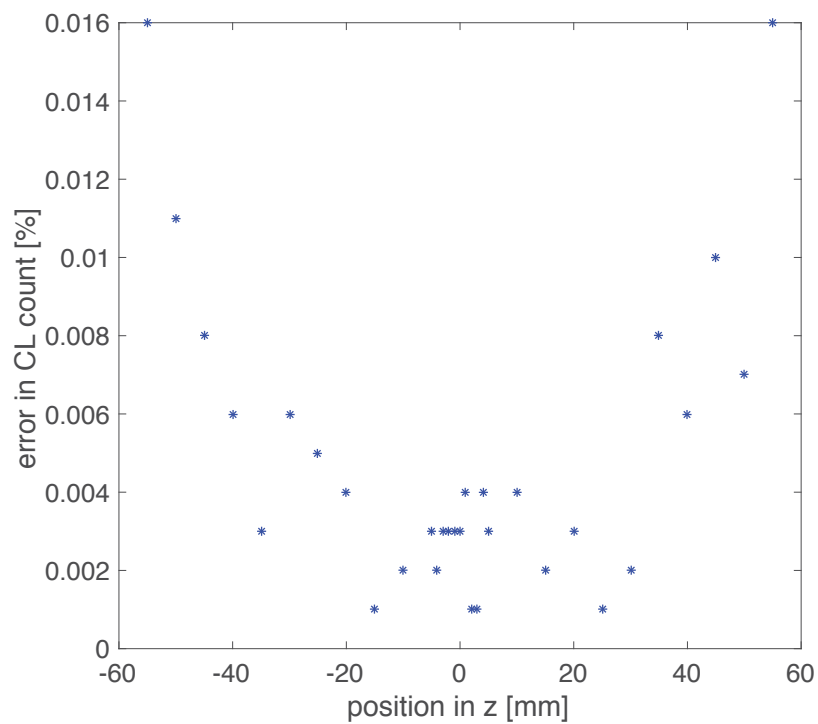
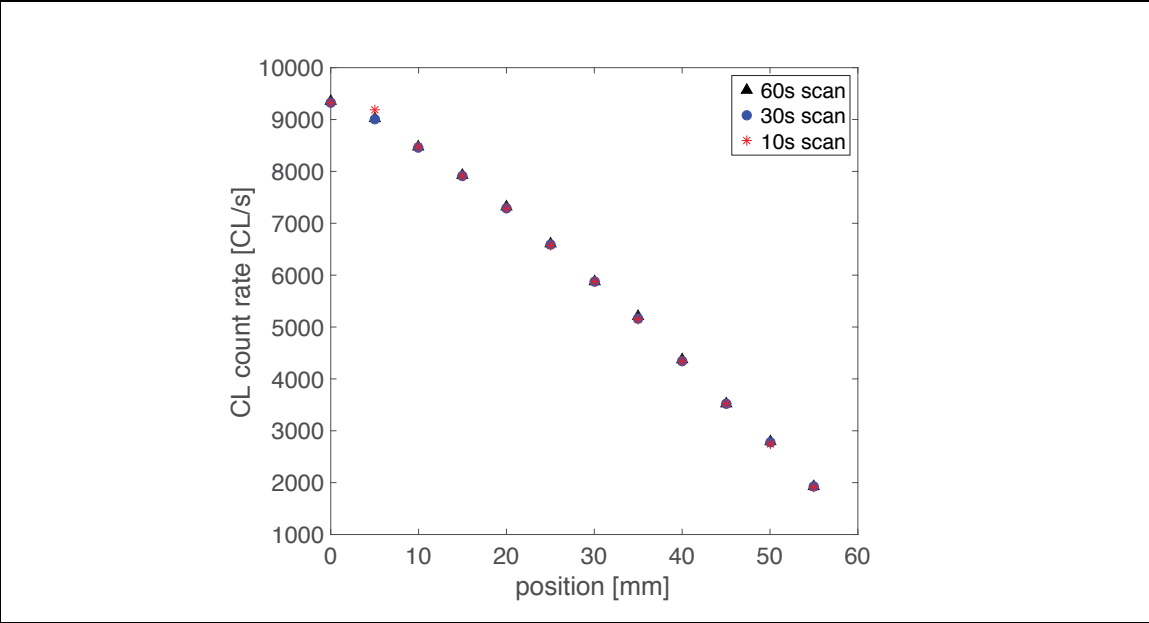
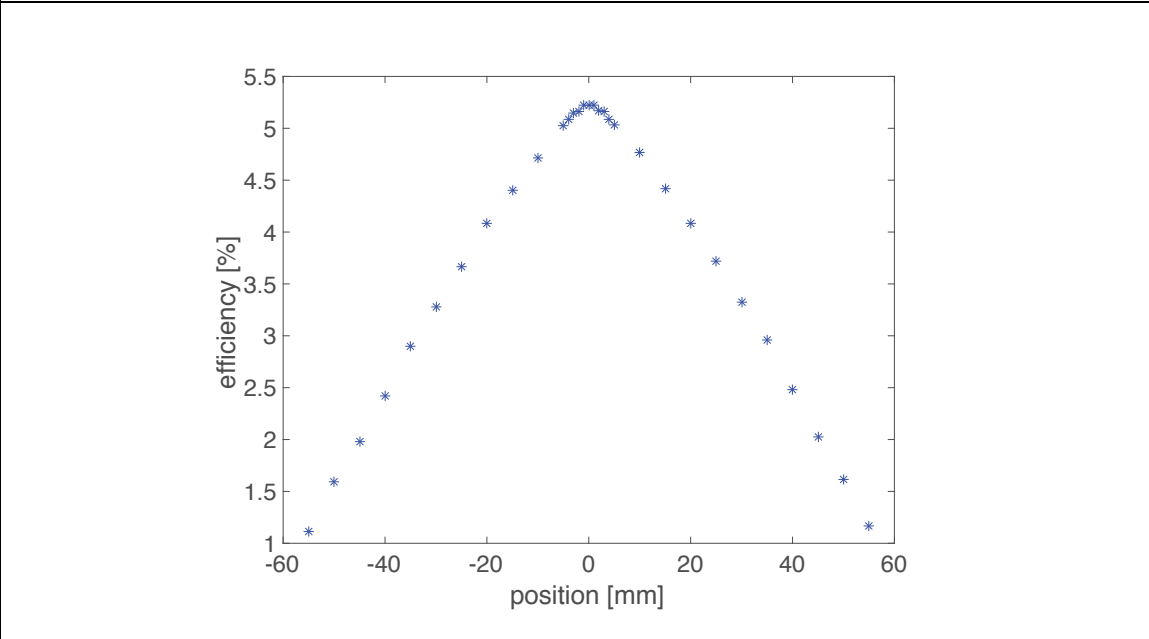


Figure 4.1. Comparison between CL count in inveon log file and M-PEPT's CL count



A) CL count at different time windows



B) CL count at different locations inside the FOV

Figure 4.2. CL count at different time windows and at different locations inside the FOV

dissertation are listed in Table 4.1. As one opens the energy window with center set to 525 keV, the efficiency also increases. However, the probability of scatter detection also increases. Additionally, an increase in the energy window facilitates the detection of background. This last factor is very important in the Inveon, since it has ^{176}Lu in the detector that decays naturally. At 425 625 keV most of the coincidences produced by ^{176}Lu decay are removed (McIntosh et al., 2011).

2. Evaluation of GATE simulated Inveon

Sources definition in GATE

In Chapter 3 GATE models to define the source were introduced. The specific use of these models is not deeply described in the literature available, and trial and error is necessary to find the best way to model the source in GATE.

The first model used is a combination of back to back gamma emission (B2B) plus positron decay. Even though the simulated CL count is three times as big as the experimental count, some results obtained with this model were published (Wiggins et al., 2017), with clear notation of the artifact previously mentioned and results were normalized by CL used per detection.

The first attempt to correct this discrepancy is to multiply the activity of the source prescribed in GATE times a scaler that yields CL count similar to the experimental count. In order to obtain this scaler, the experimental CL count at each location is divided by the simulated CL count. Then an averaging of these results in the region -40 to 40 mm is performed. The value obtained with this procedure is 0.3264. Figure 4.3 shows the results achieved with this scaler in comparison with the experimental results. The correction underestimated the CL count at the center of the FOV and overestimated the count at the edges. The error obtained with this correction is less than 40% in the range -40 to 40 mm.

Detailed comparison of the results at the CL detection level was conducted to understand differences. Figure 4.4 shows the simulated CL visualization vs experimental CL visualization. The simulated data, in red, correspond to the definition B2B +positron emission. The data in blue are the experimental CL detected by the Inveon. Plots correspond to the FOV as viewed from the entrance of the bore. Since the particle is located at the center of the FOV, the CLs should be drawn from the center to the edges of the bore. CLs that do not follow this pattern must correspond to scatter and false CLs. Figure 4.4 shows more scattered CL in the simulation than in the experimental results. Both data sets correspond to a 10 second scan of a particle located at the center of the FOV.

Table 4.1. Efficiency of the Inveon as function of the energy window

Energy Window	Efficiency [%]
425 – 625	4.97%
400 – 650	5.46%
375 – 675	5.98%
350 – 700	6.69%

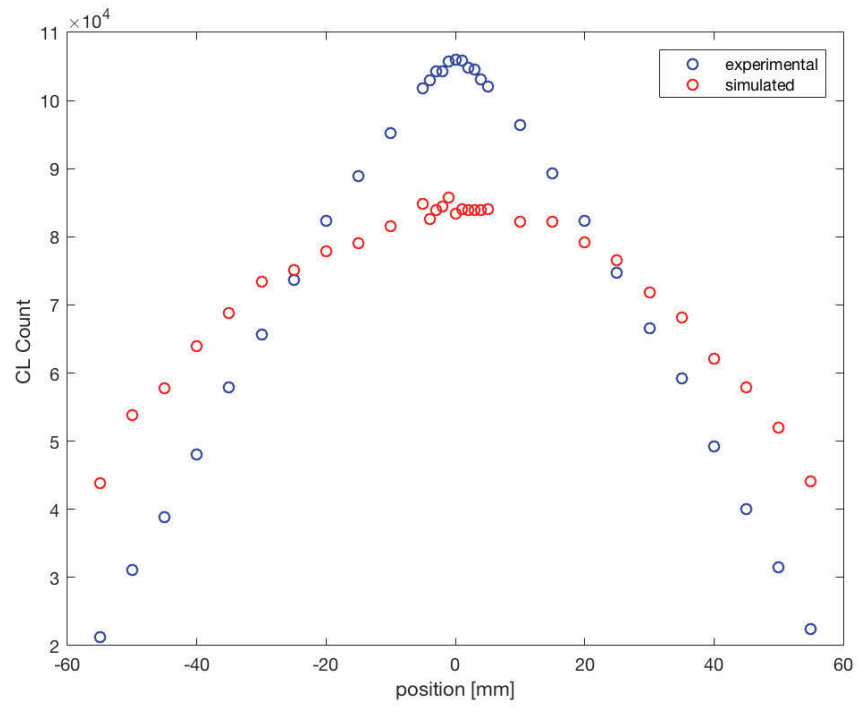


Figure 4.3. CL count comparison between simulated and experimental setups. The source definition used is back to back gamma emission plus positron emission.

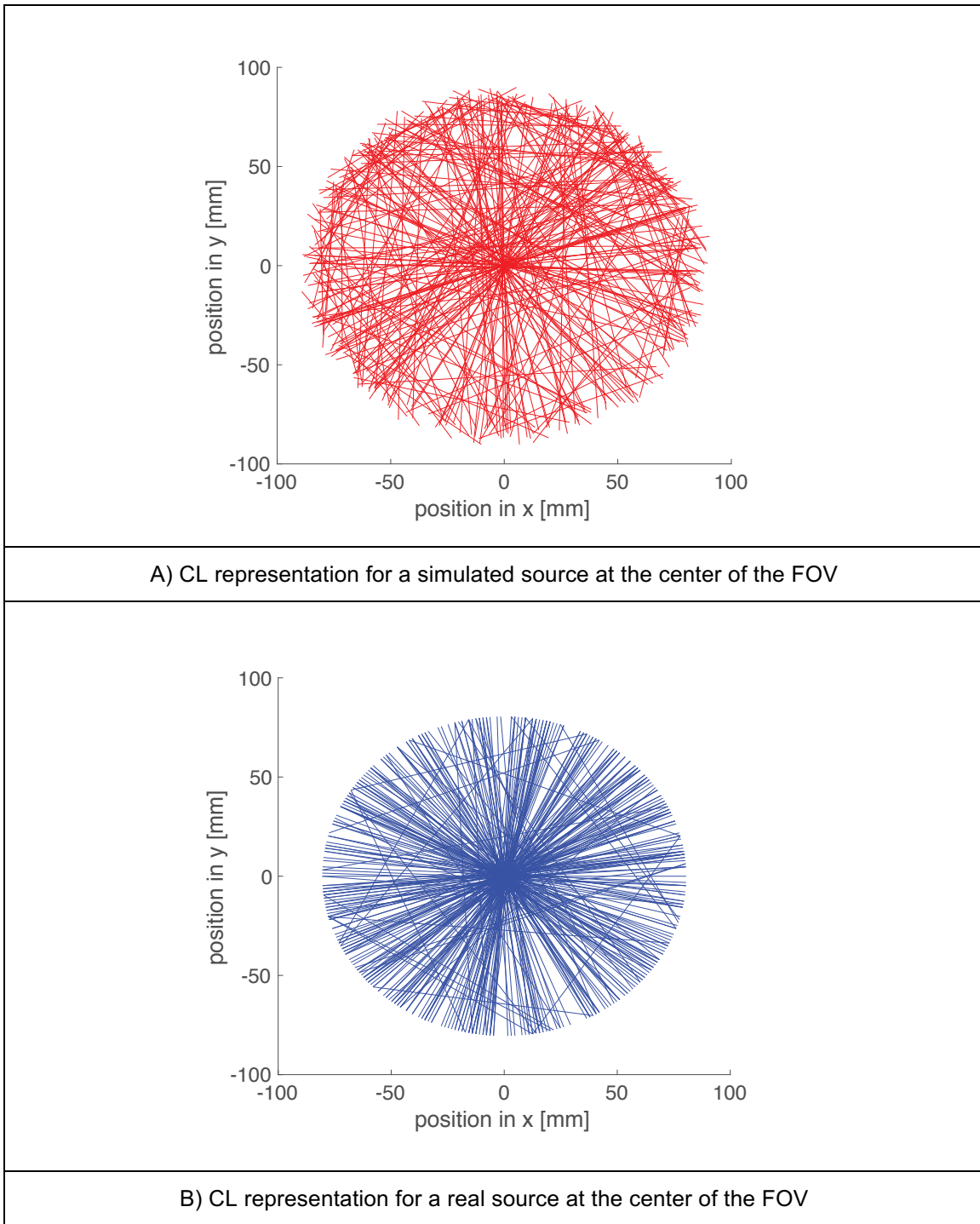


Figure 4.4. Comparison in CL representation for a simulated and experimental point source at center FOV. Back to back gamma emission plus positron emission source definition.

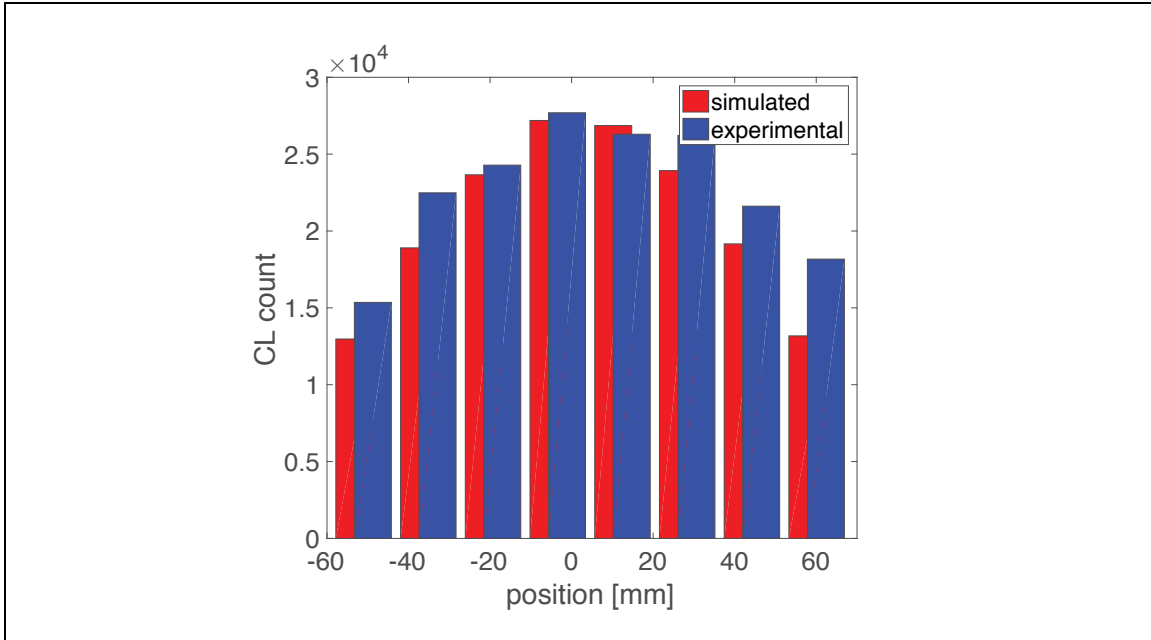
The scaler corrects the simulated CL count, but it does not change the rate of scattered CL creation. This creates a situation similar to that of a high background environment with scattered lines evenly distributed inside the FOV. The effect of this feature can be seen in Figure 4.5. Figure 4.5A shows the experimental and simulated distribution of detection sites along the z direction for a particle located at the center of the FOV. For this case both profiles are similar. However, in Figure 4.5B the detection positions are plotted for a point source located at z equal 25mm. In the case where the point source is located at z equal 25mm the detection location profiles are different. The experimental distribution is located nearer to the particle placed at z=25 mm. This discrepancy lead to the investigation of other ways to define the source.

After careful review of the GATE manual, six models of source definition are identified. Table 4.2 shows the simulated CL count generated for each of the six models. The best results are achieved when the QGSP_BERT_EMV physics list is used. Since the experimental CL count is about 109000, the model that best approaches this result is the Positron Particle + QGSP_BERT_EMV.

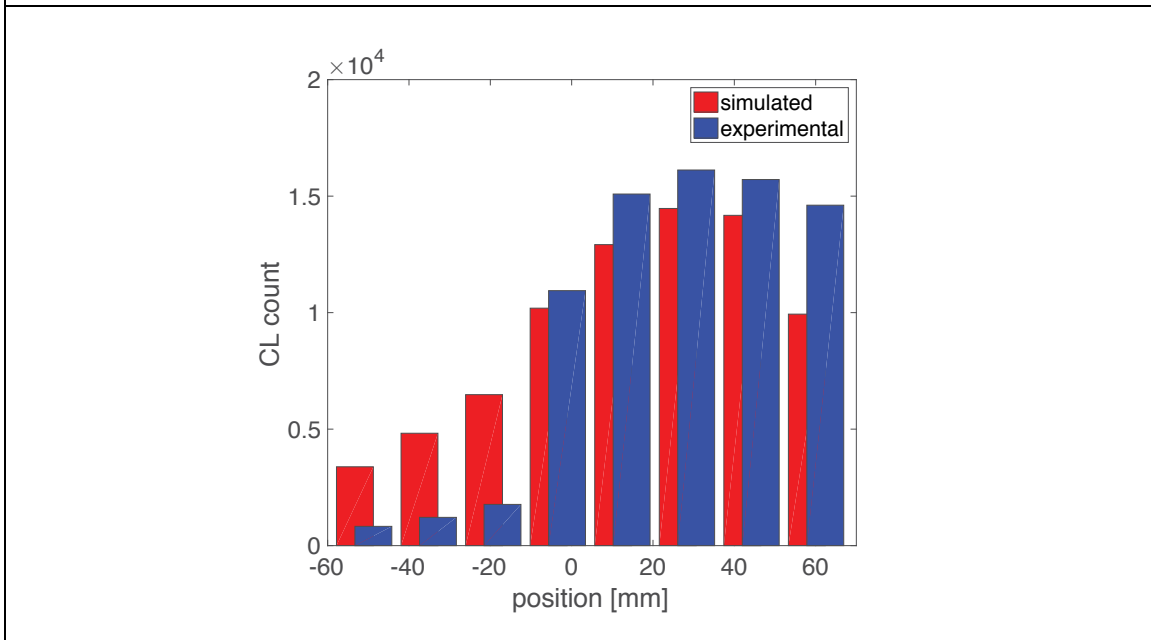
In order to evaluate the amount of scattered CL presented in each model, the distance of each CL to the center of the FOV where the source is located is calculated and the results are plotted. In all the simulations the particle is located at the center of the FOV, so the plots are also the distance of the CL to the center of the point source. Figure 4.6 shows the CL distribution relative to the center of the particle for the model B2B and Positron Particle + QGSP_BERT_EMV.

The experimental distribution shows that about 80% of the CL pass within a sphere of 5mm radius around the center. For the B2B model, this fraction is higher than 80%. In the B2B model the total count is also higher than the experimental count. The positron model, which has a CL count similar to the experimental, presents a fraction of less than 60%. This means that about 40% of the particles are scattered lines or the positron range is unusually large. This result however, is better for M-PEPT purposes, since it gives the code a conservative number of CL to detect and locate the particles. This means that if a particle is located in the simulation, it will be located more easily in the experiment. It is important to recall that M-PEPT uses only the CL that pass inside a region around the center of the particle. This region is defined by the boxcar, and typically exceeds the positron range, so most of the true CL should be captured in this cube. We note also that the small bore of the Inveon limits the impact of gamma non collinearity on detection location, such that the positron range is the primary contributor to uncertainty in true CL locations assuming perfect detection.

A complement to this analysis can be seen in Figure 4.7 which shows the



A) CL detection site distribution for a particle at the center of the FOV



B) CL detection site distribution for a particle at 25 mm away from the center of the FOV

Figure 4.5. CL detection sites distribution along the z direction for experimental and simulated particle located at the center of the FOV and at 25 mm away from the center in the z direction.

Table 4.2. CL count for the six models of source definition

Source Definition	Physics list Used	Simulation CL count (10 seconds)	Experimental CL count (10 seconds)
Bac2Back (B2B)	emstandard_opt3	296941	108883
Positron particle	emstandard_opt3	228786	
Isotope Decay	emstandard_opt3	25437	
Bac2Back (B2B)	QGSP_BERT_EMV	147024	
Positron particle	QGSP_BERT_EMV	112455	
Isotope Decay	QGSP_BERT_EMV	No run	

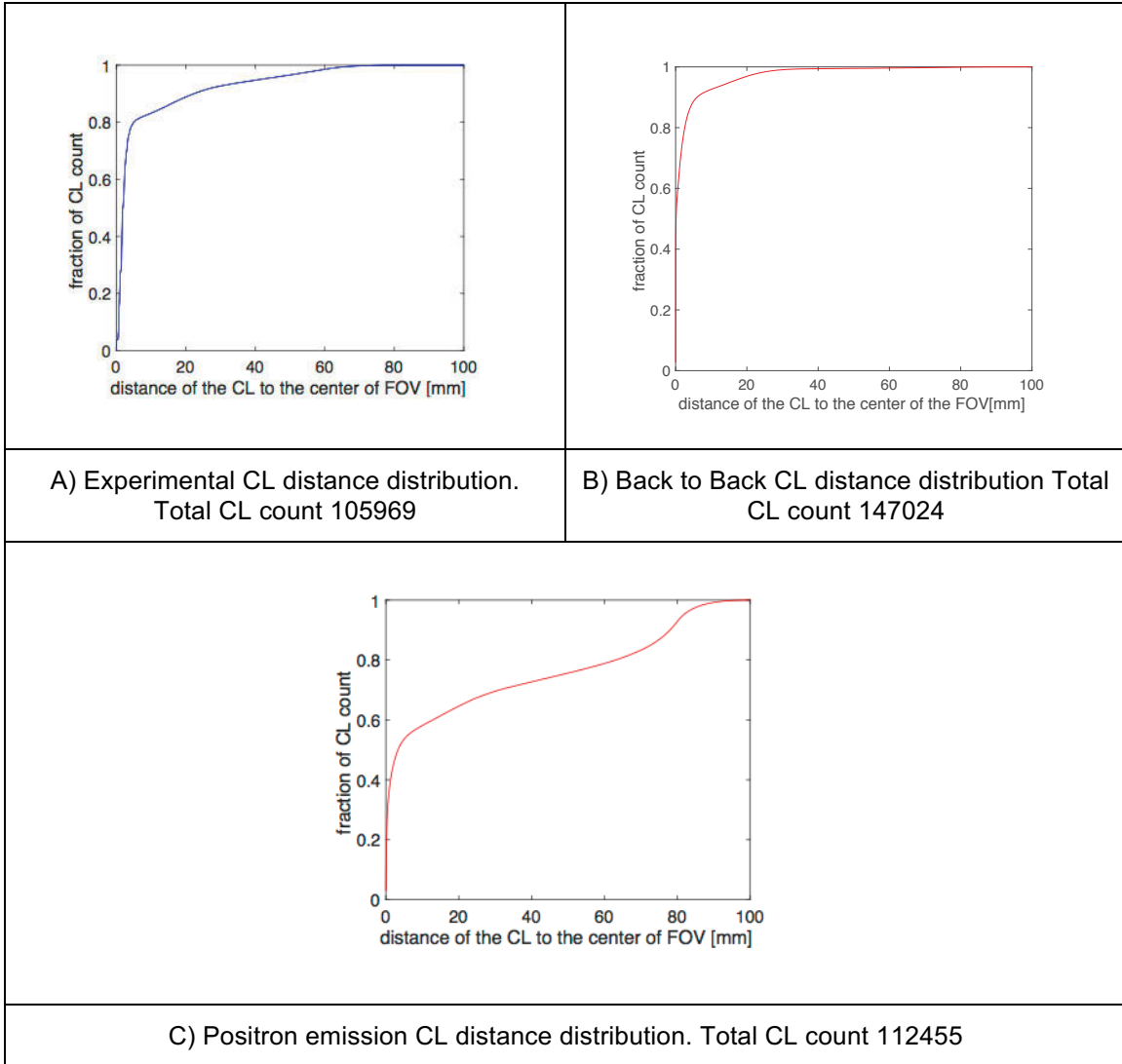
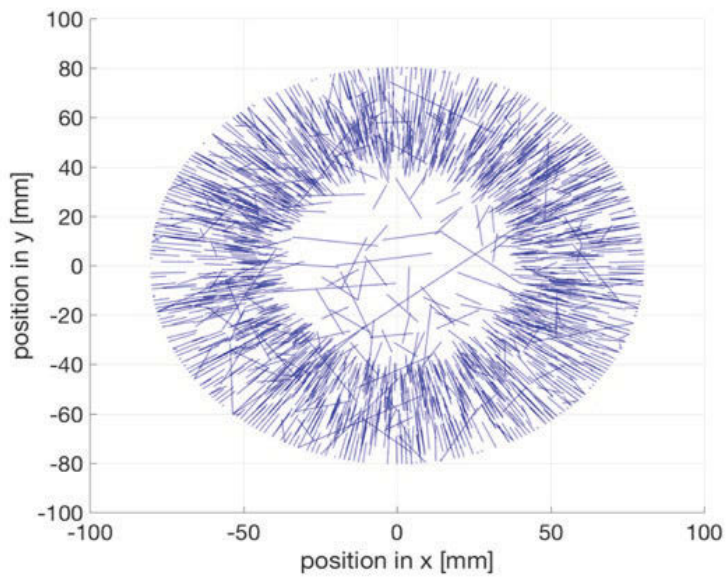
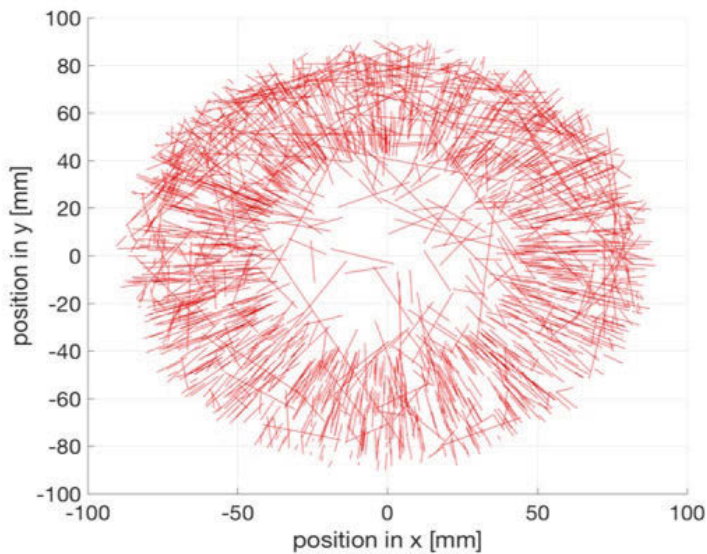


Figure 4.6. Comparison of the CL distance distribution, relative to the center of the particle, for the three model of source defintion in GATE.



A) CL representation for the actual scanner. The section plotted goes from 30 to 35 mm in z direction



B) CL representation for the simulated scanner. The section plotted goes from 30 to 35 mm in z direction

Figure 4.7. Comparison of experimental and simulated CL in the region 30 to 35 mm in the z direction

experimental and simulated CL representation in the region for 30 to 35 mm in the z direction. 5000 CL are used in the plot. The CL ring that can be seen in both plots is a visualization of the solid angle of the detector. In this regard, the CL lines present in the center, as well as those that do not have a radial direction, are scattered CL. The simulated plot displays more scattered CL than the experimental result, which is consistent with the results seen before.

Even though the positron emission source has the problem of the presence of more CL than the experiment, the distribution of CL through the bore is improved with this source definition. Figure 4.8 shows the profiles are consistent at the center, as well as at $z=25$ mm. The plot that corresponds to $z=25$ mm still presents more scattered CL in the simulation.

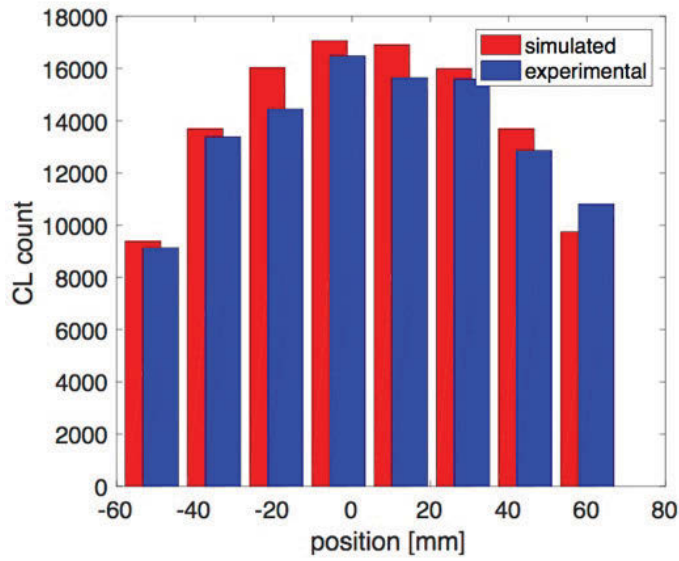
After this comparison process, the source model selected is positron emission + QGSP_BERT_EMV.

An additional difference with GATE simulation lies in the end point locations along the crystal detectors. CL end location are infinite, taken where the gamma interacted in the detector for the GATE model used in this study. For experimental results, the CL end is limited to 25,600 discrete crystal locations. The number of available LOR for the real Inveon is around 65 million. Figure 4.9 illustrates this feature. In the experimental result, the CL form a geometrical pattern. This geometrical pattern is the representation of the limited LOR present in the Inveon and the regular rows of crystals around the FOV. The location of the end point of a CL is given in terms of the centroid of the crystal at which the interaction is detected. The simulated results do not show this pattern because the end point location of the CL is given in terms of coordinates x and y where the detection took place.

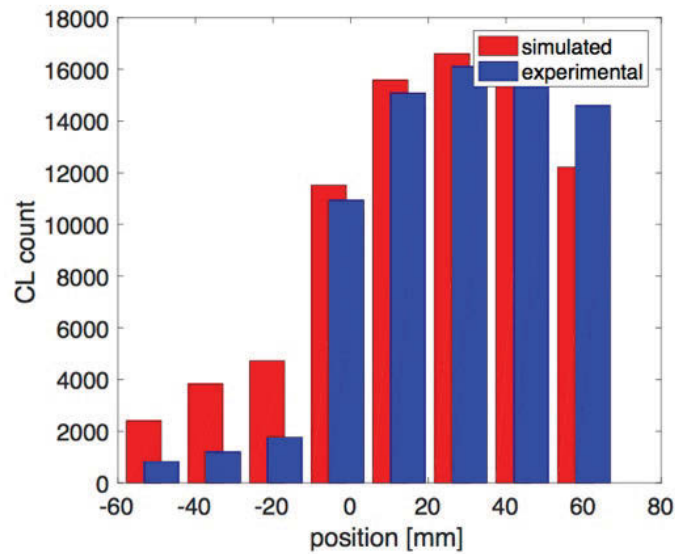
There exists an option in GATE to emulate use of nearest crystal address, but Lee's model does not incorporate this feature. The operation of this feature in GATE may be part of future work

As mentioned before, M-PEPT does not use the total CL count to detect the particle. Instead it uses only the lines that pass inside a region around the possible particle location. This region is defined by the boxcar, which establishes a cube of side equal to $2w+1$ blocks around the centroid of the source. For the present study, the grid size is 1 mm, so a boxcar with $w=3$ will be a cube of $(2*3+1) = 7$ mm. The size of this boxcar determines the number of CL used for detection

Four additional models of source definition are tested in GATE. None of the results show an improvement over the source definition already tried. Mainly, the tests are performed to better understand GATE features.



A) Distribution of CL count in the z direction for a particle located at z=0 mm (10s scan, 425-625 keV)



B) Distribution of CL count in the z direction for a particle located at z=25 mm (10s scan, 425-625 keV)

Figure 4.8. Detectio sites distribution along z for a particle located at the center of the FOV and 25 mm away in the z direction.

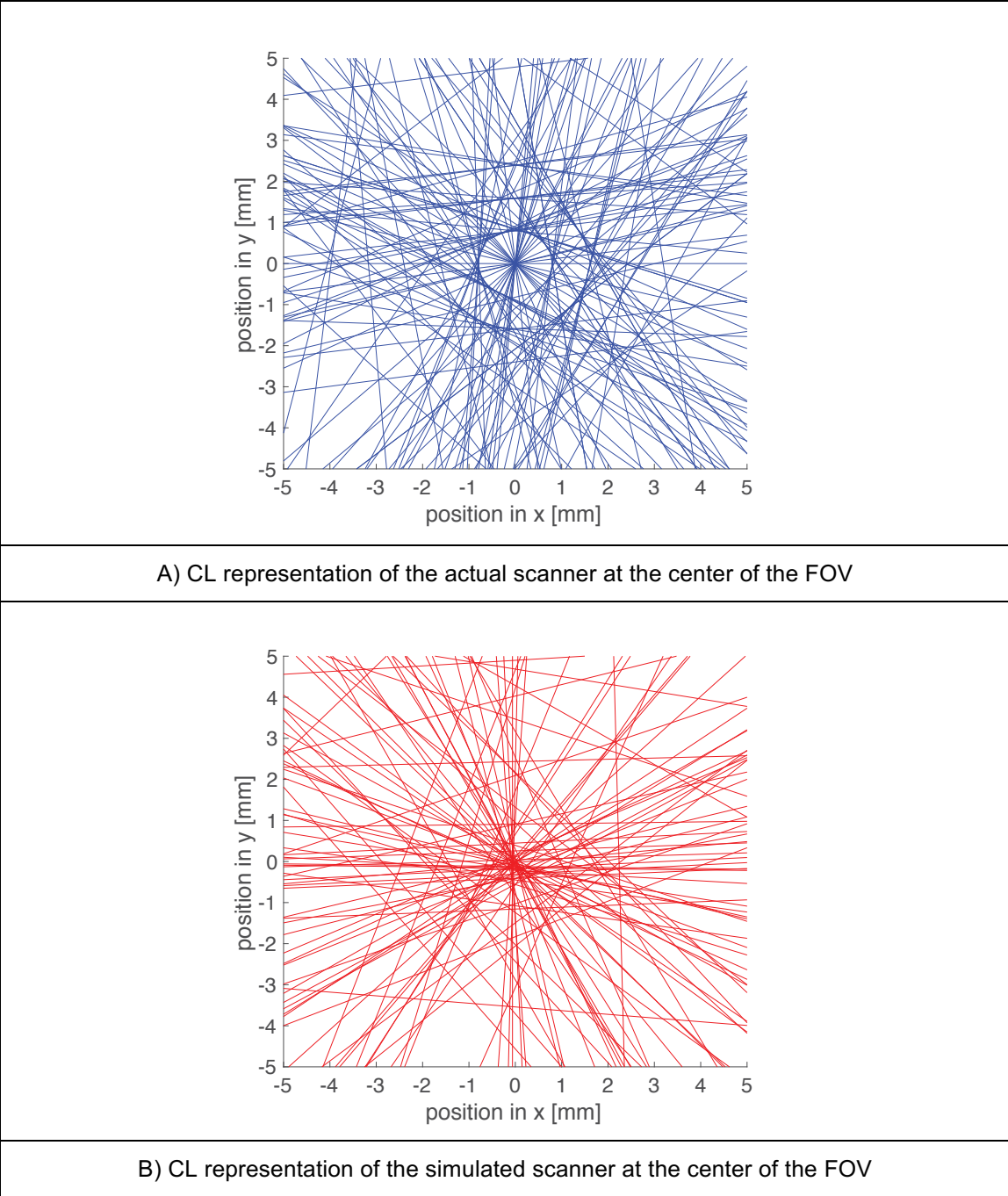


Figure 4.9. Comparison of the Experimental and simulated CL representation inside a box of 5X5X5 mm around the center of the FOV.

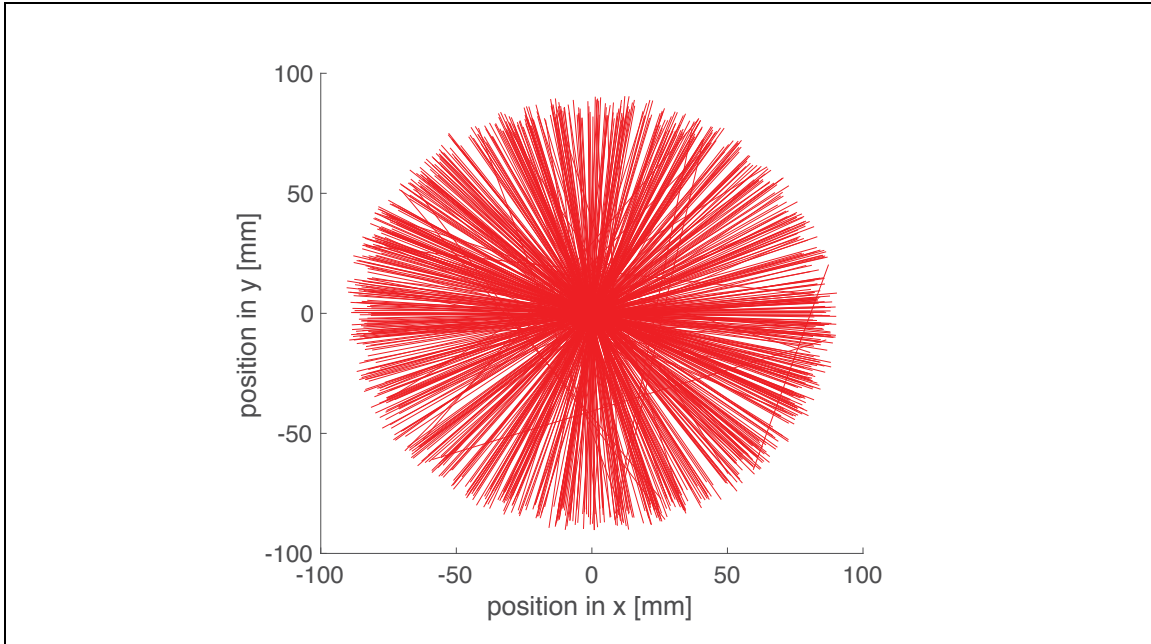
- A) **Positron emission without Physics List.** The choosing of a physics list is recommended in the GATE manual. However, the original Inveon model does not have a physics list incorporated. One simulation with no physics list is performed and the total CL count obtained is 108800, which is a similar result to the model selected, and close to the scanner count of 108883. The distribution of the CL does not show any improvement.
- B) **Positron Emission without Physics List with Ring Difference.** GATE offers a command line to define the maximum acceptance angle, this is the Ring Difference command line. A simulation with a ring difference of 3, similar to that defined in the actual Inveon, is performed. The total CL count obtained is 96908, which is less than the experimental result of 108883.
- C) **Back to Back Photon Emission without Physics List or Ring Difference.** The total CL count obtained is 150577.
- D) **Back to Back Photon Emission with Physics List and Ring Difference.** The total CL count obtained is 104266, which is close to the experimental result of 108883. However, more than 95% of these CL are within a sphere of 5 mm radius around the center of the particle. This means that the CL count used for detection for this simulation model is larger than the CL count found in experiment.

Finally, the system is modeled without the support phantom to visualize the effect of positron transport in different media. In this simulation, the positron emission + QGSP_BERT_EMV model is used. All the other parameters in GATE are the same. The results show a CL count used for detection equal to 149155, and a total CL count equal to 170293.

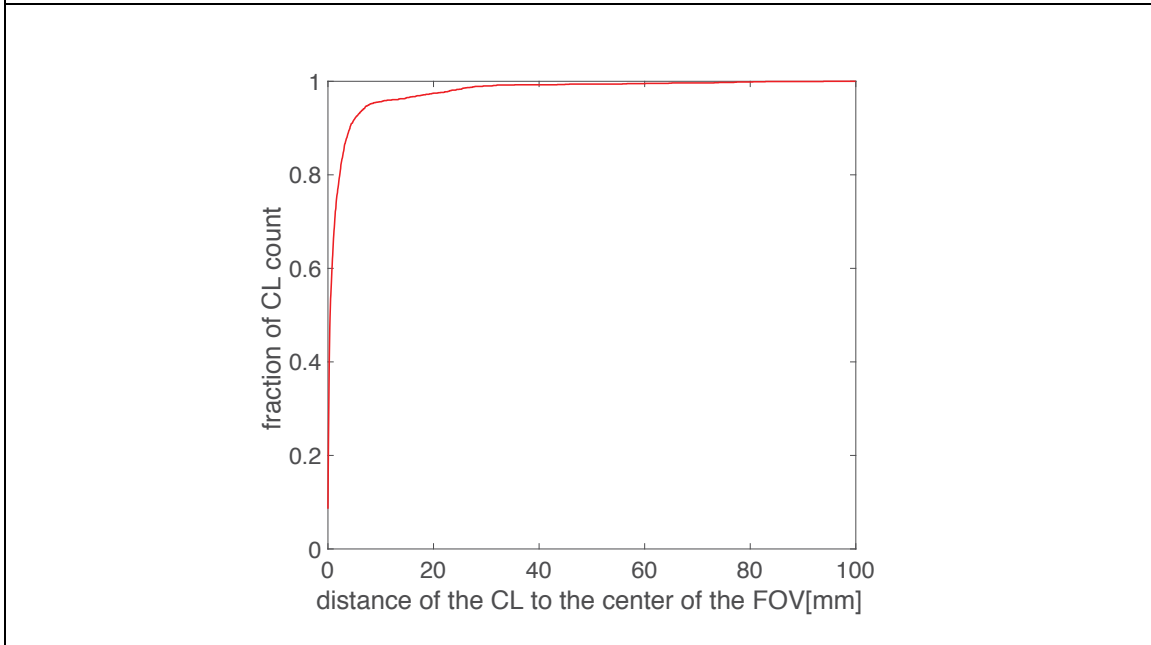
Figure 4.10 shows the CL representation and the CL distance distribution obtained for the simulation without the support. There are many less scattered CL and both plots resemble better the experimental results, however the CL count is far larger for the simulation. Also, the CL distance distribution is similar to the experimental one with the fraction of CL close to the point source near 95%.

The simulation without the support phantom does not have scattering medium so most of the CL have radial orientation. However, the experimental results show the same behavior but with the phantom. The Inveon may have a mechanism of filtering the scattered fraction, or GATE may have a deficiency in simulating the scattering in some materials.

One last concern is how the time slice prescribed in the GATE simulation affects the results. As detailed in Chapters 2 and 3, GATE does not simulate a continuous process, but instead generates a series of static simulations that resemble motion. For this reason, different time slices are prescribed in the



A) Simulated CL of a particle without the support phantom at the center of the FOV



B) Simulated CL distance distribution of a particle without the support phantom at the center of the FOV

Figure 4.10. CL plot and CL distance distribution for a point source modeled with the positron emission model but without the presence of the phantom support

GATE simulation to test impact of selected values on a 10 second scan simulation. Table 4.3 shows the results obtained. For time slices less than 200 ms, the time slice prescribed in the simulation does not significantly change the CL count result. Another criterion for time slice selection is rate of motion, and the associated change in geometry with each time step. The velocity 0.18 cm/s moves the source 0.36 mm in one 200 ms time slice. This is less than half the point source radius and is small enough to simulate near continuous simulation results. However, all the simulations use a time slice of 5 ms. This value is smaller than time step used in the M-PEPT. This assures the M-PEPT time slice is sampling data for a moving source during the trajectory reconstruction.

Inveon efficiency curve

The energy window used for detection in the actual and simulated Inveon is changed. The point 525 keV, which is the middle of the window 425-625 is fixed. Windows of 425-625 keV, 400-650 keV, 375-675 keV and 350-700 keV are used. The variation in CL count rate as function of this window is shown in Figure 4.11. For the last three cases, the simulated count rate is smaller than the experimental count rate. The error at the smallest energy window is less than 1%, the error at the largest energy window is about 10%. The difference between measured and simulated CL count increases as the energy window opens. This difference may be due to the absence in the simulation of the gamma rays produced by the decay of the ^{176}Lu .

The total experimental CL count is compared with the simulated CL count along the centerline of the FOV in Figure 4.12. The simulated results are larger than the experimental ones. The experimental efficiency at the center of the FOV is 5.22% while the simulated efficiency at the same place is 6%. At the center of the FOV the difference in CL count is less than 5%. At the edges, this difference is near 40%.

Overestimation of the CL count by GATE is also reported by others (Schmidtlein et al., 2006). They argue that the differences in results might be due to variation in the energy resolution inside a block, coupling deficiencies between the detector and the PMT tube, and incomplete geometrical information. Larger results in simulation are also reported by (Lee et al., 2015), but the authors do not provide information about possible reason for this discrepancy.

3. Evaluation of the standard deviation in reconstructed positions

Figure 4.13 shows the comparison between the prescribed position in GATE and the measured position by M-PEPT. The results correspond to the simulation of a 10 second scan of a particle located at different places along the z direction. The

Table 4.3. Results obtained at different time slice prescribed in GATE simulation. 5 ms time slice is used for GATE Simulations of moving sources.

Time slice [ms]	CL count
5	111323
10	111167
20	110721
50	111395
100	111375
200	111398

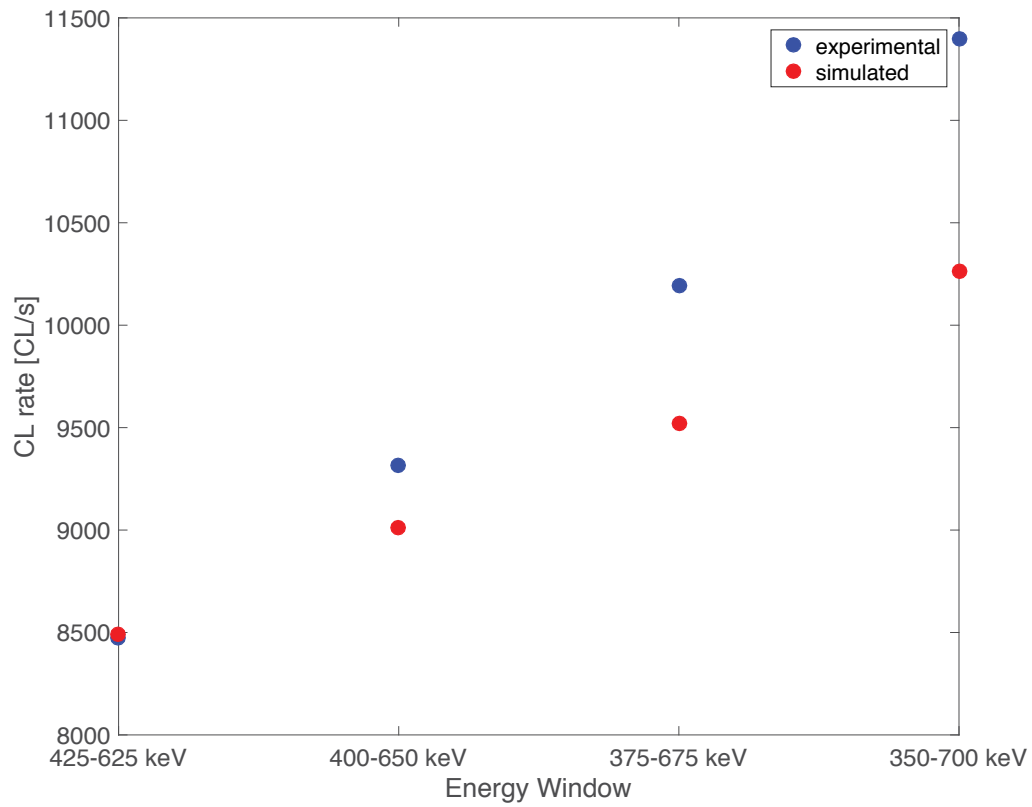


Figure 4.11. Experimental and simulated CL count rate as function of the energy window used in the Inveon setup

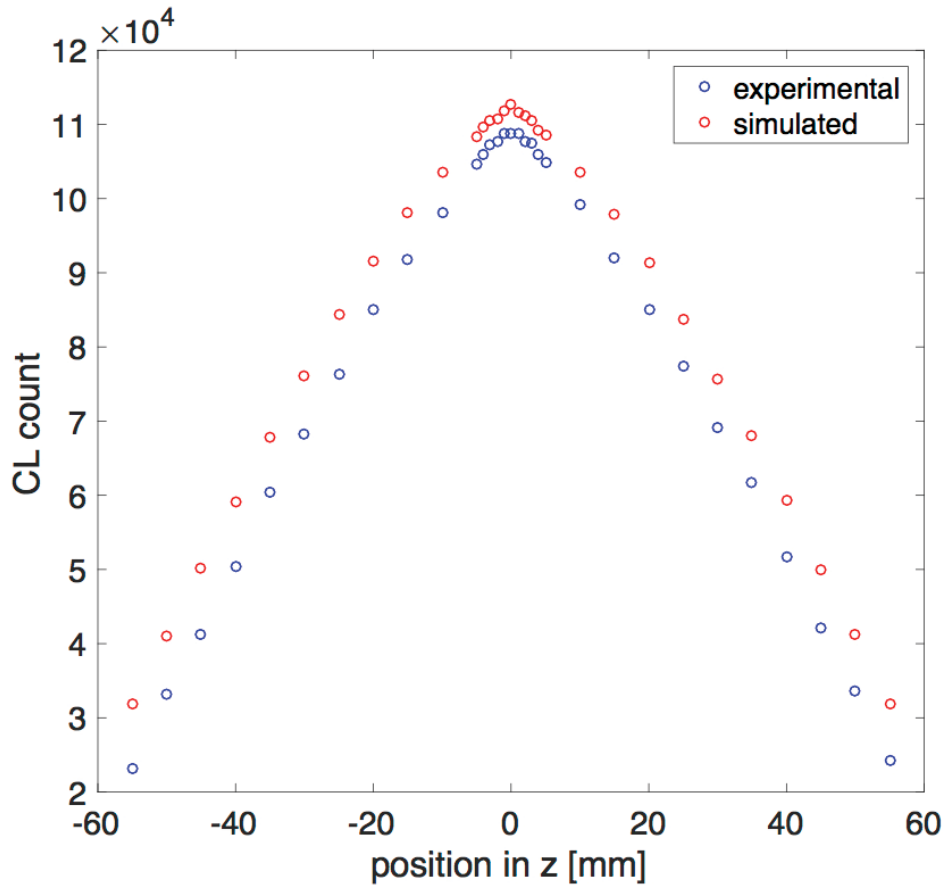
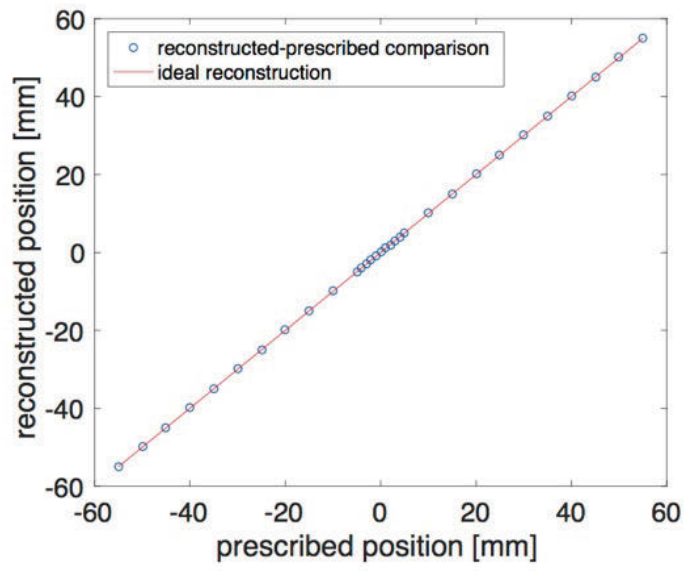
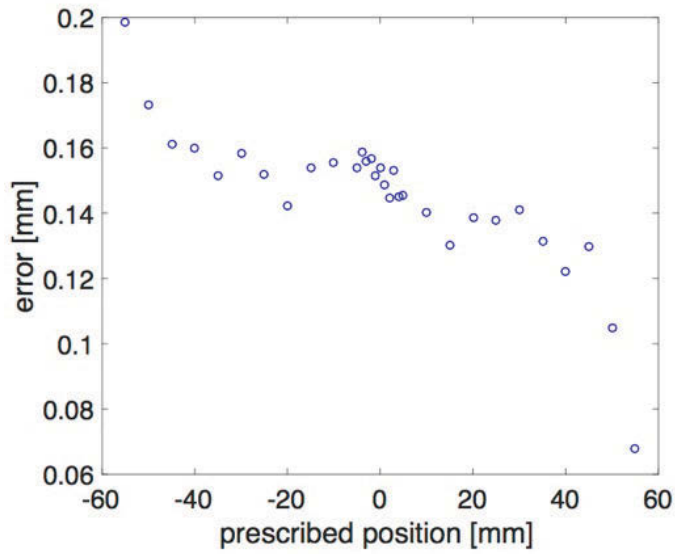


Figure 4.12. Experimental CL count comparison to Simulated CL count as function of the axial position along the center line of the FOV. 425 – 625 keV positron emission source.



A) Comparison between prescribed position in GATE and measured position with M-PEPT



B) Error in location simulated static particle at different location along the z direction

Figure 4.13. Comparison of the prescribed position in GATE and measured position for the simulated static data

total CL count used for detection is around 69000, or around 60% of the total count of 115000 CL. For the reconstruction the parameters in M-PEPT are 1 mm grid size and 10 second time step. In the Figure 4.13A, the red line corresponds to the ideal detection, in which the measured position in M-PEPT is equal to the prescribed position in GATE simulation. Figures 4.13A and 4.13B show that the location information defined in GATE is properly retrieved by M-PEPT, and provides information on the confidence in GATE results. As can be seen in Figure 4.13B for any position along the z direction, the error in the location is less than 0.2 mm.

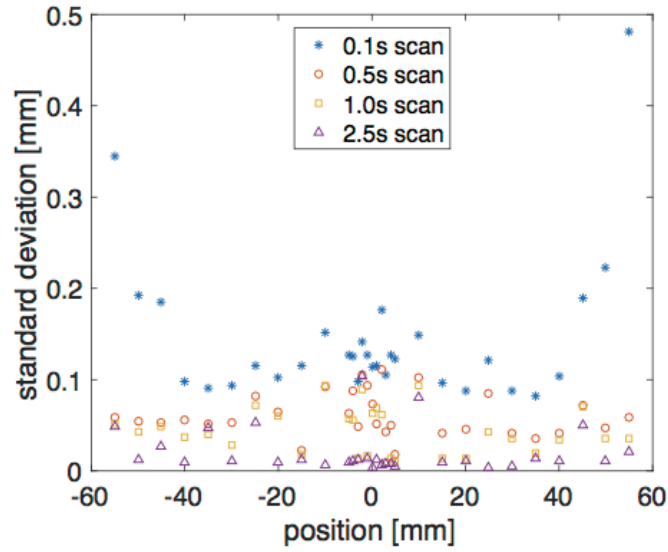
The 10 second scan of the stationary source is divided in segments of 0.1, 0.5, 1.0 and 2.5 seconds. At 0.1 seconds the CL count available for detection is around 690, while at 2.5 seconds the CL count for detection is around 17250. The CL count influences the precision of M-PEPT. Figure 4.14A shows the variation in the standard deviation for the actual scanner, while 4.14B shows the variation for the simulated scanner. As expected the efficiency degrades at the edges, and it also degrades with the decrease of the time step. Precision is reduced when there are less CL available, as expected.

4. GATE simulation of moving point source.

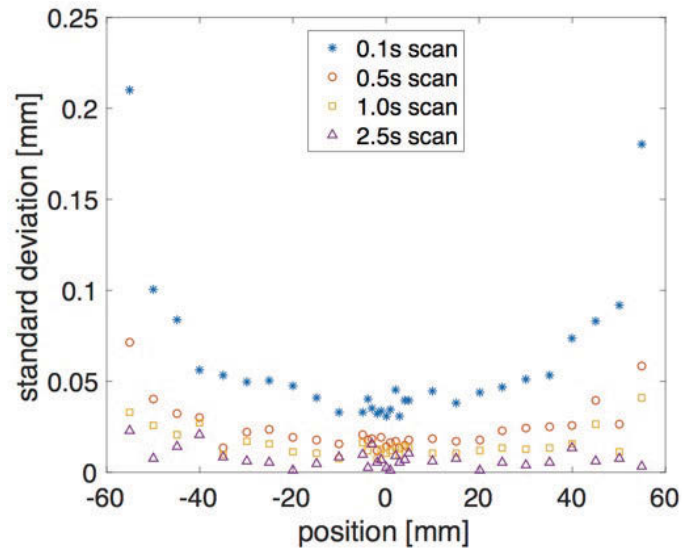
Trajectory alignment and movement

A ^{22}Na source in plastic cube is moved inside the actual Inveon FOV. The source is moved at three different velocities, and each velocity is repeated six times. This movement is done using the Inveon bed motion control. However, the precision of this motion system is not known. For this reason, the experimental data are used to define the initial position and velocity of the source. Figure 4.15 shows the overlap of simulated and experimental data for a single repetition of the three velocities tested. Once overlap of experimental and simulated data lines is achieved, the velocity and intercept of the line achieving overlap is selected as the input to the GATE simulation. The GATE simulation is then repeated five additional times with the same input file. This approach is subjective, and a more disciplined mathematical approach to this challenge is introduced in the next section.

The particle is kept in the same x and y location by using the phantom support depicted in Figure 3.2, in which the source is mounted. The Inveon scanner data, and GATE scanner data are treated by M-PEPT with 1mm grid size and 100 ms time step. Figure 4.16 shows experimental and simulated 3D result of the position reconstructed with M-PEPT for a particle moving at 0.18 cm/s. For GATE simulation, the prescribed position in x is 0mm and in y is also 0mm. The experimental particle is aligned to the center of the FOV with the procedure described in Chapter 3. The position detected by M-PEPT for the simulated



A) Standard deviation variation along the z direction in experiment.



B) Standard deviation variation along the z direction in simulation.

Figure 4.14. Comparison of the variation of the standard deviation in the detection of a static particle at different locations along the z direction

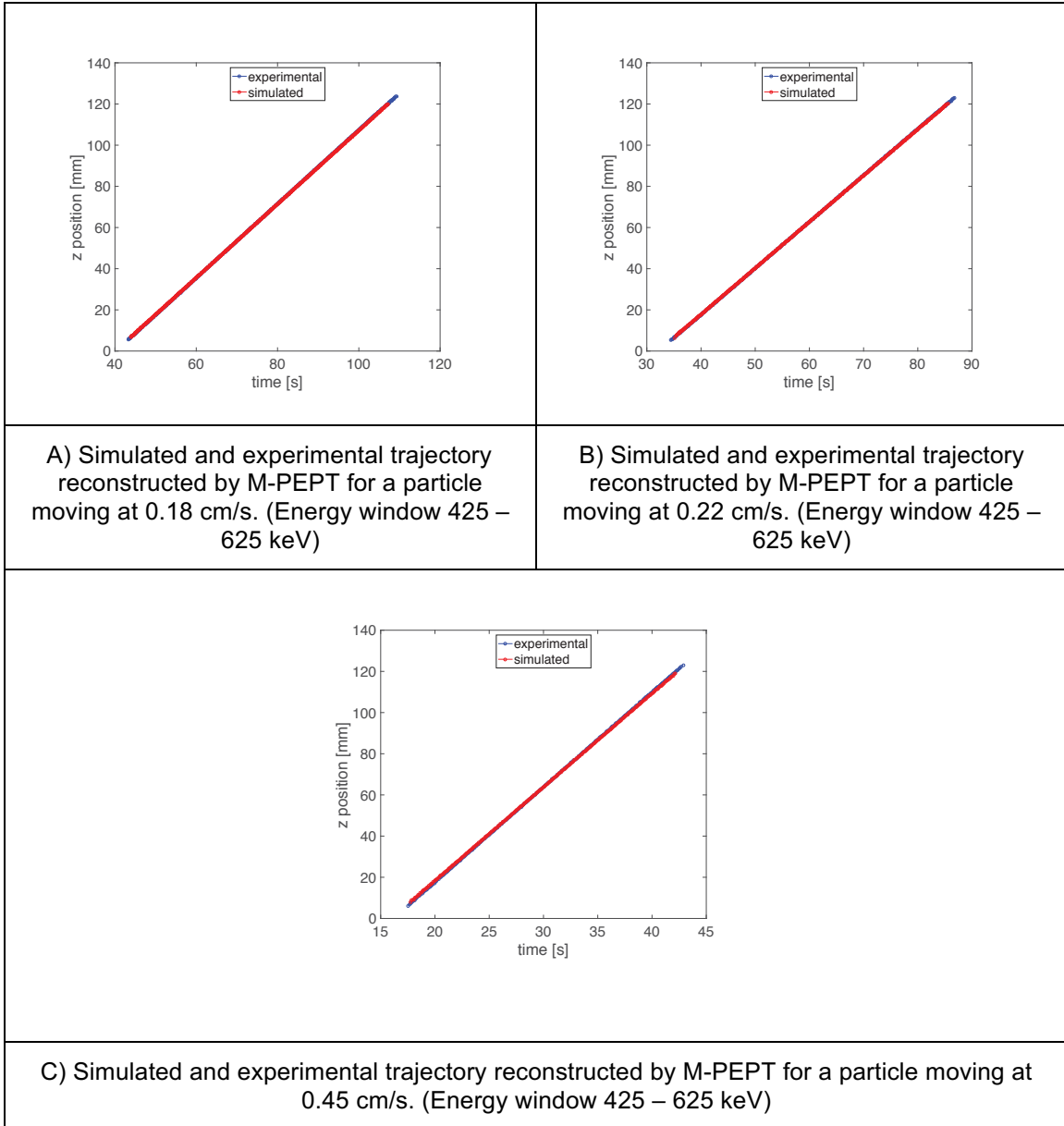


Figure 4.15. Overlapping of experimental and simulated trajectories reconstructed by M-PEPT.

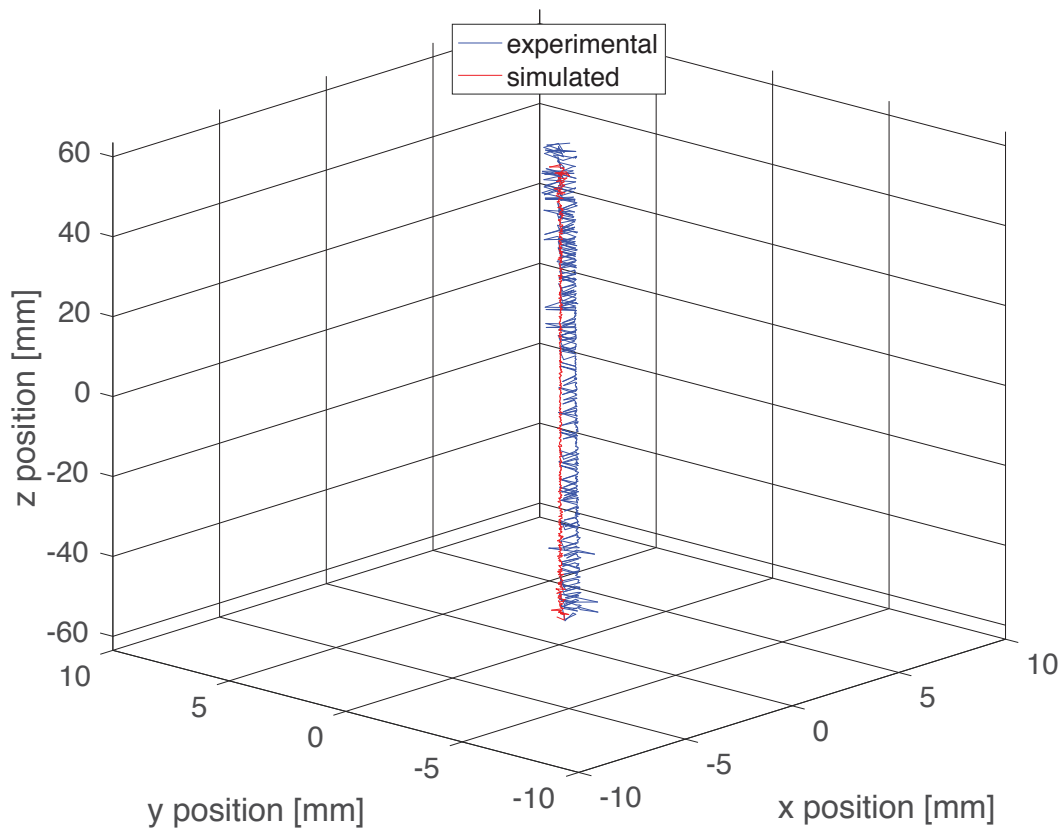


Figure 4.16. Overlapping of experimental and simulated trajectory in a 3D plot. The velocity of the particle is 0.18 cm/s (Energy window 425 – 625)

particle is ($x=0.0041\text{mm}$, $y=-0.0509\text{mm}$). The position detected for the experimental particle is ($x=0.7343\text{mm}$, $y=0.1949\text{mm}$) averaged over the entire z axis.

Figure 4.16 shows oscillation in x and y position for the experimental particle. This oscillation is due to the discrete nature of the LOR available for detection in the actual Inveon as well as the grid size used for detection in M-PEPT. A deeper explanation of these variations is written at the end of this section. This variation is not present in the simulated results because the LOR available for detection in GATE simulation are infinite.

At the center of the FOV the CL count in 100 ms is 1200 for experimental and 1400 for simulated. At the edges the CL count in 100 ms is 100 for experimental and 250 for simulated. A visual explanation of this feature is presented in Figure 4.17 where a comparison of the CL for a simulated particle is shown at two places inside the FOV. The places shown correspond to the entrance ($z = 50\text{mm}$) and the center of the bore ($z = 0\text{mm}$).

In Figure 4.17A the experimental particle at the entrance (z equal -50mm) of Inveon bore is shown. It can be seen that the CL forms a plane surface around the center of the particle. The CLs located outside this plane are scattered CLs. The orientation of the detectors allows true coincident event detection only inside this flat surface. Figure 4.17B shows the experimental particle at the center of the FOV. Now it can be seen that the CL end position forms a cylinder around the particle. The detectors are able to register events in this bigger area, increasing efficiency.

The same overall effect can be seen in the simulated particle shown in Figure 4.17 C at z equal -50mm , and in Figure 4.17 D with the simulated particle at FOV center. However, the CLs that correspond to true back to back gamma annihilation at the entrance are present in less number than in the experimental case. Meanwhile the scattered CL count for the simulation is larger than in the experiment.

Figure 4.18 shows the comparison of the CL count used to detect the simulated and experimental particle. It has to be recalled that the total CL count is not used to detect the particle by M-PEPT. Only those particles inside the boxcar are used to reconstruct the position. The experimental CL count available for detection is almost twice the simulated CL available when the support phantom is included in the simulation.

Table 4.4 compares CL count used for detection for an experimental and simulated moving particle with phantom present. The values shown are for the three first repetitions of the velocities tested.

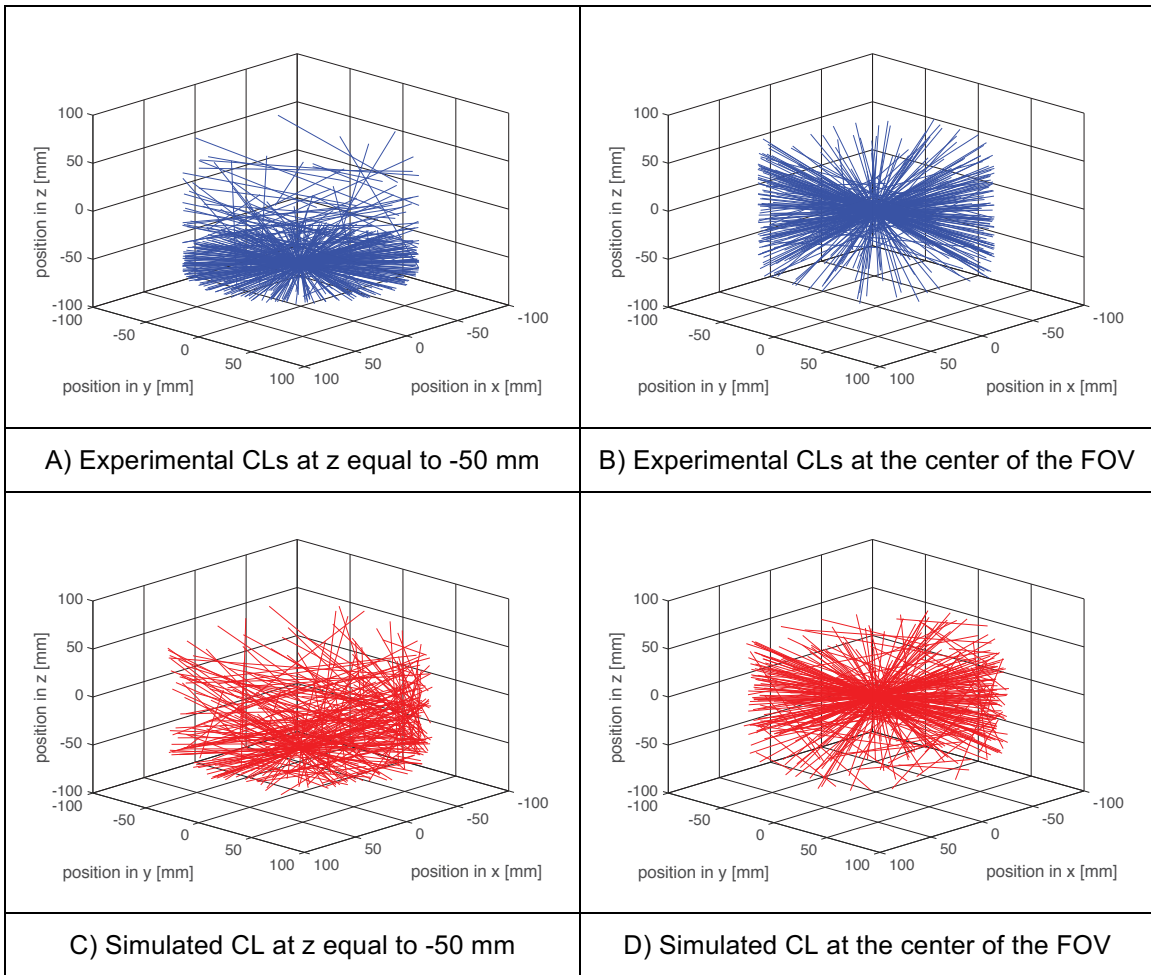


Figure 4.17. CL 3D representation at $z = -50$ mm and at the center ($z = 0$ mm) of the FOV for a moving particle. The velocity is 0.18 cm/s (Energy window 425 – 625 keV)

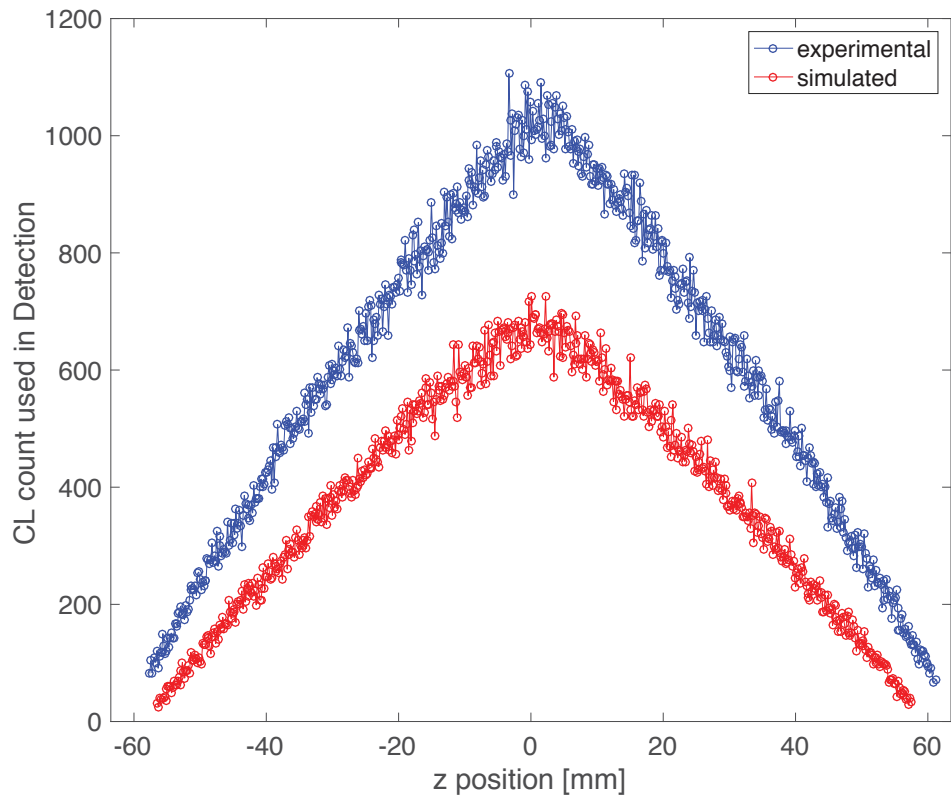


Figure 4.18. Comparison of the CL count available for detection for a particle moving at 0.18 cm/s (Energy window 425 – 625 keV)

Table 4.4. Comparison of simulated and experimental CL available for detection.

Location and velocity	CL used per detection Experimental	CL used per detection Simulated
X=0 y=0, 0.18 cm/s	1017	687
X=0 y=0, 0.45 cm/s	1013	732
X=53 y=37, 0.45 cm/s	757	543

Evaluation of the standard deviation in the reconstructed position

In the previous section and in Figure 4.16, a process to overlap the experimental and simulated results is presented to define the particle velocity to be used in GATE. Since this process is subjective, a formalization of this method is offered here by obtaining linear regressions of the experimental and simulated trajectories for each repetition. The arrays of time marks (t_k) and z positions (z_k) detected by M-PEPT are fit to Equation (4) for each of the six point-source traverse repetitions.

$$z_{k,i} = v_i \cdot t_{k,i} + z_{0i}, \quad i = 1 \dots 6, k = 1 \dots N \quad (4)$$

In Equation (4) v_i is the slope of the regression and z_{0i} is the intercept. k represents the length of the array produced by M-PEPT and i is the number of repetitions.

The results for slope and intercepts of these regressions are averaged for each nominal velocity. The slope of the regression represents the velocity of the particle and the intercepts represent the initial position of the particle. The averages and standard deviations are presented in Table 4.5. The low values of standard deviation demonstrate the repeatability of the simulation and the experimental methods used.

Table 4.6 presents the slope and intercepts obtained for the nominal velocity of 0.18 cm/s. The table shows the experimental and simulated results and includes the goodness of fit, given by the parameter R^2 . Table 4.6 shows that for this case the velocity prescribed in GATE is 0.179 cm/s

Time marks array (t_k) provided by M-PEPT are placed into Equation (4) to obtain best-fit calculated positions. These positions are subtracted from the M-PEPT measured positions (z_k) in order to obtain local variations from the linear fit, $\delta z_{k,i}$ according to equation (5)

$$\delta z_{k,i} = z_{Calculated_{k,i}} - z_{Measured_{k,i}}, \quad i = 1 \dots 6, k = 1 \dots N \quad (5)$$

Direct comparison of experimental and simulated data is not possible because both sets are slightly different in timing, and they do not overlap each other exactly. The local variation homogenizes the data in time and space and allows generation of a standard deviation in position using the best fit line as the expected value. First, the local variation is divided in groups of six elements. Then, the standard deviation array is calculated with equation (6),

$$\sigma_{\delta z_{j,i}} = \sqrt{\frac{\sum_i (\delta z_{j,i})^2}{6}}, \quad i = 1 \dots 6, j = 1, \dots N - 1 \quad (6)$$

Table 4.5. Average slope and average Intercept and their standard deviations for experimental and simulated data sets (velocity = 0.18 cm/s, x = 0, y = 0, Energy Window 425 – 625 keV)

Pres. Vel. (cm/s)	Mean exp. Intercept mm (σ mm)	Pres. GATE Intercept mm (σ mm)	Mean sim. Intercept mm (σ mm)	Mean exp. Slope cm/s (σ cm/s)	Pres. GATE Slope cm/s (Vel.)	Mean sim. Slope cm/s (σ cm/s)
0.18	-135.7784 (0.0142)	-135.5	-135.2343 (0.0108)	0.17969 (0.00014)	0.179	0.17890 (0.00012)
0.22	-136.1031 (0.0186)	-135.9	-135.6817 (0.0111)	0.22563 (0.00031)	0.225	0.22491 (0.00018)
0.45	-138.1511 (0.0383)	-136.5	-136.1011 (0.0227)	0.46153 (0.00081)	0.461	0.45472 (0.00061)

Table 4.6. Experimental and simulated intercepts for a particle moving at 0.18 cm/s along the z axis of the detection bore.

N	Experimental Intercept (mm)	Experimental Slope (cm/s)	R²	Simulated Intercept (mm)	Simulated Slope (cm/s)	R²
1	-135.7963	0.17969	1.0000	-135.2231	0.17888	1.0000
2	-135.7675	0.17968	1.0000	-135.2254	0.17889	1.0000
3	-135.7765	0.17969	1.0000	-135.2525	0.17892	1.0000
4	-135.7934	0.17971	1.0000	-135.2343	0.17890	1.0000
5	-135.7768	0.17968	1.0000	-135.2409	0.17890	1.0000
6	-135.7600	0.17967	1.0000	-135.2374	0.17890	1.0000

Figure 4.19 shows the variation in the standard deviation as function of the axial position for a moving particle. This plot uses the best-fit z position as expected value for the calculation of the standard deviation. Different velocities and different locations inside the FOV are presented in Figure 4.19. Standard deviation of the experimental data and the simulation data nearly overlap each other. The standard deviation increases at the edges of the bore and is smaller toward the center. This follows the tendency previously described by the CL count and the efficiency. Additionally, the profile depicted by the data in Figure 4.19 is consistent with the profile of Figure 4.14 for static data. The results are the same for the other five repetitions and can be seen in the Appendix 4.

Evaluation of the standard deviation in the reconstructed position in x and y direction

There exists a spurious incremental variation in the reconstructed position of a moving particle when experimental data are used. This can be seen in the experimental trajectory in Figure 4.16. The amplitude of the variation for simulated particles is less than or equal to 0.1 mm. For the experimental particle the amplitude is near 1.0mm and it occurs in all directions, as seen in Figure 4.20. Since the amplitude of the oscillation is bigger in the experimental trajectory than in the simulated, the reason for this artifact may be in the way Inveon records data, or in a combination of data acquisition and M-PEPT settings.

Figure 4.20 also shows that both particles are not located exactly at (0,0) mm. The position in x and y are locally homogenized in order to make possible a comparison between experimental and simulated sets following the same procedure used to homogenize the data in z. The local average position is used as the expected value for the standard deviation calculation. Table 4.7 shows the average location in x and y for the simulated and experimental moving particle at different velocities and at different locations. The standard variation among repetitions is also presented in the table.

The local standard deviation is calculated using groups of six positions per equation (6), and the results are presented in Figure 4.21. A particle moving at an eccentric position ($x=35\text{mm}$ $y=19\text{mm}$) at 0.45 cm/s is also presented in Figure 4.21. The oscillation in the standard deviation is similar in amplitude to that found along the primary z axis of the FOV.

The reason for these variations is further investigated. Figure 4.22 compares the CL count as function of time and the position reconstruction as function of time. The area marked in pink is expanded in order to check if there is a direct correlation between the CL count and the presence of the jumps. Figure 4.22 is made with 1 mm grid size and 100 ms time step in M-PEPT. None of the advanced user features are changed.

Figure 4.23 is the magnification in of the region marked in pink. The figure shows

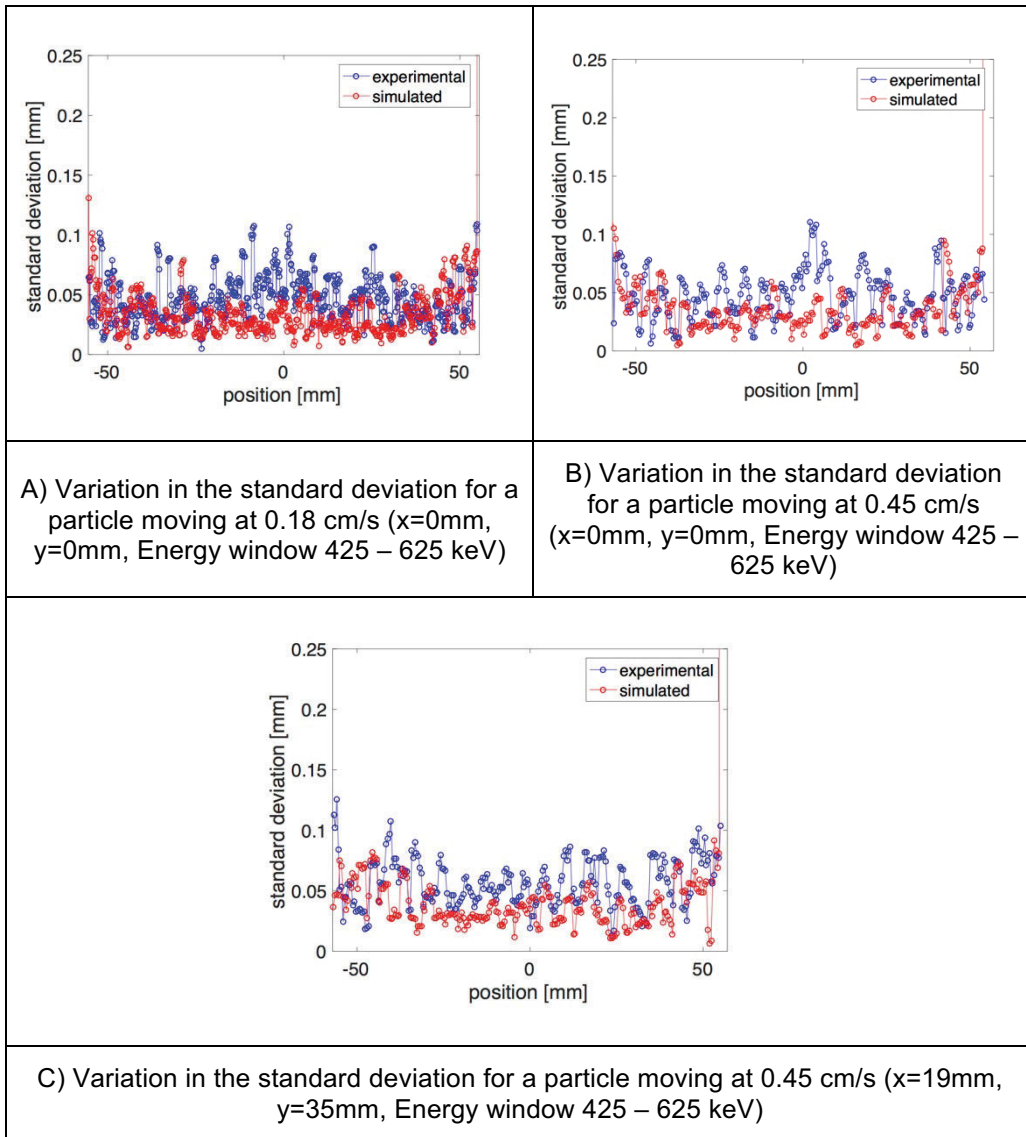
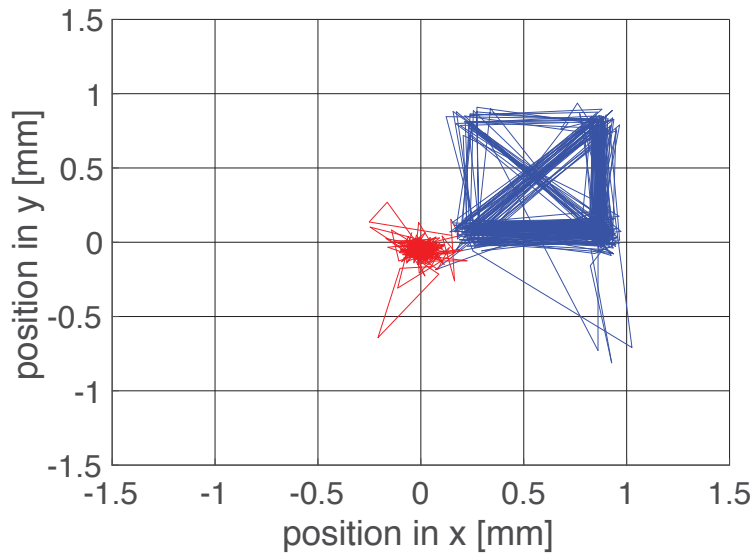
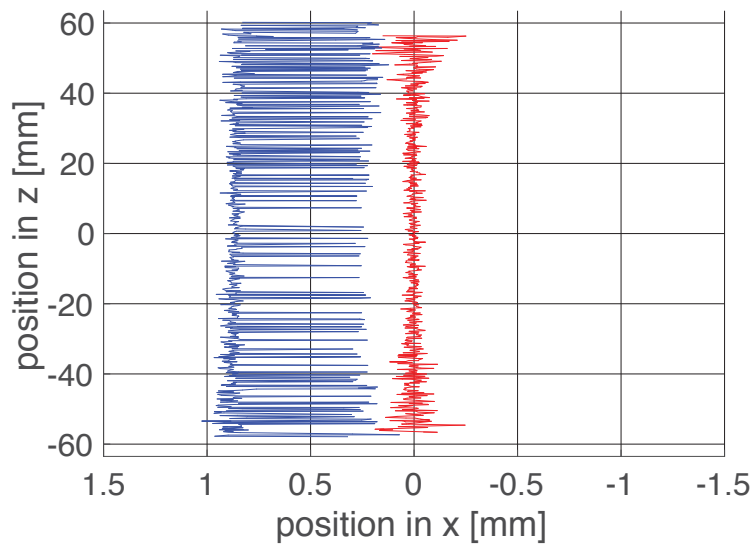


Figure 4.19. Variation in the standard deviation along the z directions for different velocities.



A) Frontal View of the FOV

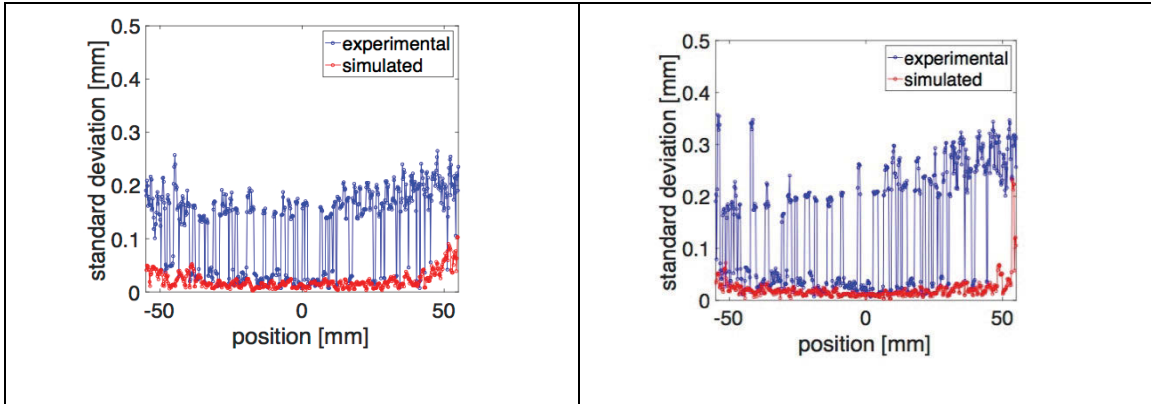


B) Lateral View of the FOV

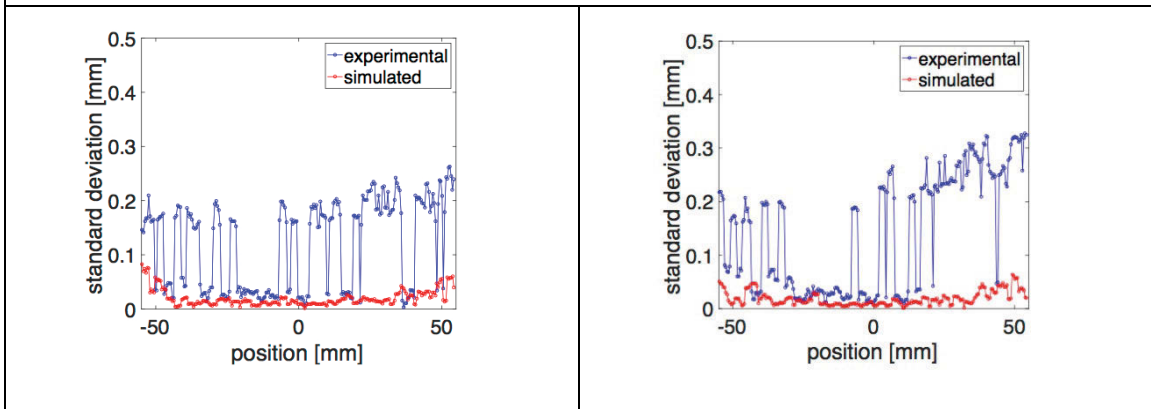
Figure 4.20. Frontal and lateral view of the FOV of the Inveon when a particle is moving at 0.18 cm/s

Table 4.7. Average position for the x and y at different velocities and different location inside the Inveon's FOV

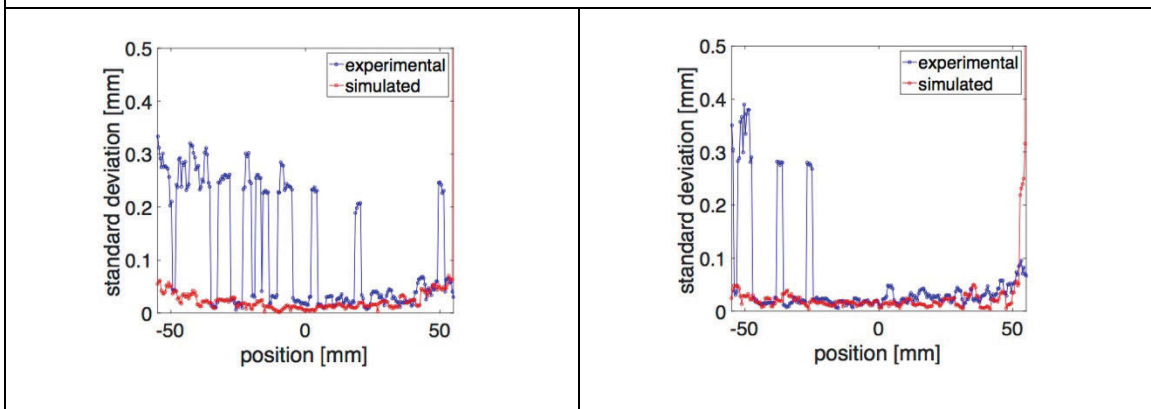
Velocity and position	x position (standard deviation) Experimental	x position (standard deviation) Simulated	y position (standard deviation) Experimental	y position (standard deviation) Simulated
0.18 cm/s (x=0, y=0)	0.7255 mm (0.0171 mm)	0.0023 mm (0.0021 mm)	0.1910 mm (0.0068 mm)	-0.0510 mm (0.0021 mm)
0.45 cm/s (x=0, y=0)	0.7354 mm (0.0066 mm)	0.0015 mm (0.0014 mm)	0.2046 mm (0.0081 mm)	-0.0646 mm (0.0028 mm)
0.45 cm/s (x=18, y=37)	17.7760 mm (0.0048 mm)	18.9615 mm (0.0020 mm)	33.8656 mm (0.0043 mm)	34.9197 mm (0.0037 mm)



A) Standard deviation in the components x and y for a particle moving at 0.18 cm/s along z at $x=0\text{mm}$ $y=0\text{mm}$



B) Standard deviation in the x and y components for a particle moving at 0.45 cm/s along z at $x=0\text{mm}$ $y=0\text{mm}$



C) Standard deviation in the x and y components for a particle moving at 0.45 cm/s along z at $x=35\text{mm}$ $y=19\text{mm}$

Figure 4.21. Variation in experimental and simulated standard deviation along the z direction for x and y positions

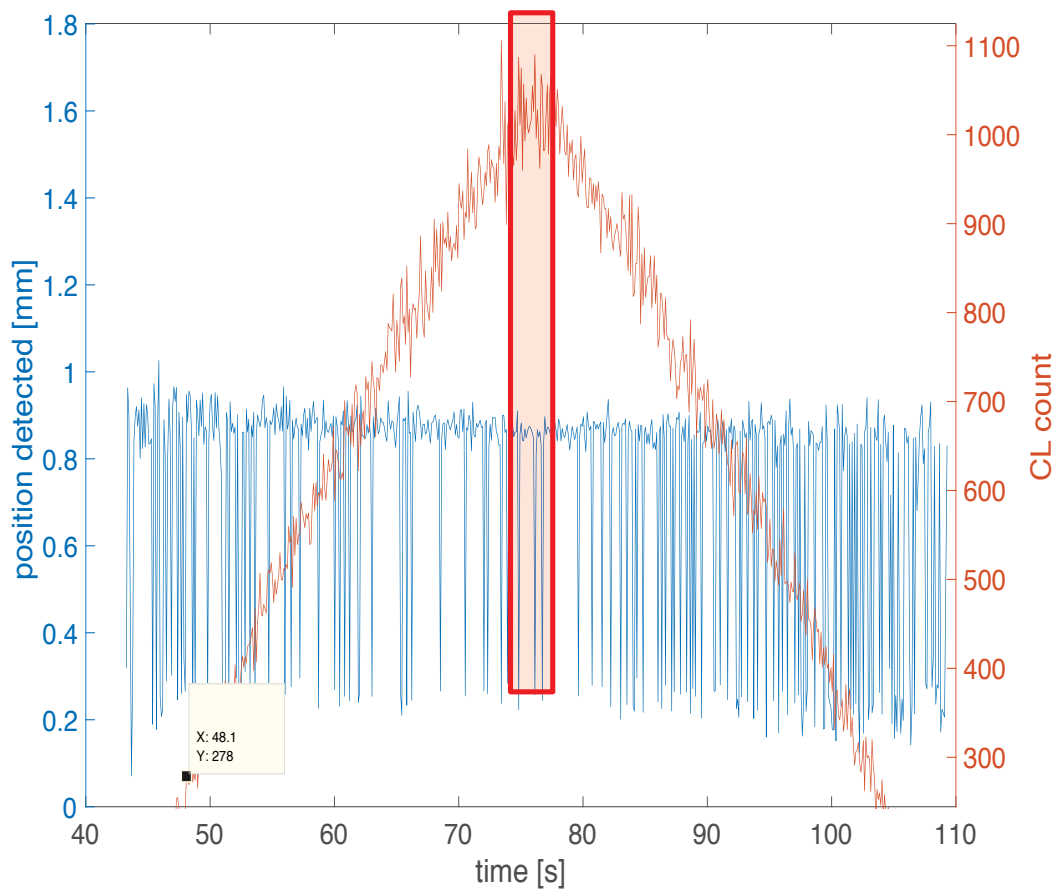


Figure 4.22. Variation CL count as function of position super imposed on position reconstruction as function of position for a particle moving at 0.18cm/s

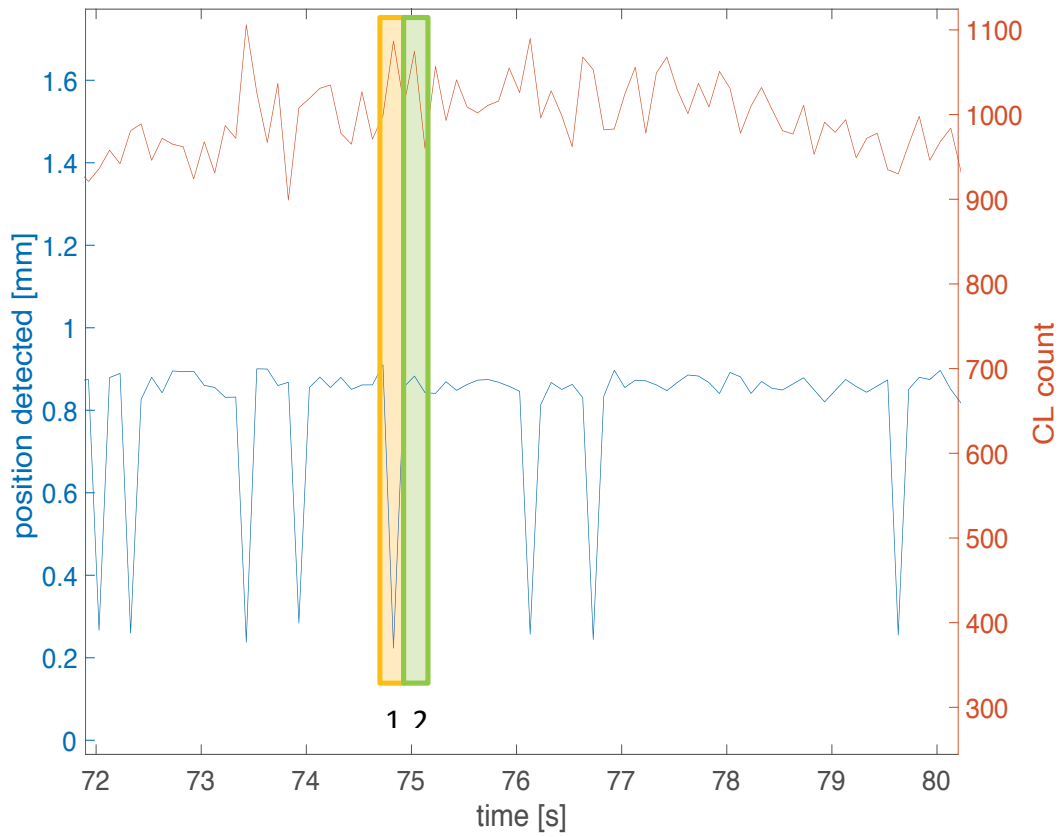


Figure 4.23. Close up of the CL count vs time superimposed to position reconstruction vs time

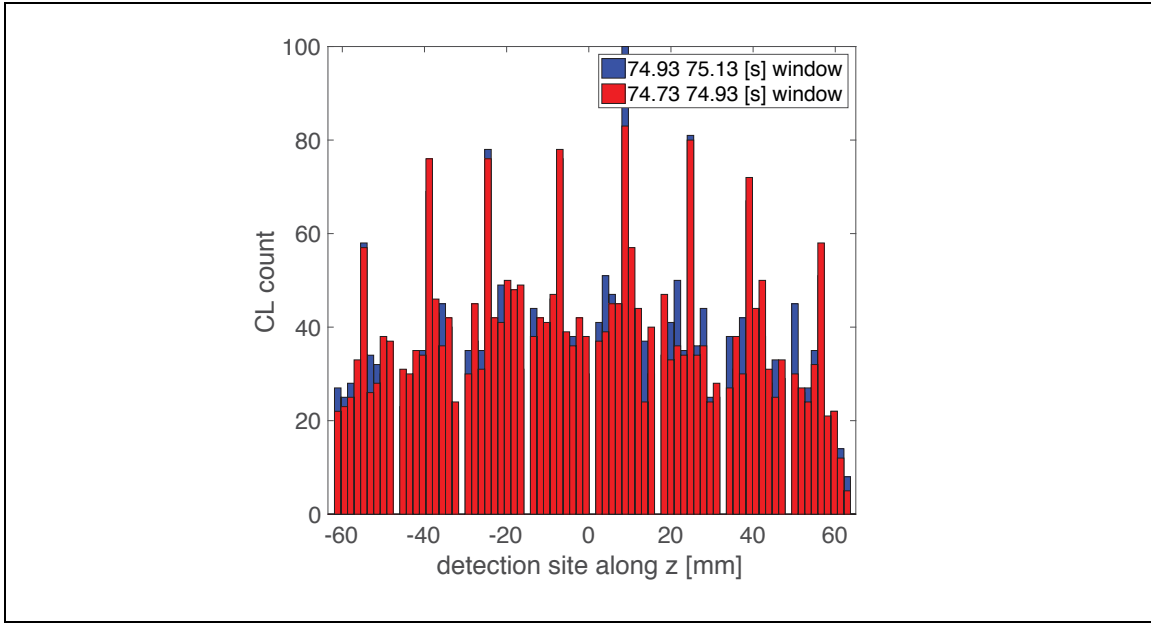
no direct correlation with the CL count and the presence of the jumps. The detection site distribution along the z direction is obtained for the regions marked in the plot. The yellow region presents a jump while the green region does not.

In Figure 4.24A the detection site distribution of the zone 1 is superimposed on the detection site distribution of the zone 2. Zone 1 corresponds to the time window of 74.73 to 74.93 s. Zone 2 goes from 74.93 to 75.13 seconds. The superimposed regions do not show differences in the detection of photon interaction along the z axis of the crystal detectors. The bins are 1.59 mm width based on the pitch size of the LSO crystals. Both distribution shows empty bins, which are evidence of the granular nature of the available LOR inside the scanner. In contrast, the distribution for GATE simulations shows all the bins occupied as seen in Figure 4.24B.

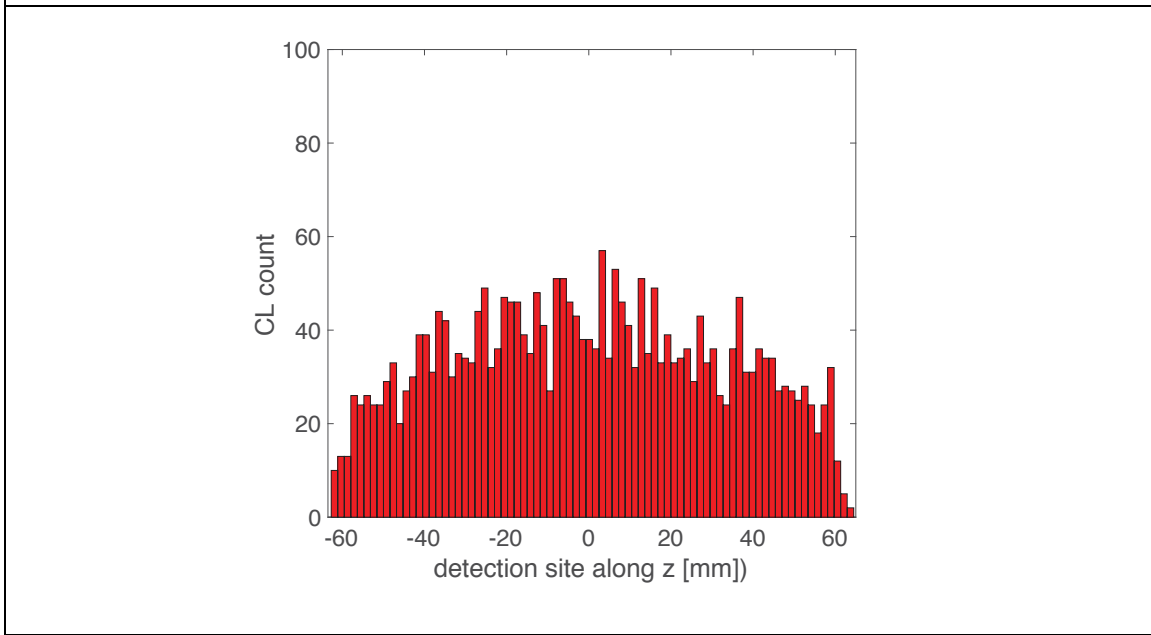
To establish if there is a link between the presence of the oscillations and the settings of M-PEPT, the same list mode file is fed into the code with different settings. The data set used corresponds to a particle moving at 0.18 cm/s. Grid sizes of 0.5, 1, 2 and 3 mm are used. The time step is 100 ms. The results of this first test for a particle moving at 0.18 cm/s is shown in Figure 4.25. Figure 25 suggests a correlation between the grid size and the presence of the artifact. However, this correlation is mainly present in the experimental results, suggesting the distortion is affected by the nature of the scanner data acquisition. Figure 4.26 shows the results of a grid size variation study in M-PEPT obtained for a particle moving at 0.22 cm/s. Figure 4.27 shows the results of a grid size comparison in M-PEPT for a particle moving at 0.45 cm/s. All tests of the impact of grid size selection in M-PEPT indicate an interplay between the real scanner data and grid size selection for grid elements less than 3 mm.

An additional interrogation of the experimental data is performed in order to understand better the variation in the predicted particle location. The information regarding the location of the endpoints of CL is retrieved in a one hundred millisecond time window. The CL are visually represented in a 3D plot, and a comparison frame by frame is performed. Figure 4.28 shows the time frames from 76.03 to 76.13 s and 76.13 to 76.23 s corresponding to the initial location of jump. A careful observation of the second frame shows that the source is “brighter” in this frame than in the previous one. In this case bright is related to the presence of CLs. Additional to this brightness, the CLs in the second frame are concentrated to the bottom. In the first frame, the CL show no explicit orientation. This change in the appearance of CL might be related to the granular nature of available LOR. Every time the source passes through regions of the scanner where LOR are “available”, its brightness increases and the position of available LOR may bias the predicted location.

The information gathered in this section suggest the oscillation in the detection is



A) Experimental detection site distribution. Regions 1 and 2 of Figure 4.24 are superimposed



B) Simulated detection site distribution

Figure 4.24. Detection site distribution for experimental and simulated results

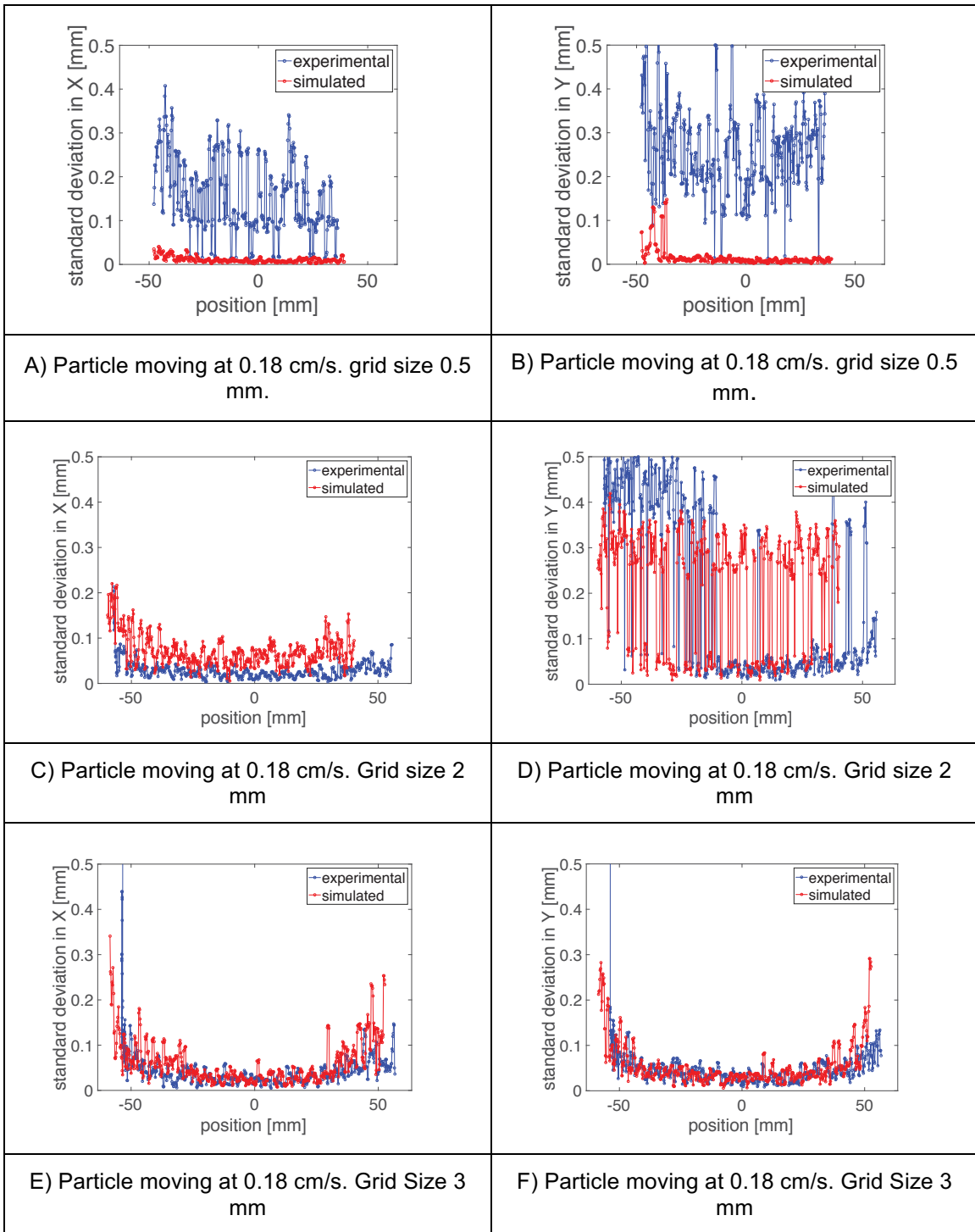


Figure 4.25. Standard deviation comparison for different grid size. Particle moving at 0.18 cm/s.

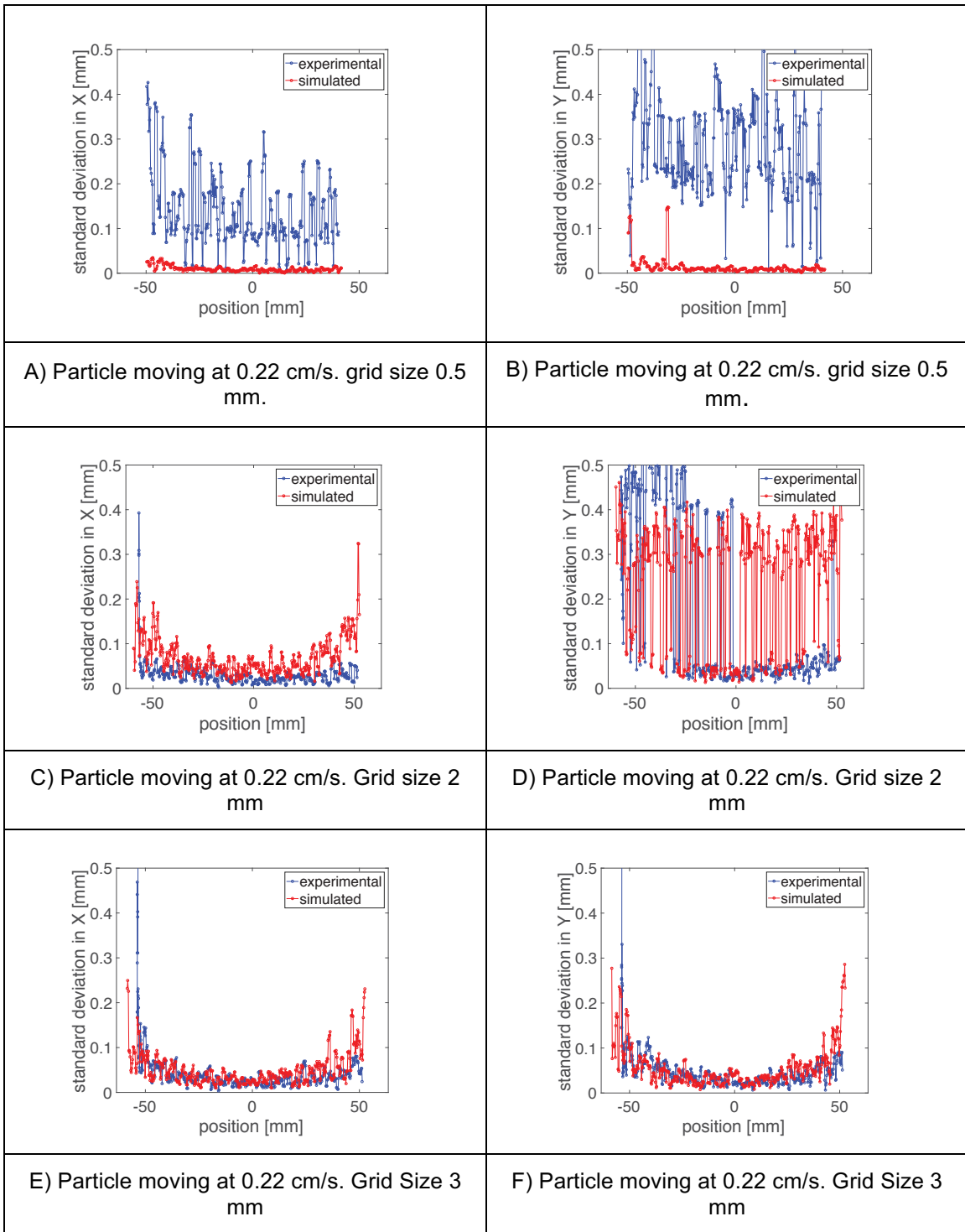


Figure 4.26. Standard deviation comparison for different grid size. Particle moving at 0.22 cm/s.

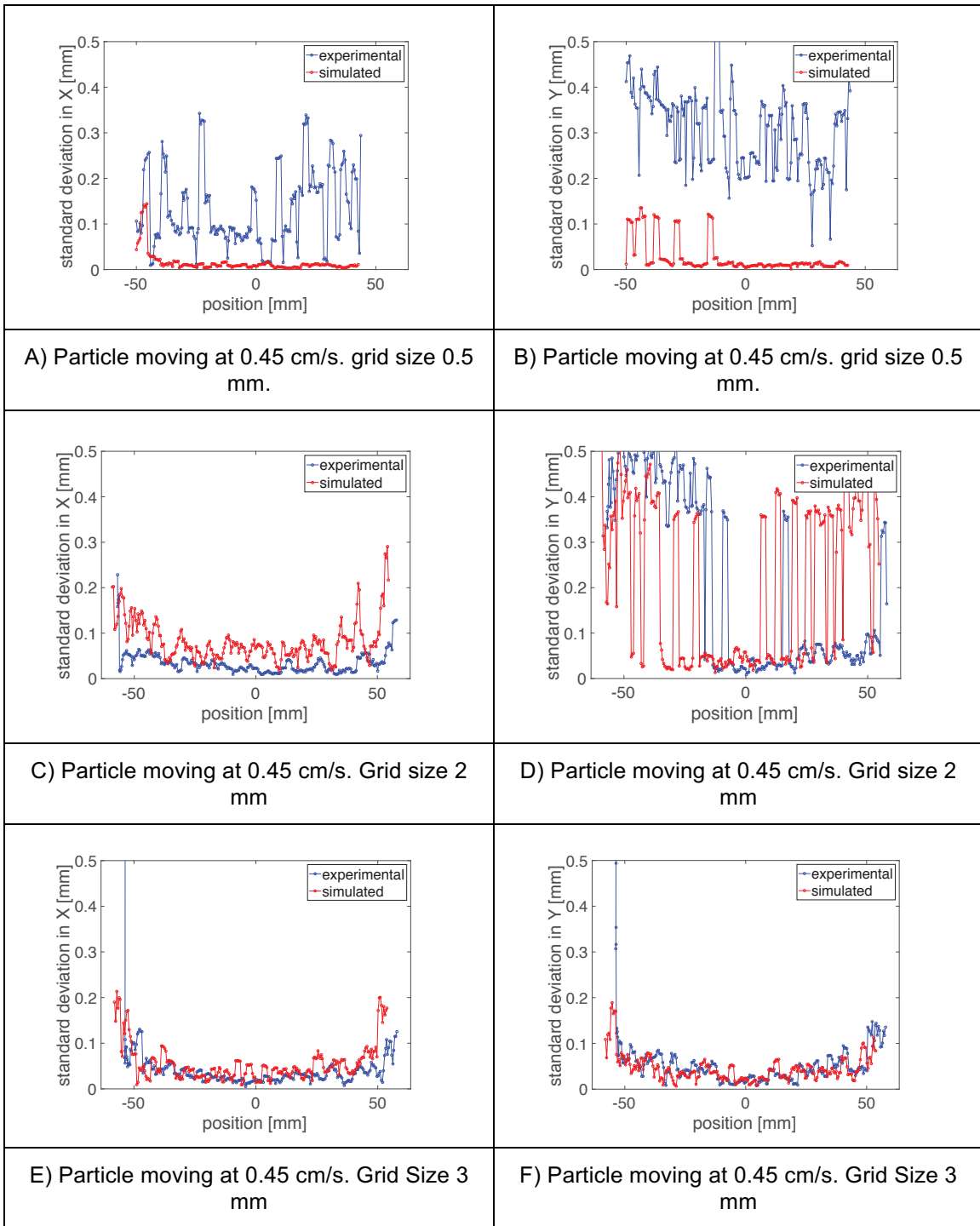
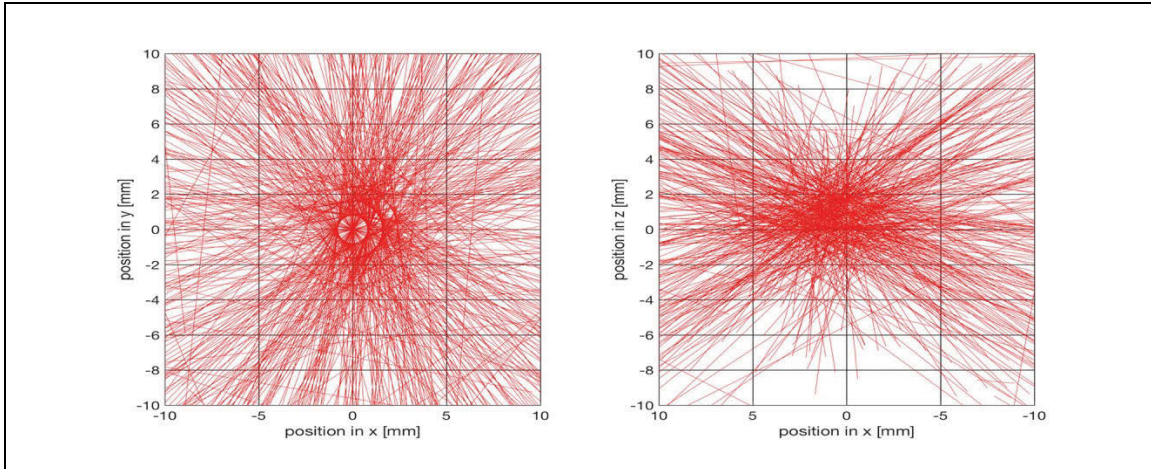
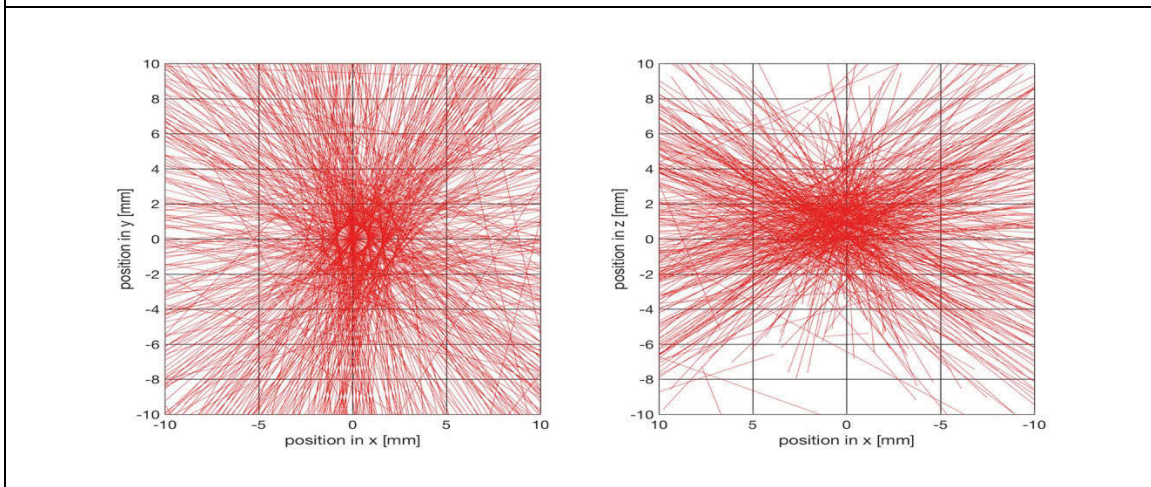


Figure 4.27. Standard deviation comparison for different grid size. Particle moving at 0.45 cm/s.



A) CL representation of a particle moving inside the FOV for the time interval from 76.03 s to 76.13 s



B) CL representation of a particle moving inside the FOV for the time interval from 76.13 s to 76.23 s

Figure 4.28. Comparison frame by frame of the CL representation of a particle moving inside the FOV

a combination of the discrete nature of the available LOR in the scanner and the grid settings used in M-PEPT. Additional research is required to fully understand this feature and to implement correction in the M-PEPT code.

CHAPTER FIVE

CONCLUSIONS, AND FUTURE WORK

1. Conclusions

This is the first validation of GATE for the M-PEPT application. Experimental data obtained from two experiments are compared with equivalent data obtained from GATE simulations. The comparison shows that GATE generates results that resemble, but not completely imitate the experimental data. The definition of the source used in GATE is the main feature of the simulation that was adjusted in order to obtain better approximations.

Three models of source definition are tested: Back to back photon annihilation, positron emission and isotope decay. The best results are achieved with the positron emission model. Other variants of this model are also tested. The results show that the presence of the source holder scattering media greatly changes the simulated results. When no holder is present, 90% of the CL are located within 5 mm around the particle source, while when the holder is present, this fraction is equal to 60%. The actual scanner with the source holder present produces 80% of the CL within a 5 mm radius of the source with the holder present.

The first experiment for GATE validation examines a single particle located at different places along the z direction of the detector bore. Through this experiment, the efficiency of the Inveon is investigated, and results are equal to 5.22% at the center of the FOV for the 425 – 625 keV energy window. The same procedure is simulated in GATE and the CL count at each location is compared to the experiment. The data show that GATE overestimates the CL count at each location. This overestimation is 3% at the center of the FOV producing efficiency 5.40% for the simulation. The overprediction in CL count is almost 40% at the edges of the FOV.

The second validation experiment for GATE is to move a particle inside the FOV at different velocities. Experimental and simulated results are treated with M-PEPT. Experimental and simulated data sets produce similar standard deviation in predicted position when used in M-PEPT. However, the standard deviation using simulated data is smaller than the standard deviation when experimental data are used. This difference is caused by the oscillation in the detection present in the experimental results. Evidence suggests that these oscillations are due to the combination of the granular nature of LOR available in the Inveon and the parameters used in M-PEPT.

The granular nature of the LOR of the Inveon is due to the limited number of LOR available for detection and the regular geometry of available crystal addresses for LOR end points. LOR are the addressable lines at which a back to back photon annihilation can be detected. In the Inveon, this number is limited and is function of the 25,600 crystal locations inside the detector and limits on acceptance angle. Any detection inside a specific crystal is processed as it occurs at the center of this crystal, thus there are locations inside the scanner where the presence of annihilation is not recordable. This feature of the physical detector is not present in GATE. In GATE, any interaction that occurs inside a crystal is recorded with the exact coordinates at which the interaction occurs, thus the LOR available in GATE are infinite.

2. Future Work

Full understanding of the reasons for the disparity in scatter fraction and true CL in the simulation relative to the Inveon will require more investigation. This would lead to a deeper understanding in the way GATE is modelling the positron and photon transport, and may also disclose some special treatments of data inside the Inveon. In this work an existing GATE model validated for PET was tested. Future work will extend this model for M-PEPT application.

The inclusion of the discrete nature of scanner data acquisition is required in GATE in order to make the simulation more representative of the scanner. GATE has the option to mimic the limited number of LOR present in the actual PET scanners. However, the activation of this option requires a new compilation of GATE. During attempts to implement this feature, simulations failed without any result. Additional features of the PET scanner may also be investigated, among them: ring difference definition, quantum efficiency, crystal to crystal variation in blurring and efficiency, and dead time.

Experiments to test simulated results at different source activities are also required. This is necessary to understand if the approximation in GATE for dead time and random coincidence is accurate when activities and count rates are high.

CHAPTER SIX

ADDITIONAL CONTRIBUTION TO M-PEPT DEVELOPMENT

1. Feature Point Identification Method Evaluation

Several additional efforts were performed supporting the thermal fluids group research that are relevant to M-PEPT, but not directly related to GATE validation for M-PEPT. An effort to evaluate the Feature Point Identification Method performed by Wiggins et al (Wiggins et al., 2017) included a GATE simulation set up by the author of this work. Simulations of 25, 50, 75 and 100 particles are performed. The particles are located in random stationary positions inside of an 80 mm diameter and 80 mm height cylinder. The simulated particles are ^{22}Na sources located inside cubes of 0.5 mm side. The simulations are done with the back to back gamma emission source definition plus the positron emission definition. This means that the actual activity of the source is 0.3264 times the activity prescribed in the simulation. For this reason the results are presented in terms of the number of LOR used for particle location (Wiggins et al., 2017).

FPI and G-means M-PEPT software are applied to detect the particles. The objective of the test is to evaluate the performance of FPI in comparison with G-means (Wiggins et al., 2016). In both methods a grid size of 0.5 mm is used. The time step used is 100 ms.

2. Movement of several particles in GATE (General Movement)

The objective of using GATE is to simulate the movement of radioactive particles inside fluids. In order to design real experiments, GATE must be able to simulate several particles at the same time. One of the first jobs done with GATE was to test this ability. For several particles, the definition of the source, and the attachment of these sources to their moving volumes has to be done in a defined order inside the mac file. Additionally, in order to create several moving particles, the motion of the moving volumes has to be the “generic move” method. A matlab script was coded to generate the mac files required to simulate several particles in GATE. This code is presented in Appendix 5. An example of a source definition and source attachment for 2 moving particles is presented in Appendix 6.

For the definition of the particle motion, the creation of a placement file is required. An example of this file is presented in Appendix 7. The three first lines of this file defines the units to be used for time, rotation and translation. Then an

array of 8 columns follows. This array will indicate what is the position and the orientation of the source as a function of time. The first column is time; the second is the rotation angle; the third, fourth, and fifth are the rotation axes. The sixth, seventh and eight columns are the translation in x, y and z. A comparison between the two definitions of movements (translation and generic move) is present in Appendix 8.

In this test, the simulation of one particle moving inside the FOV at 0.18 cm/s is done. Only the particle is simulated without any source support. The position of the source is written as a function of time in a placement file. The data for the file are obtained with the equations:

$$x = 0 \quad (7)$$

$$y = 0 \quad (8)$$

$$z = -135.5 + 1.79 * time \quad (9)$$

Figure 6.1 presents a comparison of CL count used for detection between simulated and experimental data. As expected, the CL count without the source support is higher than the experimental CL count. This simulation was done without the support in order to represent an experiment scenario in which only the particle will be present in the medium.

With this method up to 100 particles are able to be simulated. However, depending on the activity of the sources, the dead time of the simulated scanner starts to impact the results, and in some simulations, with 100 particles at 10 μ Ci each, the simulated Inveon was not able to detect any particle inside the bore.

This kind of simulation was used to simulate 20 yeast cells activated to 50 Bq/cell, as discussed in the next section.

3. Activated Yeast Simulation

M-PEPT is used to identify 20 yeast cells activated with 50 Bq/cell of ^{18}F (Langford et al., 2017). To support this effort, a GATE simulation of 20 ^{18}F particles of 50 Bq/cell is performed. The particles are placed inside a cylinder of water. The total length of the simulation is 20 minutes. The movement of the particles is simulated with the “generic move” definition in GATE. The placement files are provided by Cody Wiggins as part of the work performed for the reference (Langford et al., 2017). The settings used in M-PEPT are grid size of 2 mm and time step of 3000 ms. The objective of the simulation is to evaluate the ability of M-PEPT to identify all the trajectories input, or the possible identification of non-existent trajectories. 17 of 20 particles simulated are detected. The

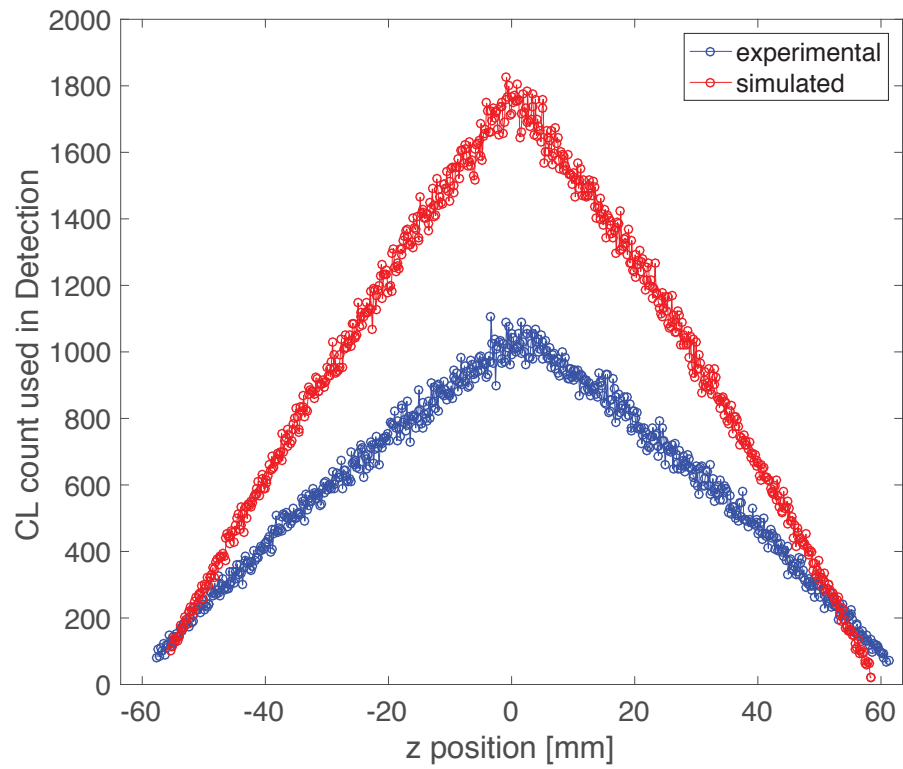


Figure 6.1. Comparison of the CL count available for detection for a particle moving at 0.18 cm/s without the phantom support. (Energy window 425 – 625 keV)

detected particles superimposed to their prescribed trajectories are shown in Figure 6.2.

Even though M-PEPT is able to detect the particles, the reconstruction of the trajectories is not perfect. In most cases, the reconstructed trajectory only covers part of the total length followed by the particle. For this reason, a comparison with all the prescribed trajectories is not possible. Instead, starting with the first time mark identified in M-PEPT, the prescribed array of time and positions are sampled every 3 seconds up to the last time mark registered in M-PEPT. In this way, the prescribed arrays have the same length as the detected arrays. Figure 6.3 shows the comparison of the sampled prescribed positions with the detected positions by M-PEPT. Figure 6.4 shows that the profile followed by the detected particle is similar, but not exactly the same as the prescribed profile. Figure 6.4 shows one particle located at the entrance of the bore, and one particle that passes through the center of the FOV. The comparison of these two plots shows that the difference between prescribed and detected trajectory is not related to the position of the particle inside the FOV.

Figure 6.4 shows the absolute difference between the prescribed position values of GATE and the detected values of M-PEPT for the same two particles mentioned above. The figure also shows the difference in the time marks of both data sets. The data indicates that the difference in position is less than 2 mm in most of the cases. However, the difference in time marks can be as large as 5 s. However, it is necessary to remember that the total length of the simulation is 20 minutes. The CL count used for detection all cases is less than 100 at each time step of 3000 s. The model of the source definition is positron emission, with the use of the defined F-18 positron distribution built in GATE. This means that even with this small amount of activity, M-PEPT is able to identify and reconstruct, with good approximation, the trajectories followed by the particles.

4. Funding

The PET scanner was procured via the U.S. Dept. of Energy National Nuclear Security Administration (NNSA)DE-NA0001983. The views presented here are those of the author and do not necessarily reflect those of the U.S.DOE or NNSA. The author's tuition was covered by the Department of Nuclear Engineering at UTK through a Graduate Teaching Assistantship. Additional fees and stipend for two years was provided by the Fulbright Program. The aim of this program is to create bonds among American and Foreign people through the exchange of culture and knowledge. This exchange is experienced in academic environments inside the United States or in any other country that participates in the program. Additional funding through the whole duration of the program was provided by the Escuela Politecnica Nacional (EPN) in Quito, Ecuador. The EPN

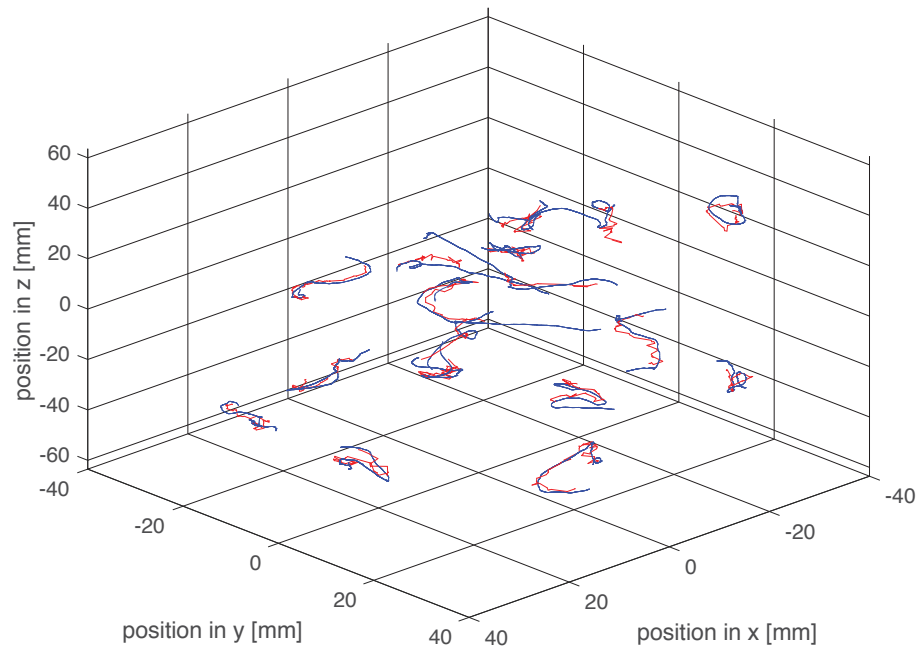


Figure 6.2. Superimposition of the particles detected in M-PEPT and their trajectories prescribed in GATE for a simulation of 20 F-18 particles of 50 Bq each. Only 17 particles are detected

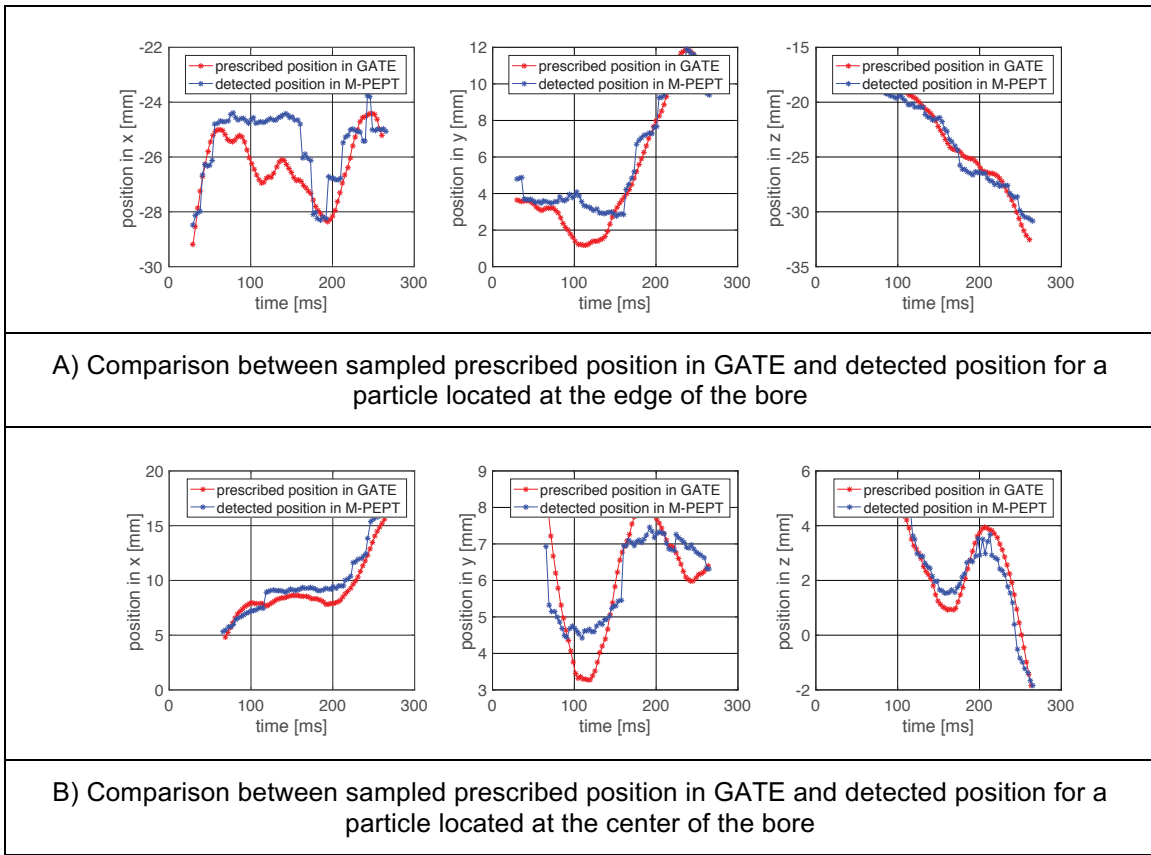
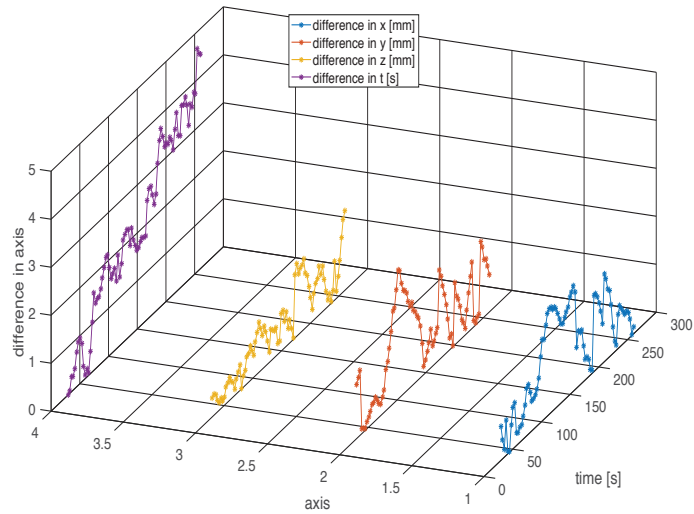
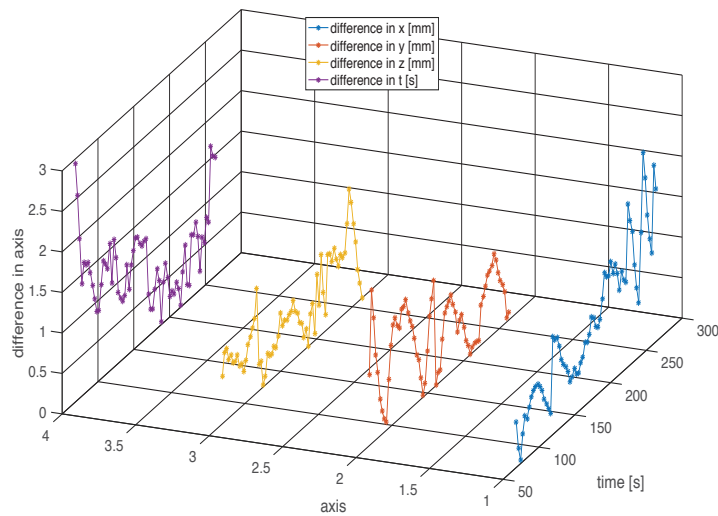


Figure 6.3. Comparison of the prescribed position in GATE and the detected particles in M-PEPT



A) Difference in prescribed and detected position for a particle located at the edge of the bore



B) Difference in prescribed and detected position for a particle located at the center of the bore

Figure 6.4. Absolute difference of the values prescribed for position in GATE and those detected with M-PEPT. The difference in the time mark of detection is also included.

is ranked as the best university in Ecuador and is part of the top 75 universities in Latin America.

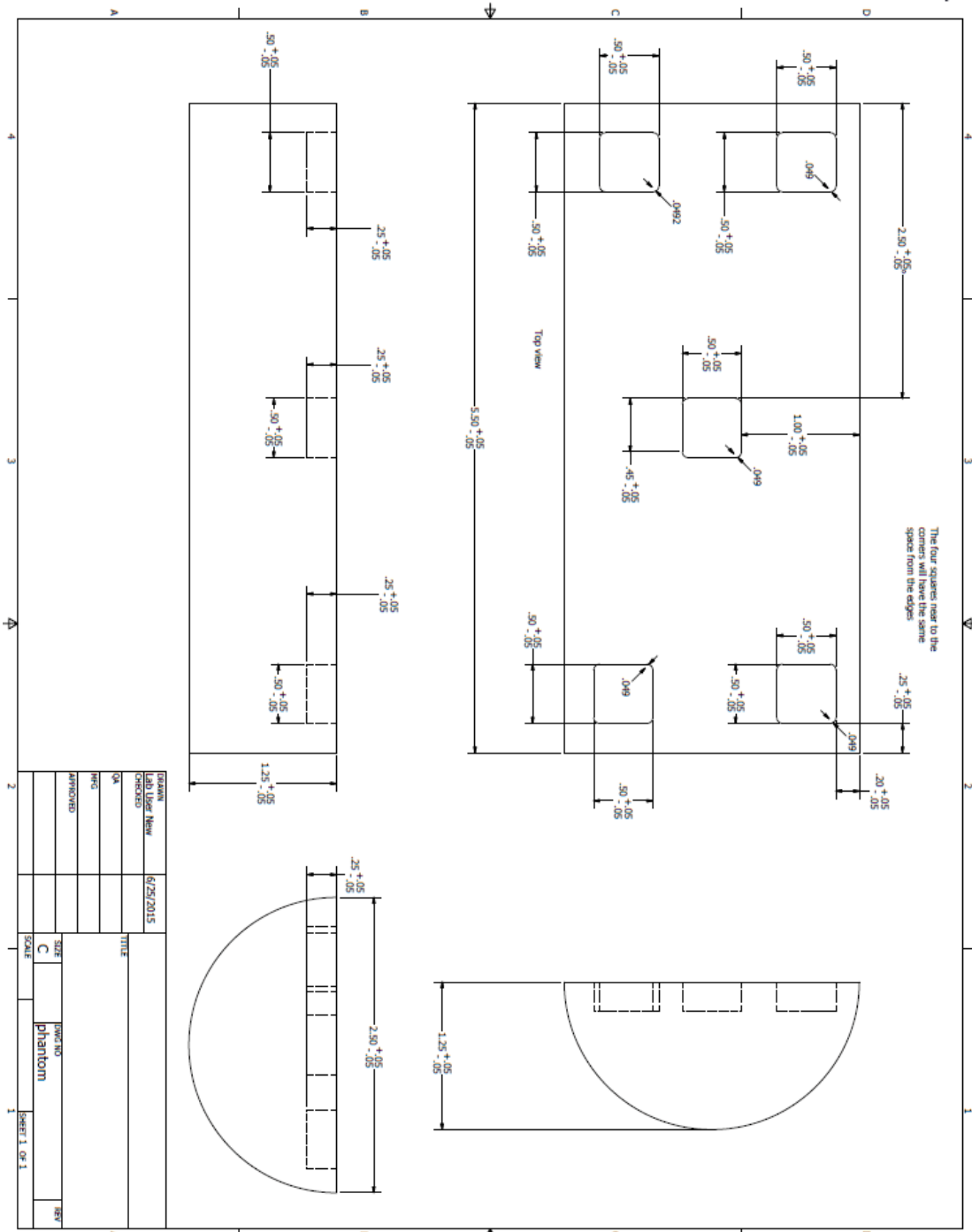
LIST OF REFERENCES

- AGOSTINELLI, S., ET AL, Geant4—a simulation toolkit. *Nuclear Inst. and Methods in Physics Research, A*, 506, 250-303.
- BAO, Q., CHEN, M., STOUT, D. B., CHATZIOANNOU, A. F. & NEWPORT, D. 2009. Performance evaluation of the Inveon dedicated PET preclinical tomograph based on the NEMA NU-4 standards. *Journal of Nuclear Medicine*, 50, 401-408.
- BICKELL, M., BUFFLER, A., GOVENDER, I. & PARKER, D. J. 2012. A new line density tracking algorithm for PEPT and its application to multiple tracers. *Nuclear Inst. and Methods in Physics Research, A*, 682, 36-41.
- I.F. SBALZARINI, P. K. 2005. Feature point tracking and trajectory analysis for video imaging in cell biology. *Journal of Structural Biology*, 151, 182-195.
- JAN, S. 2004. Gate: a simulation toolkit for pet and spect. *Physics in Medicine and Biology*, 49, 4543-4561.
- KUHN, H. W. 2005. The Hungarian method for the assignment problem. *Naval Research Logistics (NRL)*, 52, 7-21.
- LANGFORD, S., WIGGINS, C., TENPENNY, D. & RUGGLES, A. 2016. Positron Emission Particle Tracking (PEPT) for Fluid Flow Measurements. *Nuclear Engineering and Design*, 302, 81-89.
- LANGFORD, S. T., WIGGINS, C. S., SANTOS, R., HAUSER, M., BECKER, J. M. & RUGGLES, A. E. 2017. Three-dimensional spatiotemporal tracking of fluorine-18 radiolabeled yeast cells via positron emission particle tracking. *PLOS ONE*, 12, e0180503.
- LEE, K. S., KIM, T. J. & PRATX, G. 2015. Single-Cell Tracking With PET Using a Novel Trajectory Reconstruction Algorithm. *Medical Imaging, IEEE Transactions on*, 34, 994-1003.
- LEE, S., GREGOR, J. & OSBORNE, D. 2013. Development and Validation of a Complete GATE Model of the Siemens Inveon Trimodal Imaging Platform. *Molecular Imaging*, 12.
- LU, L., MA, J., BIAN, Z., CHEN, W., HAN, Y., KARAKATSANIS, N., RAHMIM, A. & TANG, J. 2013. Performance evaluation of the Inveon PET scanner using GATE based on the NEMA NU-4 standards.
- MCINTOSH, B., STOUT, D. B. & GOERTZEN, A. L. 2011. Validation of a GATE Model
Lu-176 Intrinsic Radioactivity in LSO PET Systems. *Nuclear Science, IEEE Transactions on*, 58, 682-686.
- MUNKRES, J. 1957. Algorithms for the Assignment and Transportation Problems. *Journal of the Society for Industrial and Applied Mathematics*, 5, 32-38.
- NEMA STANDARDS PUBLICATION. 2008. Performance measurements of small animal positron emission tomographs. *National Electrical Manufacturers Association NU(4)*, Rosslyn, VA
- PARKER, D. J., BROADBENT, C. J., FOWLES, P., HAWKESWORTH, M. R. & MCNEIL, P. 1993. Positron emission particle tracking - a technique for

- studying flow within engineering equipment. *Nuclear Inst. and Methods in Physics Research*, A, 326, 592-607.
- PATEL, N., WIGGINS, C. & RUGGLES, A. 2017. Positron emission particle tracking in pulsatile flow. *Experiments in Fluids*, 58, <xocs:firstpage xmlns:xocs=""/>.
- PHELPS, M. E. 2006. PET : physics, instrumentation, and scanners. *Positron-emission tomography : physics, instrumentation, and scanners*. New York Berlin: New York Berlin : Springer.
- PROSPER, H. B., DANILOV, M. & SPRINGERLINK 2003. *Techniques and Concepts of High-Energy Physics XII*, Dordrecht : Springer Netherlands : Imprint: Springer.
- S. JAN, G. S., D. STRUL, S. STAELENS, K. ASSIÉ, ET AL 2014. GATE Users Guide V7.1. . In: S. GLICK, S. K., F. MAYET (ed.).
- SAHA, G. B. 2016. *Basics of PET Imaging : Physics, Chemistry, and Regulations*, Cham : Springer International Publishing : Imprint: Springer.
- SARRUT, D. ET AL. 2014. A review of the use and potential of the GATE Monte Carlo simulation code for radiation therapy and dosimetry applications. *Medical Physics*, 41.
- SCHMIDTLEIN, C. R., KIROV, A. S., NEHMEH, S. A., ERDI, Y. E., HUMM, J. L., AMOLS, H. I., BIDAUT, L. M., GANIN, A., STEARNS, C. W., MCDANIEL, D. L. & HAMACHER, K. A. 2006. Validation of GATE Monte Carlo simulations of the GE Advance/Discovery LS PET scanners. *Medical Physics*, 33.
- SHAW, R. F. 1978. *Signaling particles for introduction into blood flow through a vessel of interest*. United States patent application.
- SIEMENS 2011. Inveon's User Manual. United States of America: Siemens.
- TURNER, J. E. 2007. *Atoms, Radiation, and Radiation Protection*, Federal Republic of Germany, WILEY-VCH Verlag GmbH
- WIGGINS, C., SANTOS, R. & RUGGLES, A. 2016. A novel clustering approach to positron emission particle tracking. *Nuclear Inst. and Methods in Physics Research*, A, 811, 18-24.
- WIGGINS, C., SANTOS, R. & RUGGLES, A. 2017. A feature point identification method for positron emission particle tracking with multiple tracers. *Nuclear Inst. and Methods in Physics Research*, A, 843, 22-28.

APPENDIX

Appendix 1: Design drawings of the phantom support



Appendix 2: Mac file for the definition of the source

```
#=====
#Source definition positron emission model
#=====

#multiple    source    try    one
/gate/source/addSource    Na22_1    gps
/gate/source/Na22_1/setActivity    231990 becquerel
/gate/source/Na22_1/gps/particle    e+
/gate/source/Na22_1/setForcedUnstableFlag    true
/gate/source/Na22_1/setForcedHalfLife    82268906.02 s
/gate/source/Na22_1/gps/energytype    UserSpectrum
/gate/source/Na22_1/gps/setSpectrumFile    distribution.txt
/gate/source/Na22_1/gps/angtype    iso
/gate/source/Na22_1/gps/mintheta    0    deg
/gate/source/Na22_1/gps/maxtheta    180    deg
/gate/source/Na22_1/gps/minphi    0    deg
/gate/source/Na22_1/gps/maxphi    360    deg
/gate/source/Na22_1/gps/type    Point
```

Appendix 3: Inveon header file

```
40_PET_SensitivityCurve425625ener10sec_v1.pet.img.hdr
~/Documents/InveonResults/425625ener10sec/40/40_PET_SensitivityCurve425625ener10sec_v1.pet.img.hdr
842 # Following parameters are used for PET or SPECT modalities.
843 #
844 #
845 # Deadtime correction for data set (float)
846 #     NOTE: Scale factor INCLUDES this value.
847 #
848 deadtime_correction 1.05618
849 #
850 # Global decay correction applied to data set (float)
851 #     NOTE: Scale factor INCLUDES this value.
852 #
853 decay_correction 1
854 #
855 # Prompts count for data set (64-bit ints)
856 #
857 #     NOTE: The 3 values represent histogrammed prompts,
858 #           unhistogrammed prompts, and prompts at coincidence detection.
859 #
860 prompts 109219 5356 114411
861 #
862 # Prompts countrate per sec before histogramming (int)
863 #
864 prompts_rate 5200
865 #
866 # Following parameters are used for PET modality only.
867 #
868 #
869 # Delays count for data set (64-bit ints)
870 #
871 #     NOTE: The 3 values represent histogrammed delays,
872 #           unhistogrammed delays, and delays at coincidence detection.
873 #
874 delays 172 95 249
875 #
876 # Trues count for data set (64-bit ints)
877 #
878 #     NOTE: The 3 values represent histogrammed trues,
879 #           unhistogrammed trues, and trues at coincidence detection.
880 #
881 trues 109047 5261 114162
882 #
883 # Delays countrate per sec before histogramming (int)
884 #
885 delays_rate 10
886 #
887 # Singles rates array (integer float float)
888 #     block_number  singles/sec  raw_singles/sec  xy_stored_singles/sec  block_s:
889 #
890 singles 0 2432.54 6560.14 6213.6 2432.54 24.5045 24.5045 0.315315 0.315315
891 singles 1 2410.32 6583.47 6220.36 2410.32 25.045 25.045 0.0900901 0.0900901
```

Appendix 4: Standard deviation distribution for the three velocities tested and at the different repetitions.

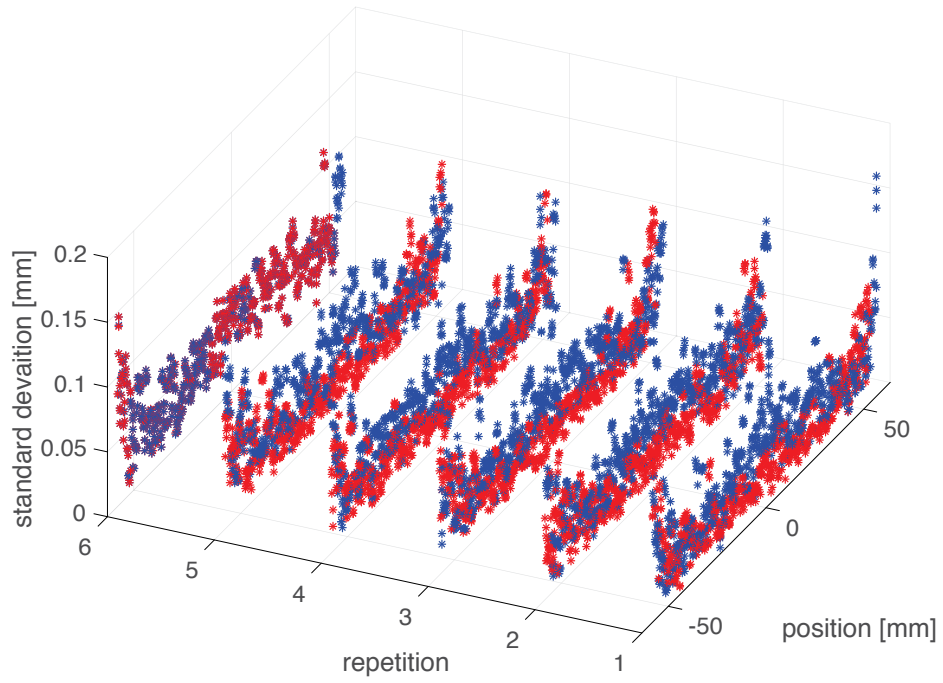


Figure A.1. Standard deviation comparison for 0.18 cm/s

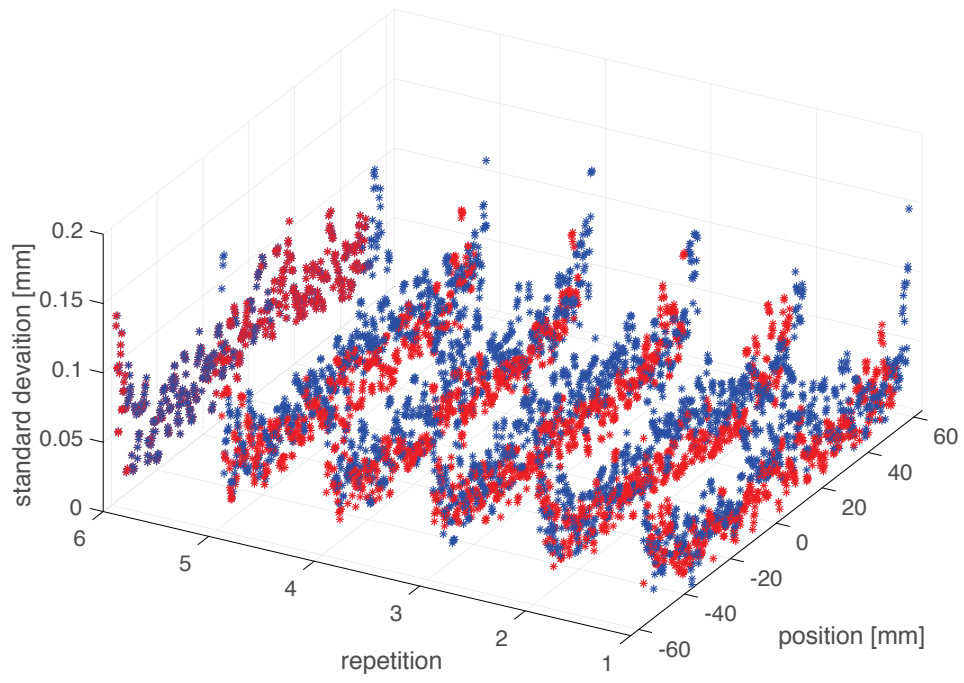


Figure A.2. Standard deviation comparison for 0.22 cm/s

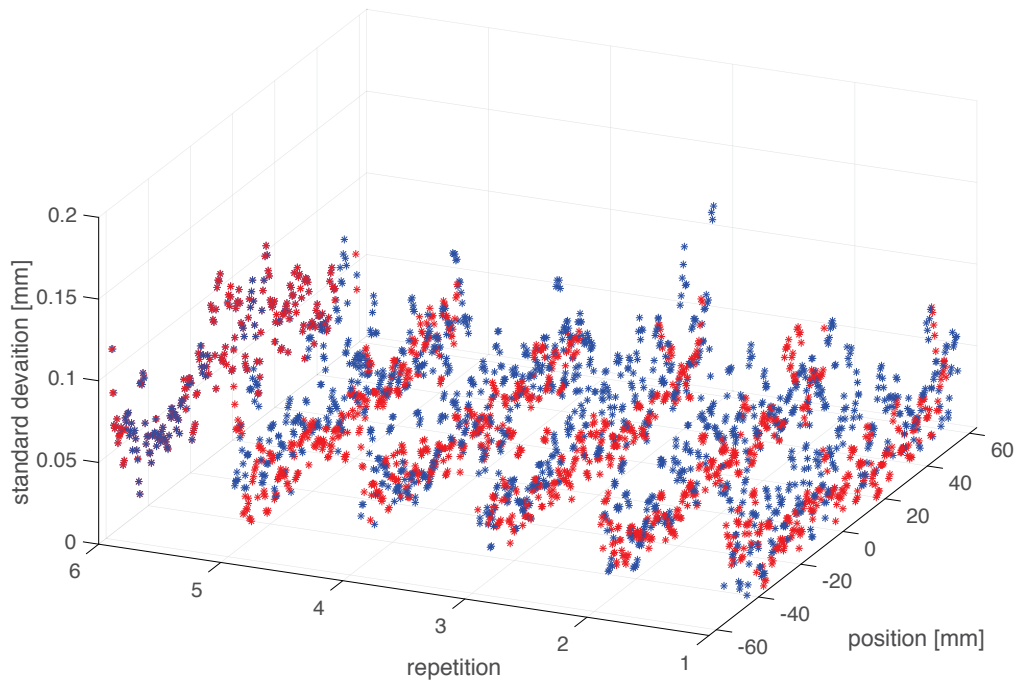


Figure A.3. Standard deviation comparison for 0.45 cm/s

Appendix 5: GateFileCreator

```
%volumeGenericMovePlacements
clc
clear all
close all
%create a txt file that lists the displacemnts file for generic moves
in
%Gate
NumberOfSources=2;
NameoftheSources=['Na22Cubes'];
Movement=2;%input('Type of move\1-translation \2-genericMove ');
TypeofSource=1;%1-Na22 2-F18

%%
%volumeVelocities.mac
for i=1:NumberOfSources

    N=num2str(i);
    if Movement==1
        movement=['translation'];
        A{i,1}=['/gate/',NameoftheSources,N,'/moves/insert ',movement];
        B{i,1}=['/gate/',NameoftheSources,N,'/',movement,'/setSpeed 0 0
0 cm/s'];
    else
        movement=['genericMove'];
        A{i,1}=['/gate/',NameoftheSources,N,'/moves/insert ',movement];

B{i,1}=['/gate/',NameoftheSources,N,'/',movement,'/setPlacementsFilenam
e data/',NameoftheSources,N,'.placement'];
        end
    end

end

[nrow,ncols]=size(A);
fid=fopen('volumeVelocities.mac','wt');
for row=1:nrow
    fprintf(fid,'%s\n',A{row,:},B{row,:});
end
fclose(fid);

%%
%SourceAttachto.mac
%NameofMovingSources=input('Name of the files to be moved (Seth)
','s');
for i=1:NumberOfSources

    N=num2str(i);

    if TypeofSource==1
        A{i,1}=['/gate/source/Na22_',N,'/attachTo
',NameoftheSources,N];
    else
```

```

                A{i,1}=[ '/gate/source/F18_',N,'/attachTo
',NameoftheSources,N];
                end

end

[nrow,ncols]=size(A);
fid=fopen('sourceAttachto.mac','wt');
for row=1:nrow
    fprintf(fid,'%s\n',A{row,:})
end

fclose(fid);

%%
%sourceDefinition.mac
for i=1:NumberOfSources

    N=num2str(i);

    if TypeofSource==1
        A{i,1}=[ '/gate/source/addSource Na22_',N,' gps'];
        B{i,1}=[ '/gate/source/Na22_',N,'/gps/particle e+'];
        C0{i,1}=[ '/gate/source/Na22_',N,'/setActivity 72460
becquerel'];
        C{i,1}=[ '/gate/source/Na22_',N,'/setForcedUnstableFlag
true'];
        D{i,1}=[ '/gate/source/Na22_',N,'/setForcedHalfLife
82268906.02 s'];
        E{i,1}=[ '/gate/source/Na22_',N,'/gps/energytype
UserSpectrum'];
        F{i,1}=[ '/gate/source/Na22_',N,'/gps/setSpectrumFile
distribution.txt'];
        G{i,1}=[ '/gate/source/Na22_',N,'/setType backtoback'];
        H{i,1}=[ '/gate/source/Na22_',N,'/gps/angtype iso'];
        I{i,1}=[ '/gate/source/Na22_',N,'/gps/mintheta 90 deg'];
        J{i,1}=[ '/gate/source/Na22_',N,'/gps/maxtheta 90 deg'];
        K{i,1}=[ '/gate/source/Na22_',N,'/gps/minphi 0 deg'];
        L{i,1}=[ '/gate/source/Na22_',N,'/gps/maxphi 360 deg'];
        M{i,1}=[ '/gate/source/Na22_',N,'/gps/type Point'];

    else

        N0{i,1}=[ '/gate/source/addSource F18_',N,' gps'];
        O{i,1}=[ '/gate/source/F18_',N,'/gps/particle e+'];
        P{i,1}=[ '/gate/source/F18_',N,'/gps/energytype Fluor18'];
        Q{i,1}=[ '/gate/source/F18_',N,'/setForcedUnstableFlag
true'];

        R{i,1}=[ '/gate/source/F18_',N,'/setForcedHalfLife 6586 s'];
        S{i,1}=[ '/gate/source/F18_',N,'/setActivity 10000 Bq'];
        T{i,1}=[ '/gate/source/F18_',N,'/gps/angtype iso'];
        U{i,1}=[ '/gate/source/F18_',N,'/gps/mintheta 0 deg'];
        V{i,1}=[ '/gate/source/F18_',N,'/gps/maxtheta 180 deg'];
    end
end

```

```

        W{i,1}=['/gate/source/F18_',N,'/gps/minphi 0 deg'];
        X{i,1}=['/gate/source/F18_',N,'/gps/maxphi 360 deg'];
        Y{i,1}=['/gate/source/F18_',N,'/gps/type Point'];
    end
end

if TypeofSource==1

    [nrow,ncols]=size(A);
    fid=fopen('sourcesDefinition.mac','wt');
    for row=1:nrow

        fprintf(fid,'%s\n',A{row,:},B{row,:},C0{row,:},C{row,:},D{row,:},E{row,
        :},F{row,:},G{row,:},H{row,:},I{row,:},J{row,:},K{row,:},L{row,:},M{row
        ,:})
        end

        fclose(fid);
    else

        [nrow,ncols]=size(N0);
        fid=fopen('sourcesDefinition.mac','wt');
        for row=1:nrow

            fprintf(fid,'%s\n',N0{row,:},O{row,:},P{row,:},Q{row,:},R{row,:},S{row,
            :},T{row,:},U{row,:},V{row,:},W{row,:},X{row,:},Y{row,:})
            end

            fclose(fid);
        end

%%
%%sourcePlacement.mac
for i=1:NumberOfSources

    N=num2str(i);

    if TypeofSource==1;
        A{i,1}=['/gate/source/Na22_',N,'/gps/centre 0 0 0 mm'];
    else
        A{i,1}=['/gate/source/F18_',N,'/gps/centre 0 0 0 mm'];
    end
end

[nrow,ncols]=size(A);
fid=fopen('sourcesPlacement.mac','wt');
for row=1:nrow
    fprintf(fid,'%s\n',A{row,:})
end

```

```

fclose(fid);

%%
%visualizeSources.mac
for i=1:NumberOfSources

    N=num2str(i);

    if TypeofSource==1
        A{i,1}=['/gate/source/Na22_',N,'/visualize 50 yellow 3'];
    else
        A{i,1}=['/gate/source/F18_',N,'/visualize 50 yellow 3'];
    end
end

[nrow,ncols]=size(A);
fid=fopen('visualizeSources.mac','wt');
for row=1:nrow
    fprintf(fid,'%s\n',A{row,:})
end

fclose(fid);

%%
%volumeTomove.mac
for i=1:NumberOfSources

    N=num2str(i);

    A{i,1}=['/gate/WaterCylinder/daughters/name
',NameoftheSources,N];
    B{i,1}=['/gate/WaterCylinder/daughters/insert box'];
    C{i,1}=['/gate/',NameoftheSources,N,'/setMaterial Air'];
    D{i,1}=['/gate/',NameoftheSources,N,'/vis/forceSolid'];
    E{i,1}=['/gate/',NameoftheSources,N,'/vis/setColor red'];
    F{i,1}=['/gate/',NameoftheSources,N,'/vis/setVisible'];
    G{i,1}=['/gate/',NameoftheSources,N,'/geometry/setXLength 0.5
mm'];
    H{i,1}=['/gate/',NameoftheSources,N,'/geometry/setYLength 0.5
mm'];
    I{i,1}=['/gate/',NameoftheSources,N,'/geometry/setZLength 0.5
mm'];
end

```

```
[nrow,ncols]=size(A);
fid=fopen('volumesTomove.mac','wt');
    for row=1:nrow

fprintf(fid,'%s\n',A{row,:},B{row,:},C{row,:},D{row,:},E{row,:},F{row,:
},G{row,:},H{row,:},I{row,:})
    end
    rowf=nrow+1
    I{rowf,1}=['/control/execute VolumePlacement.mac'];
    J{rowf,1}=['/control/execute volumeVelocities.mac'];
    fprintf(fid,'%s\n',I{rowf,:},J{rowf,:})
    fclose(fid);
```

Appendix 6: Examples of Mac files

A) Source definition for two particles moving inside the bore (valid up to 100 moving particles)

```
#source 1
/gate/source/addSource Na22_1 gps
/gate/source/Na22_1/gps/particle e+
/gate/source/Na22_1/setActivity 72460 becquerel
/gate/source/Na22_1/setForcedUnstableFlag true
/gate/source/Na22_1/setForcedHalfLife 82268906.02 s
/gate/source/Na22_1/gps/energytype UserSpectrum
/gate/source/Na22_1/gps/setSpectrumFile distribution.txt
/gate/source/Na22_1/setType backtoback
/gate/source/Na22_1/gps/angtype iso
/gate/source/Na22_1/gps/mintheta 90 deg
/gate/source/Na22_1/gps/maxtheta 90 deg
/gate/source/Na22_1/gps/minphi 0 deg
/gate/source/Na22_1/gps/maxphi 360 deg
/gate/source/Na22_1/gps/type Point
#source 2
/gate/source/addSource Na22_2 gps
/gate/source/Na22_2/gps/particle e+
/gate/source/Na22_2/setActivity 72460 becquerel
/gate/source/Na22_2/setForcedUnstableFlag true
/gate/source/Na22_2/setForcedHalfLife 82268906.02 s
/gate/source/Na22_2/gps/energytype UserSpectrum
/gate/source/Na22_2/gps/setSpectrumFile distribution.txt
/gate/source/Na22_2/setType backtoback
/gate/source/Na22_2/gps/angtype iso
/gate/source/Na22_2/gps/mintheta 90 deg
/gate/source/Na22_2/gps/maxtheta 90 deg
/gate/source/Na22_2/gps/minphi 0 deg
/gate/source/Na22_2/gps/maxphi 360 deg
/gate/source/Na22_2/gps/type Point
#source...
```

B) Source attachment to moving volume (valid up to 100 particles)

```
/gate/source/Na22_1/attachTo Na22Cubes1
/gate/source/Na22_2/attachTo Na22Cubes2
/gate/source/Na22_...
```


Appendix 7: Example of placement file (for Yeast simulation)

```
#=====
#Fragment of the mac file that indicates the locations of the particle
#as function of time
#=====
Time s
Rotation deg
Translation mm
0.000000 0 0 0 0 -16.683512 3.596253 -38.745572
0.005000 0 0 0 0 -16.683193 3.596821 -38.745439
0.010000 0 0 0 0 -16.682864 3.597381 -38.745300
0.015000 0 0 0 0 -16.682535 3.597942 -38.745163
0.020000 0 0 0 0 -16.682219 3.598496 -38.745010
0.025000 0 0 0 0 -16.681899 3.599046 -38.744853
0.030000 0 0 0 0 -16.681570 3.599598 -38.744696
0.035000 0 0 0 0 -16.681237 3.600152 -38.744534
0.040000 0 0 0 0 -16.680909 3.600703 -38.744369
0.045000 0 0 0 0 -16.680586 3.601255 -38.744205
0.050000 0 0 0 0 -16.680264 3.601801 -38.744036
0.055000 0 0 0 0 -16.679945 3.602345 -38.743875
0.060000 0 0 0 0 -16.679610 3.602890 -38.743711
0.065000 0 0 0 0 -16.679277 3.603436 -38.743548
0.070000 0 0 0 0 -16.678942 3.603984 -38.743381
0.075000 0 0 0 0 -16.678612 3.604532 -38.743209
0.080000 0 0 0 0 -16.678271 3.605086 -38.743027
0.085000 0 0 0 0 -16.677931 3.605643 -38.742839
0.090000 0 0 0 0 -16.677595 3.606195 -38.742667
0.095000 0 0 0 0 -16.677258 3.606755 -38.742494
0.100000 0 0 0 0 -16.676910 3.607323 -38.742318
0.105000 0 0 0 0 -16.676567 3.607893 -38.742140
0.110000 0 0 0 0 -16.676225 3.608460 -38.741969
```

Appendix 8: Comparison between definition of movements

```
#=====
#mac file setting the velocity at 0.18 cm/s in the z direction
#=====
```

```
#volumeVelocities
/gate/plasticPhantom/moves/insert translation
/gate/plasticPhantom/translation/setSpeed 0 0 0.179 cm/s
```

a) General movement translation

```
#=====
#mac file setting the moving type to generic move. The file also
#indicates the file that has the array of position as function of time
#=====
```

```
#volumeVelocities
/gate/plasticPhantom/moves/insert genericMove
/gate/plasticPhantom/genericMove/setPlacementsFilename
volumeTomove_1a.placement
```

VITA

Roque Antonio Santos Torres was born in Quito Ecuador, on 20th June 1983. His elementary education was done in Colegio Cardenal Spellman, in Quito. He obtained his bachelor degree in Chemical Engineering at Escuela Politecnica Nacional, in Quito Ecuador. His first job was as technician in the Camacho Cifuentes, environmental Consultancy Group. In 2009 he obtained a scholarship to pursue his Master's degree in Nuclear Engineering and Applications at Universidad Autonoma de Madrid, Spain. He became a professor at Escuela Politecnica Nacional in 2010. In 2014 he won a Fulbright Scholarship to pursue a PHD program in Nuclear Engineering at University of Tennessee, Knoxville.

In the course of his research in Knoxville, Mr. Santos co-authored 3 refereed journal papers, 5 posters and 1 conference presentation. He has an additional journal paper as primary author in review. He is also the official Inveon PET scanner operator for the thermal fluids group M-PEPT research.